UNIVERSITÀ
DEGLI STUDI
DI PADOVA

Dipartimento di Ingegneria Industriale

Corso di Laurea Magistrale in Ingegneria Aerospaziale

Analysis of ballistic capture in the circular restricted three body problem

Relatore: Prof. Enrico Lorenzini
Co-relatore: Prof. Claudio Bombardelli

Laureando: Lorenzo Anoè
Matricola: 1234061

Anno Accademico 2020-2021

Abstract

Ballistic capture is a natural phenomenon with important potential for the saving of propellant in interplanetary orbits and for exploration of asteroids. It exploits the interactions of two celestial bodies (Sun and a planet) to insert in an orbit around the planet and spend there a period more or less long. In this work the circular restricted three body problem (CRTBP) is analyzed using curvilinear coordinates for the synodic frame. A trajectory is considered ballistic captured when it spends a significant period with negative keplerian energy with respect to the planet. Thanks to these simple considerations, a detailed analysis of trajectories leading to capture is developed when Jacobi constant has a high value, that is to say when zero velocity curves are only slightly open around the planet and therefore around Lagrangian points L1 and L2. An algorithm implemented in *MatLab* is developed to perform what said above and to compute peculiar features of the trajectories obtained, such as orbital keplerian elements of the orbit of origin. A large number of examples, important considerations and typical patterns of the capture are obtained from this study, where cases with one between Jupiter, Mars and Earth as the planet orbiting the Sun are analyzed. Finally, a preliminary investigation into the potentialities of the use of these trajectories for interplanetary missions is conducted, which shows possible savings of propellant to reach Jupiter or Mars.

Abstract

La cattura balistica è un fenomeno naturale con potenzialità importanti per il risparmio di propellente in orbite interplanetarie e per l'esplorazione di asteroidi. Essa sfrutta le interazioni di due corpi celesti (Sole e un pianeta) per inserirsi in orbita del pianeta e restarvi per tempi più o meno lunghi. In questo lavoro è analizzato il problema circolare ristretto dei tre corpi (CRTBP) utilizzando delle coordinate curvilinee per il sistema di riferimento sinodico. Una traiettoria viene considerata catturata balisticamente quando trascorre un tempo notevole con energia kepleriana negativa rispetto al pianeta. Con queste semplici considerazioni viene svolta una analisi dettagliata delle traiettorie che conducono a cattura quando la costante di Jacobi ha un valore elevato, cioè quando le *zero velocity curves* sono solo leggermente aperte intorno al pianeta e quindi ai punti Lagrangiani L1 e L2. Un algoritmo viene implementato in *MatLab* per svolgere quanto detto sopra e per calcolare le particolari caratteristiche delle traiettorie ottenute, come gli elementi orbitali dell'orbita di origine. Un gran numero di esempi, importanti considerazioni e schemi tipici della cattura sono ricavati dal presente studio, dove sono analizzati i casi in cui il pianeta che orbita intorno al Sole è uno tra Giove, Marte o la Terra. Infine viene condotta una ricerca preliminare sulle potenzialità di queste traiettorie per le missioni interplanetarie, che mostrano un possibile risparmio di propellente per raggiungere Giove o Marte.

Contents

Introduction

Ballistic capture is a natural phenomenon that was developed in literature mostly by Belbruno and Topputo [5, 7], but also by other authors [2, 8]. This phenomenon is important because it can bring a body orbiting the Sun to an orbit linked temporarily to a planet. An event like this is important for many reasons:

- A spacecraft could exploit these trajectories for an interplanetary transfer, saving a certain amount of propellant necessary to introduce itself in a stable orbit around the arrival planet [9];
- An asteroid could be ballistic captured by a planet as it happened to 2006 RH120 [10]. Answering to questions related to this event is an important step for a further comprehension and exploiting of this phenomenon [11];
- Finding an asteroid that will be captured in future could be an occasion to prepare a mission capable of reaching and exploring it. Thanks to events like this also the mining of an asteroid could be planned;
- This phenomenon could be the cause of deflection of asteroids (mainly by Jupiter) and also of the moon and planet formation [3].

In literature, the definition and the nature of ballistic capture was addressed in mainly two different ways to date: the first is by using the definition of Belbruno of weak stability boundary [5] which involves the revolutions of a body around the second primary in the synodic frame; the second is by individuating captures starting from periodical orbits [13] or from invariant manifolds [4].

The method developed in this work is based on a simplified definition of ballistic capture and on a different method implemented to find orbits that could be interested by this phenomenon. In fact, this work wants to find trajectories spending a relevant period with negative keplerian energy

relative to the second primary. This is done analysing a vast number of initial positions near the planet of interest.

The environment of simulation is the circular restricted three body problem (CRTBP) [6] that uses curvilinear coordinates [12].

The fundamental aim of the thesis is the comprehension of astrodynamics phenomena linked to the interactions of more than one body at the same time. In particular of bodies that change significantly their orbits and behave in peculiar ways that could be exploited as stated above. So the research and the characterization of trajectories that are captured by a planet is the main goal.

This document is developed in the following way. In chapter 1 the implementation of the orbital mechanics of the three bodies is introduced starting from the two body problem and validation is conducted, together with some introducing examples. The implementation and verification of the curvilinear coordinates will be addressed in chapter 2. In chapter 3 the ballistic capture will be defined as will be used in this work and a couple of examples will be shown to introduce it. Zero velocity curves and other examples will be introduced in chapter 4. Then, the preliminary search algorithm will be developed and preliminary results will be shown with some useful considerations. In chapter 5 the search will be improved to get simpler results in order to make possible a better interpretation and examine trajectories with similar features to each other. Results will be then shown when the second primary is Jupiter and an important analysis on orbits obtained will be conducted. Finally, orbits will be catalogued according to the duration of the capture obtained and examples of the outcome will be shown. In chapter 6 and 7 the same study made for Jupiter will be conducted for respectively Mars and Earth. An application of a trajectory exploiting ballistic capture is shown in chapter 8, where possible saving of propellant for interplanetary missions are discussed.

Chapter 1

Third body perturbation

The first step to implement the three body problem must be to consider the classical orbital problem with two bodies and add the third body perturbation.

In this way, it will be considered the three body problem in an inertial frame, where the most important body in terms of mass is the main body, while the second body is the satellite and has a negligible mass. The third body has not negligible mass, but lower than the first primary. It is important to define the *third body perturbation* as the gravitational influence that this body has over the satellite, which could be artificial or natural, like an asteroid.

Alternatively, the main body could be named *first primary*, the third body could be named *second primary*, while the second body *satellite*, *spacecraft*, *asteroid* or simply *body*. This recalls the usual vocabulary for the TBP: *Three Body Problem*.

In this first part of this first chapter, the values of the constants correspond to the ones characteristics to the Sun-Earth system, but in next chapters will be changed, accordingly to the system of celestial bodies considered.

The work of this first chapter consisted in the implementation of the trajectory of the third body around the main body (second primary around first primary in a circular orbit), with a simple propagation of the two body problem. Then, the perturbation will be added to the simulator, in this way all the three bodies will be considered properly. Verification of the code implemented will be conducted and finally a large number of examples will be analyzed.

1.1 Code

1.1.1 Introduction

Tho whole Matlab code is written in order to have all dimensionless parameters. Space is adimensionalized with respect to the characteristic distance between the primaries, which is the semi-major axis of the orbit of the planet around the Sun, in the Solar System. This distance will be also named *reference radius*. Time is adimensionalized with respect to the mean motion of the same orbit. In fact, it is easy to link this quantity, measured in rad/s, with semi-major axis. In this way, it is possible to obtain dimensionless position and velocity in the desired frame. This is particularly useful because the position and velocity of the second primary will always be unitary, regardless the mass of the celestial bodies considered.

1.1.2 Initial material

Firstly, the work began with a Matlab script recalling an *ODE function*. The last one uses the given initial conditions and integrates the differential equations, calculating dimensionless gravitational acceleration given by the main body in every instant. This procedure is propagated over time, with the classical procedure of the *ODE functions* used in Matlab.

Other two functions are used every time that the 6 orbital keplerian elements will be transformed in position and velocity vectors (3 plus 3 parameters), and vice versa.

1.1.3 Ode45 e ode113

Ode functions are pre-implemented routines for the solution of differential equations (or systems of differential equations, written as matrices). Various kind of them could be chosen, but the most used is without any doubt *Ode45*. This one is based on Runge-Kutta (4,5) relations and it's a single step solver, which means that it calculates new values (at the following time step) basing only on the values at the very previous instant. For this reason, it is versatile and used as a first attempt, even if in some cases another *Ode* could be a more appropriate choice.

Another example of *Ode function* is *Ode 113*, a PECE Adams-Bashforth-Moulton, *variable-step, variable-order (VSVO)* solver. It could be more efficient of *Ode45* when stricter tolerances are necessary or when the differential equation is heavy in computational terms. Being a variable step solver, it requires solutions at different previous times to calculate the current solution.

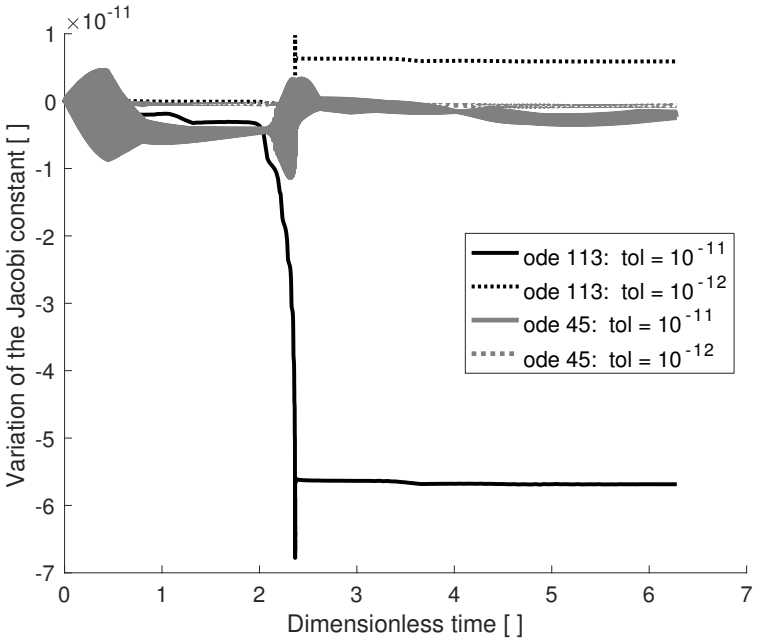

Figure 1.1: Comparison of the Jacobi constant in an inertial reference frame using Cartesian coordinates for *Ode45* and *Ode113*, with different integration tolerances.

According to the developers of the software MATLAB®, these characteristics make *Ode 113* a suitable solver exactly for orbital dynamics, where the solution is smooth and great precision in fundamental.

Retrospectively, a comparison between these two tools will be made, but results and conclusions about this topic are already shown here. For both the frames used in the propagation and, hence, in the differential equations, the resulting Jacobi constant (equation 1.4) was analyzed. To the contrary of the expected, *Ode45* gave a lower error in the Jacobi constant, keeping it more steady than *Ode113*, as can be seen in figure 1.1 and 1.2. From now on, *Ode45* will be used as the only solver for differential equations.

A peculiarity stays in the difference of the number of iterations (or steps) made automatically by *Ode45*, which are from 6 to 10 times the ones of the other solver, for a fixed tolerance. This is surely a disadvantage when long times of simulation are considered, because having a better precision will cost in terms of memory storage space needed and heaviness of the simulation. For a better understanding of this phenomenon, a simulation with a forced step was run with both solvers. The steps were the ones given by the *Ode113*, so with a number of step much lower than the ones automatically given by

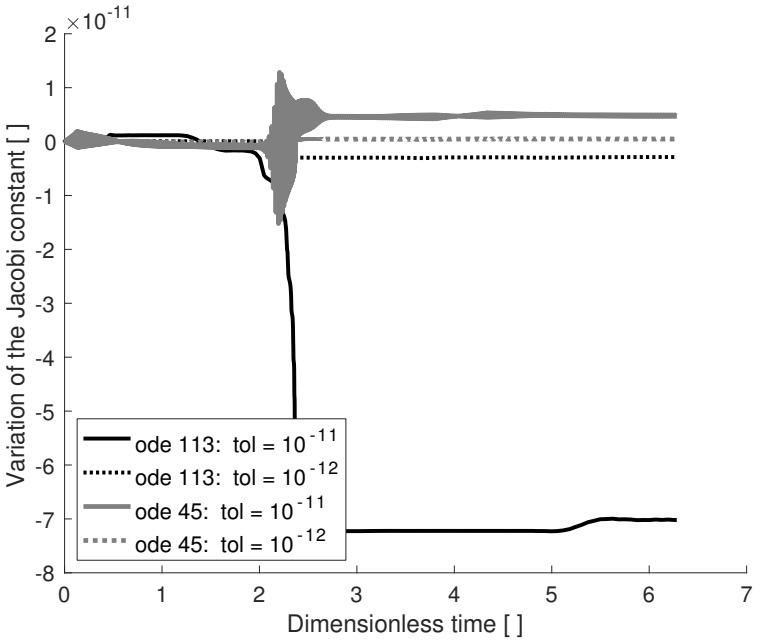

Figure 1.2: Comparison of the Jacobi constant in an synodic reference frame using curvilinear coordinates for *Ode45* and *Ode113*, with different integration tolerances.

Ode45. The result, in figure 1.3, shows only few changes in the precision of the method.

On the contrary, in some cases further explored in the end of this chapter, *Ode113* seems to give better precision: all these cases have in common the fact that they orbit durably one of the massive bodies, or in the case of Copenhagen Problem, see section 1.5.1.

1.1.4 New implementations

Modifying the code described in section 1.1.2, in the *Ode function* was added the third body perturbation, inserting its component in the acceleration term, together with the fictitious centrifugal acceleration of the third body.

$$\mathbf{a}_p = -\mu \left(\frac{\mathbf{d}}{d^3} + \mathbf{r}_2 \right) \tag{1.1}$$

where

$$\mu = \frac{m_2}{m_1 + m_2} \tag{1.2}$$

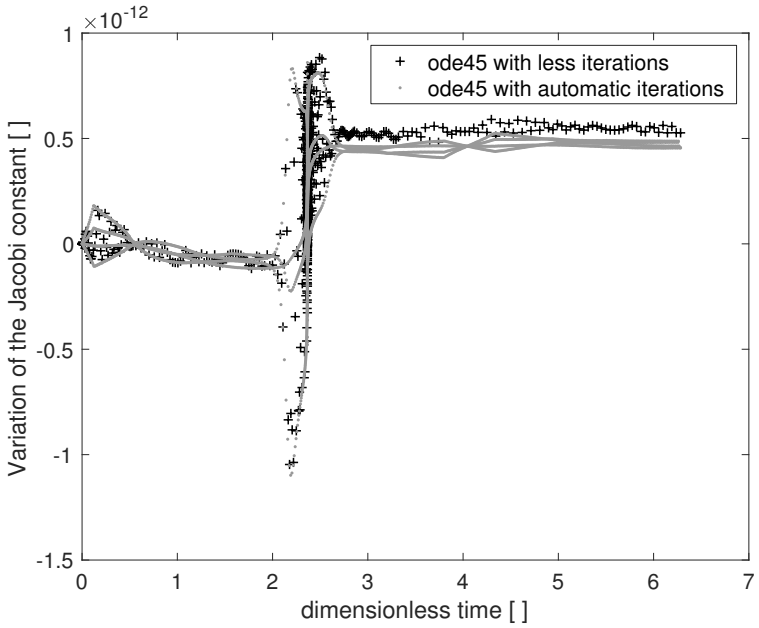

Figure 1.3: Comparison of the Jacobi constant in an synodic reference frame using curvilinear coordinates for *Ode45* with different number of integration steps.

is the mass ratio of the two massive bodies, $\mathbf{r}_2$ is the dimensionless vector of the position of the third body (or second primary) and $\mathbf{d}$ is the dimensionless vector of the position of the satellite respect to the third body (or second primary). This last vector, in our simplified case of circular orbit of the perturbing body, is defined as the difference between the position of the satellite in the inertial frame centered in the main body (or first primary) and the position of the second primary $\mathbf{r}_2$. Instead, this last position is obtained through goniometric functions that describe a unitary circle in the reference period of the orbit in the inertial frame of the first primary.

On the whole, acceleration comes from the following equation and has to be decomposed on the three axes

$$\mathbf{a} = -\frac{\boldsymbol{\rho}}{\rho^3} - \mu \left(\frac{\mathbf{d}}{d^3} + \mathbf{r}_2 \right) \tag{1.3}$$

with $\boldsymbol{\rho}$ position vector of the satellite in the inertial reference frame.

After the assignment of reference parameters for the circular orbit of the Earth around the Sun, the script mainly uses the function for the transformation between keplerian elements and position-velocity. Then, recalled the

Ode function, it makes plots in different frames and fashions.

1.2 Verification

As said before, to verify the solutions gained, it was used the Jacobi constant:

$$C_j = \frac{1-\mu}{a} + 2\sqrt{a(1-\mu)(1-e^2)}\cos i + 2R_d \tag{1.4}$$

with a, e, i semi-major axis, eccentricity, inclination of the orbit, while

$$R_d = \mu\left(\frac{1}{||\, r - r_2||} - \frac{\mathbf{r}\cdot\mathbf{r}_2}{r_2^3}\right) \tag{1.5}$$

is the *disturbing function*, which takes into account the third body perturbation. In fact, it is the inverse of the potential associated to the perturbing force (for mass unity) of the third body. In other words, it is the potential of the gravitational force and the fictitious force associated to the acceleration of the centre of the reference system (of the second primary, which generates this force) with respect to an inertial frame. Jacobi constant should result steady in the three body problem and it was verified that in various configurations of the three bodies it did so. The absolute variation of the constant was considered and all the diagrams contain this variation. Its change is in the order of 10^{-12} and it maintains this value for almost every configuration taken in consideration. In some cases it could be higher, but never over 10^{-9}, which is totally acceptable. As a consequence, the procedure implemented will be considered correct.

1.2.1 Jacobi variation changing the integration tolerance

Results for the following examples are compared here, paying attention mostly on the Jacobi constant. As shown in figure 1.4, the error follows consistently the variation of the integration tolerance applied in the *ode45*.

1.3 Examples of results

For the sake of simplicity, all the configurations analyzed here have initial position aligned with the conjunction of the primaries, so that perigee argument, argument of ascending node and true anomaly are all equal to 0° (or at most 180°). Should be noted that all diagrams are always displayed in

dimensionless coordinates with X and Y (uppercase) that indicate inertial coordinates, while x and y (lowercase) indicate coordinates relative to the second primary aligned with the inertial frame of the first primary.

1.3.1 Orbit around the second primary (Earth)

Here is simulated an orbit very close to the second primary, so this body will have a predominant contribution in the forces at stake, while the main body will be only a disturbance.

In fact, the orbit in the frame of the first primary is continuously modified by the interactions given by the Earth. With respect to it, the keplerian elements of the orbit are semi-major axis $a = 7392.3\,km$, eccentricity $e = 0.05307$, inclination of about $i = 7.5°$. The maximum error obtained for the Jacobi constant is in the order of magnitude of about $\varepsilon_{r,max} = 10^{-12}$.

Propagating the same problem with *Ode113*, it can be obtained the result in figure 1.8, slightly better than the other one above, despite the fact that this one presents almost 10 times less steps than *Ode45*.

1.3.2 Orbit around the first primary (Sun)

Another case analyzed is the one of an orbit very near to the Sun, where the perturbation of the third body will be surely negligible. A circular orbit with radius $a = 10^6$ km was studied, obtaining an error in the Jacobi conservation of the order of magnitude of 10^{-9}. This is also due to the fact that the propagation was protracted for a longer time equal to 2 years. In this way, the evolution of the constant for a long time could be displayed, highlighting its variation, much more important than in all the other cases studied.

Propagating the same problem with *Ode113*, it can be obtained the result in figure 1.11, which is much better than the other one above, despite the fact that this one presents almost 10 times less steps than *Ode45*. Also in this case, the trajectory stays very close to the primary with the mass that reach quite the total one.

1.3.3 Other orbits

For a generic orbit distant from both primaries, the maximum error in the conservation of the Jacobi constant stays in the order of magnitude of 10^{-12}.

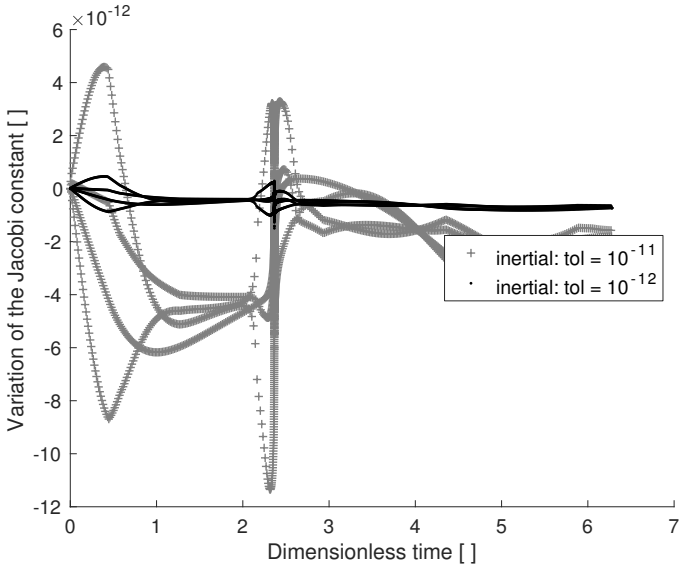

Figure 1.4: Comparison of Jacobi constant for different values of the integration tolerance.

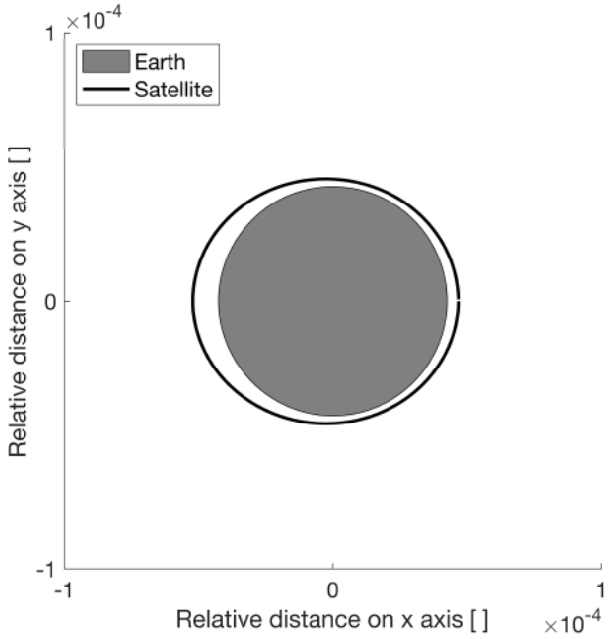

Figure 1.5: Relative motion of the satellite around the Earth (or second primary) in the ecliptic plane.

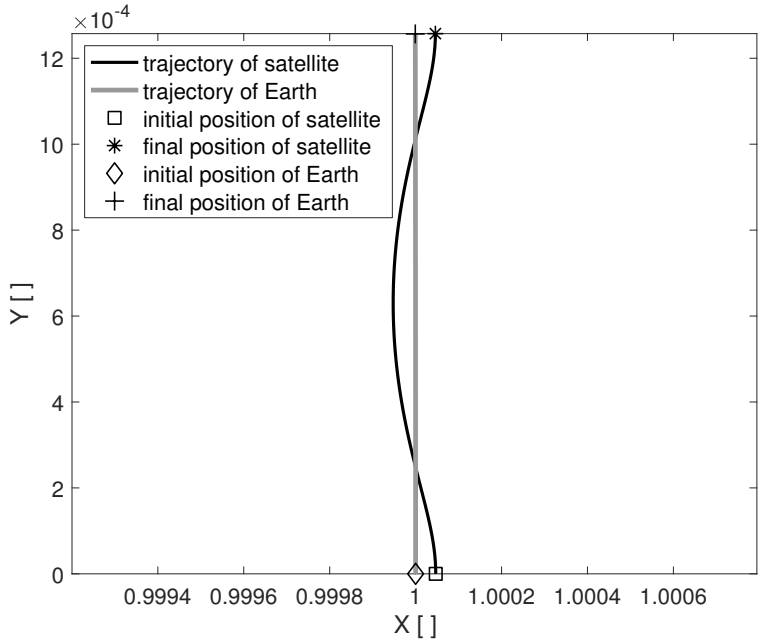

Figure 1.6: Motion of the satellite and the Earth (or second primary) in the inertial frame centered in the Sun (or first primary).

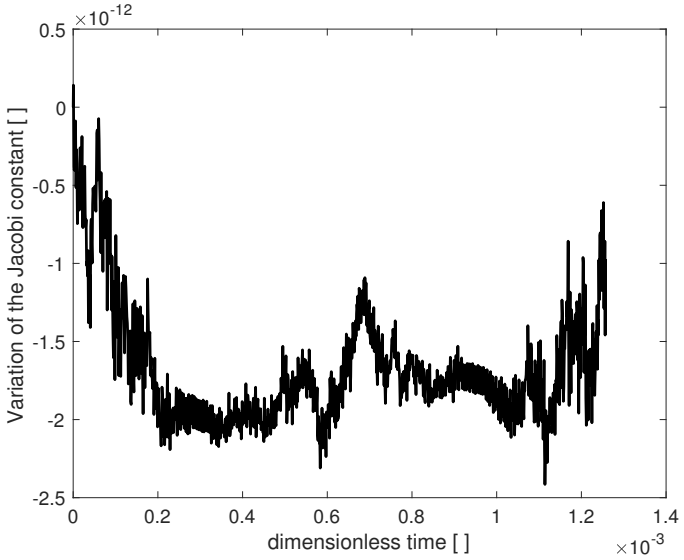

Figure 1.7: Jacobi constant for the orbit around the second primary (Earth). Its value is $C_J = 3.060743$.

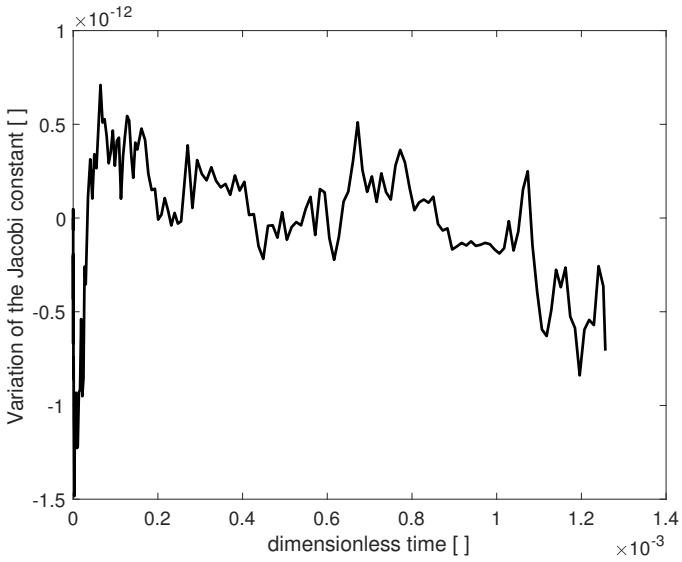

Figure 1.8: Jacobi constant with *Ode113* for the orbit around the second primary (Earth).

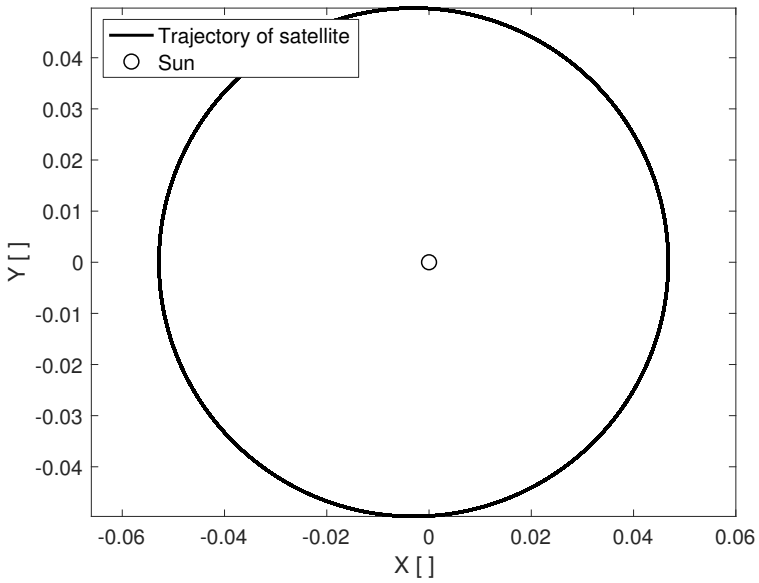

Figure 1.9: Motion of the satellite around Sun.

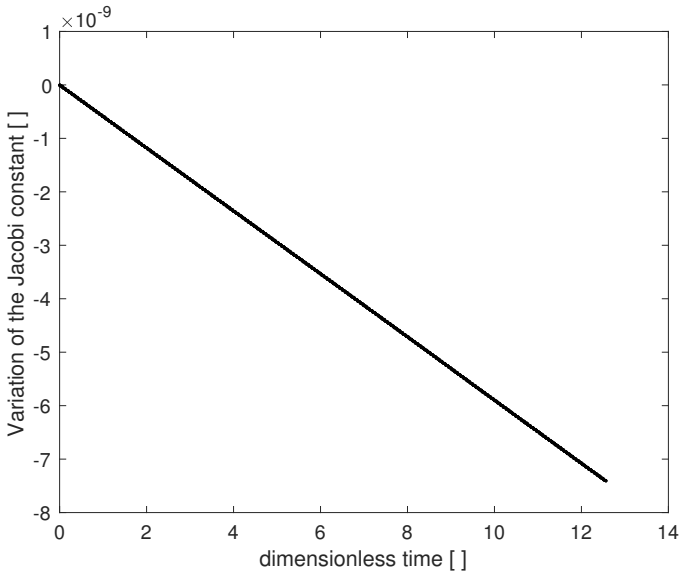

Figure 1.10: Jacobi constant for the orbit around the Sun (or first primary). Value of Jacobi constant is $C_J = 20.520589$.

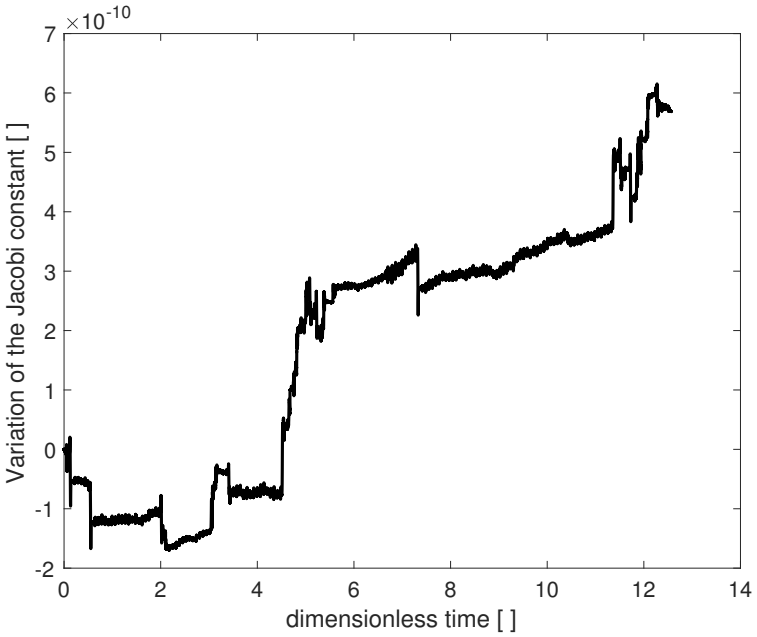

Figure 1.11: Jacobi constant with *Ode113* for the orbit around the first primary (Sun).

1.4 Flyby at Mars

From now on, a different problem will be considered involving the Sun as first primary and Mars as the second primary (or perturbing body). For this system $\mu = 3.227\,10^{-7}$.

To obtain a flyby at the planet in the inertial frame centered in the Sun, an orbit with perihelion in proximity of the Earth will be considered, so with $r_p = 1\,AU$, and aphelion at Mars. The satellite needs to have nearly the same position of the planet in the same instant, when the last one crosses the line of apsides of the satellite orbit. To set up this configuration, in the first steps the gravitational attraction of Mars will not be taken into consideration (NonPerturbed). The distance between aphelion and planet will be given by a parameter called α, but there will be also distinction among internal (between Sun and Mars) and external transfer:

1. External Flyby. In this case, aphelion will be equal to

$$r_{a,ext,NonPerturbed} = R_{ref} + (1+\alpha)\,R_M \tag{1.6}$$

   with $r_{a,ext,NonPerturbed}$ the non-perturbed aphelion in external flyby, R_{ref} the reference radius of the system (radius of the circular orbit of Mars around the Sun) and R_M the radius of the planet itself.

2. Internal flyby.

$$r_{a,int,NonPerturbed} = R_{ref} - (1+\alpha)\,R_M \tag{1.7}$$

In this way, keplerian elements such as semi-major axis a and eccentricity e are computed, knowing from the supposed configuration that the argument of perihelion will be forced to be equal to $\omega = 180°$.

$$e = \frac{r_a - r_p}{r_a + r_p} \tag{1.8}$$

$$a = \frac{r_p}{1-e} \tag{1.9}$$

Given the values described above, only from now on will be considered the gravitational attraction of the second primary.

Besides, it was implemented a control over the eventuality of collisions: for every value of α the script says whether there is a collision or not, with an additional range of distances of the radius of the planet plus a contribution of the atmosphere of nearly 200 km. In case of acceptable trajectory, minimum distance from the planet, error in the Jacobi conservation and keplerian elements after the gravity assist will be computed.

Table 1.1: Preliminary results for external flyby varying α parameter.

α	distance from Mars [km]	a [ ]	e [ ]
0.140	197.71	0.966719	0.114403
0.150	224.18	0.965839	0.114638
0.160	250.69	0.964966	0.114877
0.170	277.24	0.964100	0.115118
0.180	303.85	0.963242	0.115363
0.190	330.50	0.962390	0.115612
0.200	357.19	0.961545	0.115863
0.210	383.94	0.960707	0.116117
0.220	410.72	0.959876	0.116374
0.230	437.55	0.959052	0.116633
0.240	464.43	0.958234	0.116896
0.250	491.35	0.957423	0.117160
0.260	518.31	0.956619	0.117428

Table 1.2: Comparison of keplerian elements of the orbit before and after the external flyby with Mars, for the value of α chosen.

	a [ ]	e [ ]	i [ ]	ω []	Ω []	ν []
Pre-Flyby	0.828231	0.207433	0.000000	3.141593	0.000000	0.000000
Post-Flyby	0.966718	0.114404	0.000000	1.980508	0.000000	2.501879

1.4.1 Analysis of external flyby

The analysis of different initial configurations leads to the following results:

A minimum value $\alpha_{min} = 0.14$ was found to avoid collision and at the same time to give an efficient gravity assist in terms of semi-major axis of the final orbit. In figure 1.12 and figure 1.13 are reported trajectories and the detail of the flyby. Note how the satellites passage near the planet is "behind" it.

In the following tables are shown parameters of the chosen orbit, which is the one obtained with $\alpha = 0.14$. The maximum value for the variation of the Jacobi constant stays, as usual, in the order of 10^{-12}. In figure 1.14, this trend of the Jacobi constant is shown for the time of a period of the orbit.

In table 1.2, keplerian elements of the orbit before and after the flyby are compared, respectively: semi-major axis (dimensionless), eccentricity, inclination, perihelion argument, right ascension of the ascending node and true anomaly.

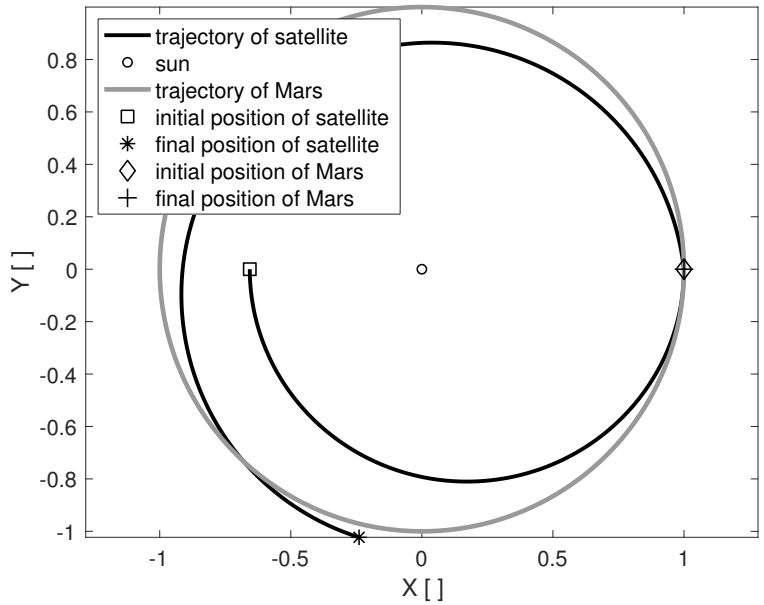

Figure 1.12: Motion of the satellite and of Mars in the case of external flyby. The reference system is inertial and centered in the Sun.

1.4.2 Analysis of the internal flyby

Analogously to the previous case, here will be analyzed some internal configurations varying the parameter α.

A minimum value of $\alpha_{min} = 2.30$ was found to avoid collision and at the same time to give an efficient gravity assist in terms of semi-major axis of the final orbit. In figure 1.15 and figure 1.16 are reported trajectories and the detail of the flyby. Note how the satellites passage near the planet is "in front" of it.

In the following tables are shown parameters of the chosen orbit, which is the one obtained with $\alpha = 2.30$. The maximum value for the variation of the Jacobi constant stays, as usual, in the order of 10^{-13}. In figure 1.17, this trend of the Jacobi constant is shown for the time of a period of the orbit.

In table 1.4, keplerian elements of the orbit before and after the flyby are compared, respectively: semi-major axis (dimensionless), eccentricity, inclination, perihelion argument, right ascension of the ascending node and true anomaly.

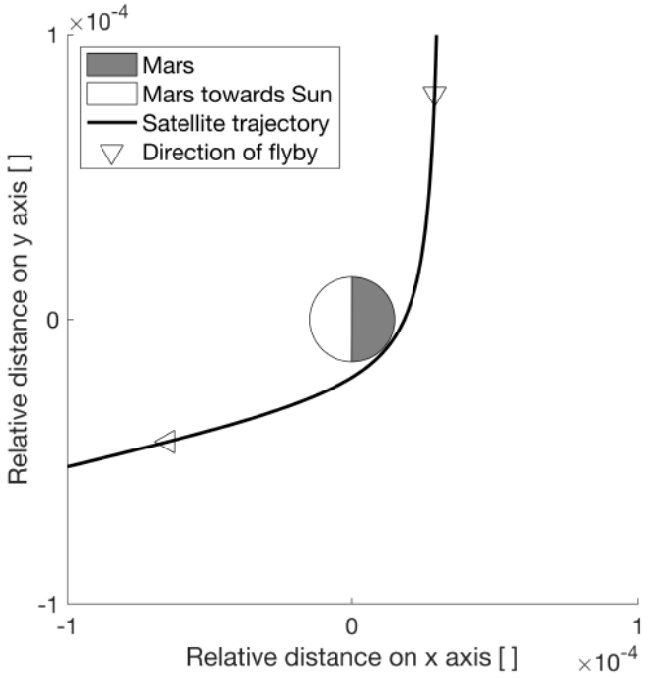

Figure 1.13: Detail of the external flyby.

Table 1.3: Preliminary results for the internal flyby in function of the parameter α.

α	distance from Mars [km]	a [ ]	e
2.30	203.41	0.968093	0.113949
2.31	229.87	0.967211	0.114176
2.32	256.37	0.966336	0.114406
2.33	282.93	0.965468	0.114640
2.34	309.53	0.964608	0.114878
2.35	336.18	0.963754	0.115118
2.36	362.87	0.962907	0.115362
2.37	389.61	0.962067	0.115608
2.38	416.39	0.961234	0.115858
2.39	443.21	0.960407	0.116110
2.40	470.08	0.959587	0.116365
2.41	496.99	0.958774	0.116623
2.42	523.94	0.957967	0.116883

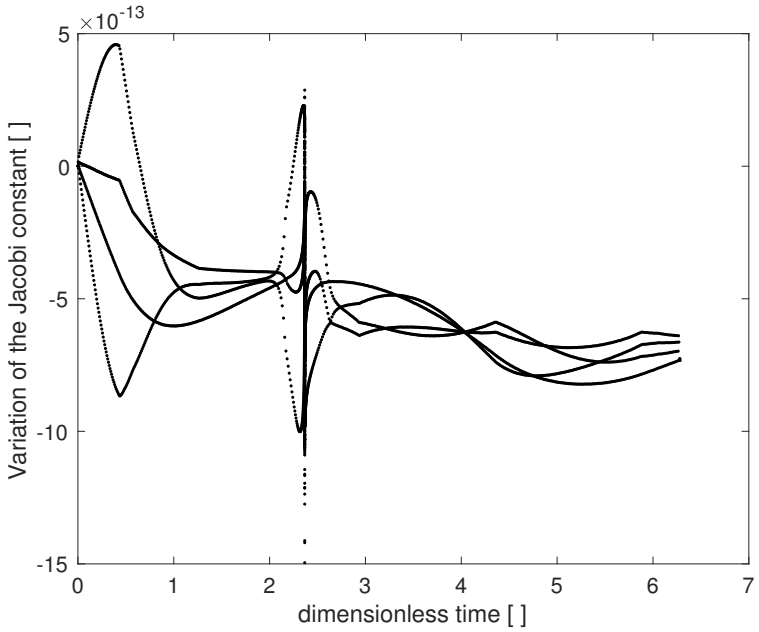

Figure 1.14: Variation of the Jacobi constant for an entire period of the orbit, in the case of external flyby. Value of the constant is $C_J = 2.987953$.

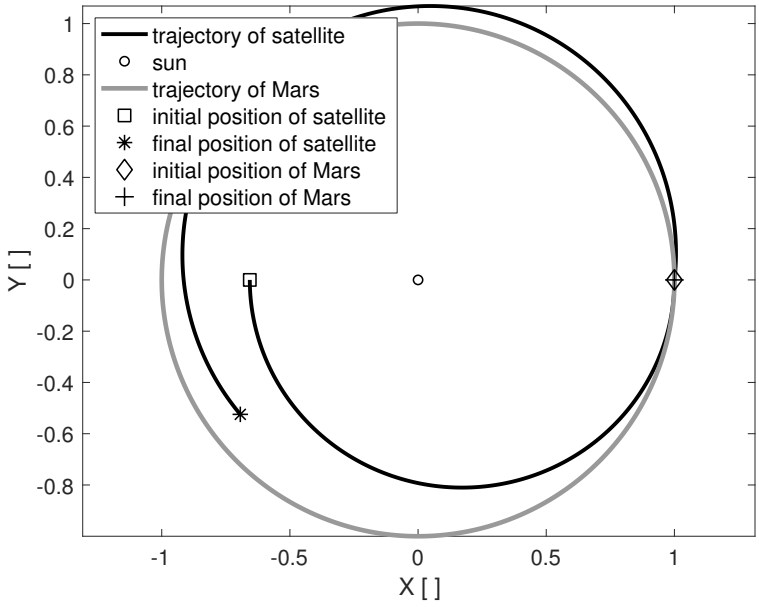

Figure 1.15: Motion of the satellite and of Mars in the case of internal flyby. The reference system is inertial and centered in the Sun.

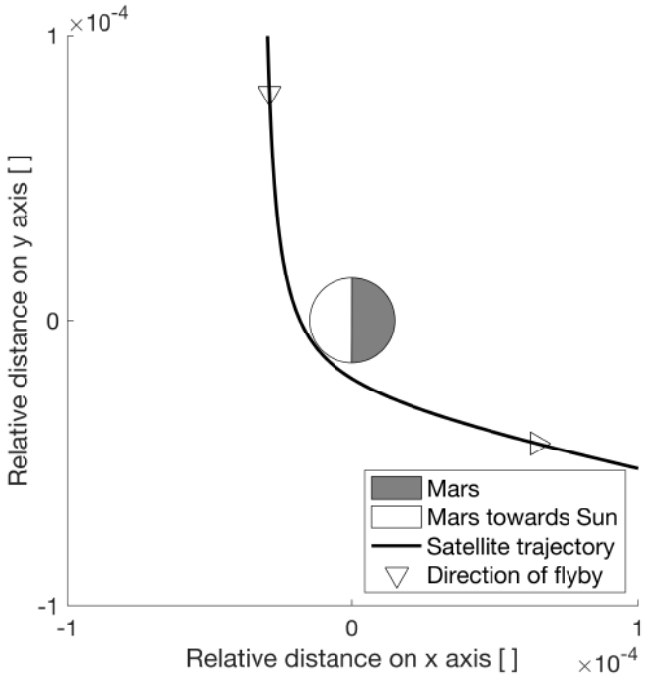

Figure 1.16: Detail of the internal flyby.

Table 1.4: Comparison of keplerian elements of the orbit before and after the internal flyby with Mars, for the value of α chosen.

	a [ ]	e [ ]	i [ ]	ω []	Ω []	ν []
Pre-Flyby	0.828180	0.207385	0.000000	3.141593	0.000000	0.000000
Post-Flyby	0.968094	0.113949	0.000000	-1.975526	0.000000	5.764664

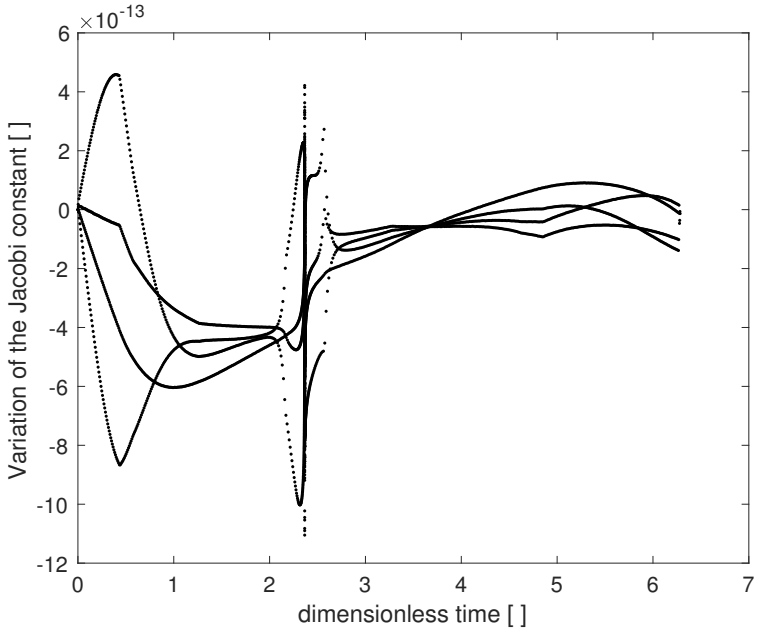

Figure 1.17: Variation of the Jacobi constant for an entire period of the orbit, in the case of internal flyby. Value of the constant is $C_J = 2.987978$.

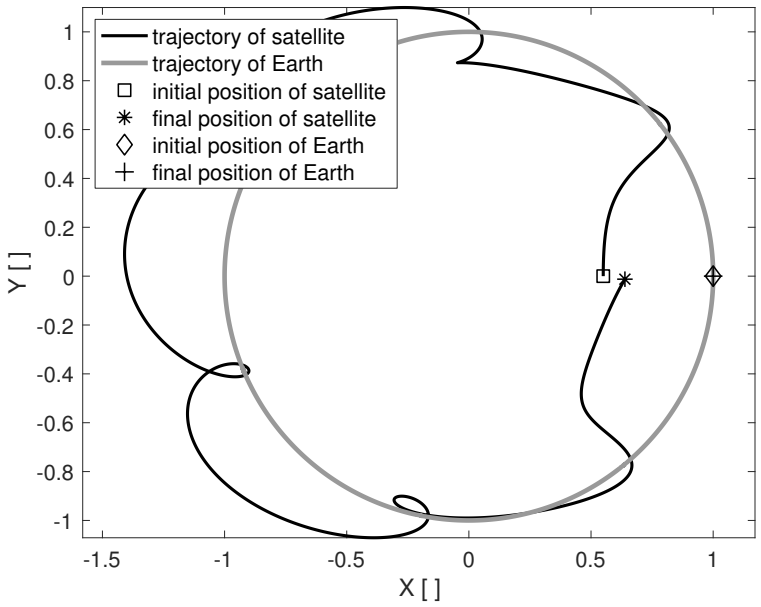

Figure 1.18: Motion in a general flyby case of the Copenhagen Problem.

1.5 Copenhagen Problem

Copenhagen Problem is a particular case of the CRTBP where primaries have the same mass, so that $\mu = \dfrac{m_2}{m_1 + m_2} = 0.5$.

1.5.1 Flyby in the Copenhagen Problem

With general initial conditions for position and velocity in the inertial frame centered in the first primary, motion tends to get forced near to one of the primaries, as shown in figure 1.18. Instead, in figure 1.19 it is shown the limited variation of the Jacobi constant, which proves the goodness of the simulation implemented, also in this particular case of the three body problem.

Propagating the same problem with *Ode 113*, it could be obtained figure 1.20, which is better than the previous diagram, mostly because here the peaks of figure 1.19 (caused by flybys) are softened.

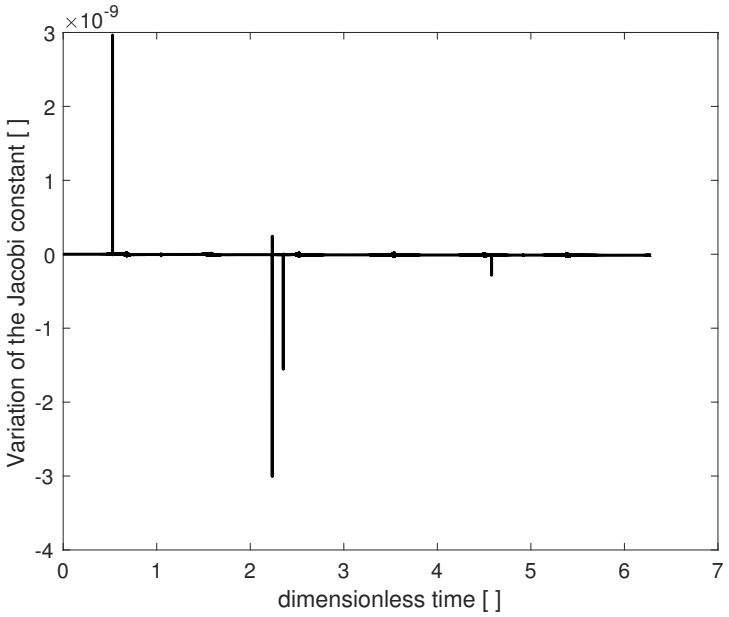

Figure 1.19: Variation of the Jacobi constant for the Copenhagen Problem. Value of the constant is $C_J = 3.489608$.

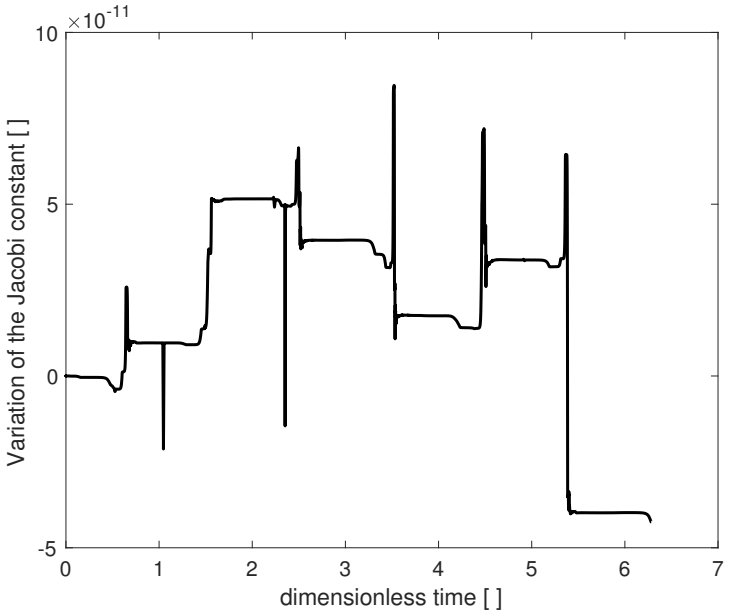

Figure 1.20: Variation of the Jacobi constant with *Ode 113* for the Copenhagen Problem.

Chapter 2

Implementation of curvilinear coordinates for CRTBP

Once implemented of the circular restricted three body problem (CRTBP) in Cartesian coordinates, it was considered a system of reference in curvilinear coordinates very similar to the cylindrical ones.

From now on, the three bodies will be referred as *first primary*, *second primary* and satellite or body. As listed here, they are in decreasing order of mass with the last body (the satellite) with negligible mass. From this last peculiarity comes the word *restricted* in the name of the problem, because it exerts negligible gravitational influences over both massive bodies.

The work summarized here consists on the implementation of equations with curvilinear coordinates in the synodic reference frame and in the verification of results, nonetheless in the study of coordinate transformations between curvilinear, inertial and keplerian elements.

2.1 Parametrization of curvilinear coordinates

The second primary m_2 moves on a circular orbit around the first primary m_1 and the satellite is subjected to the gravitational force of both of them.

All the parameters of the problem are adimensionalized using the distance between the primaries R_{ref} and their mean motion n. It should be now introduced the parameter μ, mass ratio between the primaries and, in figure 2.1, the reference system used.

$$\mu = \frac{m_2}{m_1 + m_2} \tag{2.1}$$

The three coordinates used in the new reference frame are: ρ, which versor always follows the satellite (indicated in figure with m_3) and whose module "starts" from the circumference marked by the second primary; θ (angle sweeped from the position of m_2 to m_3); z, perpendicular to the other two and, as a consequence, also to the ecliptic plane. Those parameters are obviously function of dimensionless time τ and they rotate with respect to the inertial reference frame (i, j in figure) by an angle $\tau + \theta$.

Finally, relations indicating the position r of the satellite in this frame are now introduced,

$$\mathbf{r} = r_\rho \mathbf{u}_\rho + z\mathbf{k} \tag{2.2}$$

together with the position r' of the same body m_3 with respect to the second primary m_2

$$\mathbf{r}' = (r_\rho - \cos\theta)\,\mathbf{u}_\rho + \sin\theta\,\mathbf{u}_\theta + z\,\mathbf{k} \tag{2.3}$$

where $r_\rho = 1 + \rho$, e $\{\mathbf{u}_\rho, \mathbf{u}_\theta, \mathbf{k}\}$ are the orthonormal versors of the synodic (rotating) reference system centered in the first primary.

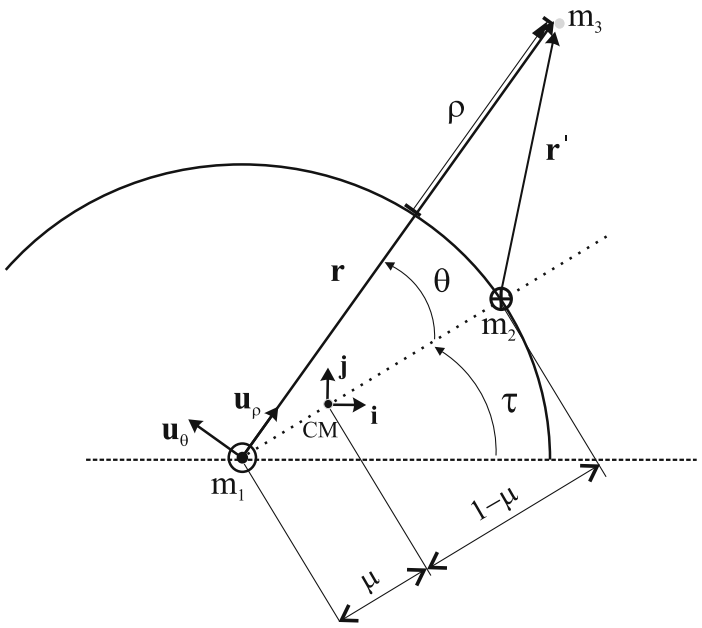

Figure 2.1: Rotating reference system in curvilinear coordinates ρ, θ and z. Credits reference [12]

2.2 Motion in curvilinear coordinates

2.2.1 Equations of motion

Equations of motion are obtained from the acceleration with respect to the rotating reference frame with the versors introduced above.

$$\frac{d^2\mathbf{r}}{d\tau^2} = -(1-\mu)\frac{\mathbf{r}}{|\mathbf{r}|^3} - \mu\frac{\mathbf{r}'}{|\mathbf{r}'|^3} - \mathbf{a}_{rel} - 2\boldsymbol{\omega}_{rel}\times\frac{d\mathbf{r}}{d\tau} - \boldsymbol{\omega}_{rel}\times(\boldsymbol{\omega}_{rel}\times\mathbf{r}) - \frac{d\boldsymbol{\omega}_{rel}}{d\tau}\times\mathbf{r} \tag{2.4}$$

with fictitious acceleration $\mathbf{a}_{rel}$ given by the motion of the second primary around the first one (centripetal relation), while $\boldsymbol{\omega}_{rel}$ is the angular velocity in the new frame with respect to the inertial system.

$$\mathbf{a}_{rel} = \mu\,\cos\theta\,\mathbf{u}_\rho - \mu\,\sin\theta\,\mathbf{u}_\theta \tag{2.5}$$

$$\boldsymbol{\omega}_{rel} = \omega_{rel}\,\mathbf{k} = \left(1+\dot{\theta}\right)\mathbf{k} \tag{2.6}$$

The following equations of motion to be implemented in Matlab could be obtained by developing equation 2.4 and the previous ones, then projecting them in the 3 axes of the curvilinear frame.

$$\begin{cases} \ddot{\rho} = r_\rho\omega_{rel}^2 - \dfrac{(1-\mu)r_\rho}{r^3} - \dfrac{\mu\,(r_\rho-\cos\theta)}{r'^3} - \mu\cos\theta \\ \\ \ddot{\theta} = -\dfrac{2\dot{\rho}\omega_{rel}}{r_\rho} + \dfrac{\mu\sin\theta}{r_\rho}\left(1-\dfrac{1}{r'^3}\right) \\ \ddot{z} = -\,(1-\mu)\,\dfrac{z}{r^3} - \mu\dfrac{z}{r'^3} \end{cases} \tag{2.7}$$

with

$$r = \sqrt{r_\rho^2 + z^2} \tag{2.8}$$

$$r' = \sqrt{(r_\rho-\cos\theta)^2 + \sin^2\theta + z^2} \tag{2.9}$$

2.2.2 Jacobi constant in curvilinear coordinates

To verify that the implementation was correct, the Jacobi constant was used.

$$C_j = -2\left(\dot{\rho}^2 + \dot{\theta}^2 r_\rho^2 + z^2\right) + r_\rho^2 + 2\frac{1-\mu}{r} + 2R \tag{2.10}$$

with

$$R = \frac{\mu}{r'} - \mu r_\rho \cos\theta \tag{2.11}$$

the *disturbing function*, which takes into account for the third body perturbation (given by the planet, or second primary), as described in chapter 1. This constant should result fixed in time in the three body problem.

Maximum variation of this value is in fact in the order of magnitude of 10^{-12} and it is maintained so in most configurations studied. Said so, the procedure implemented will be considered correct.

2.2.3 Jacobi constant in orbital parameters

It is also possible to compute the Jacobi constant by using orbital parameters.

$$C_j = \frac{1-\mu}{a} + 2\sqrt{a(1-\mu)(1-e^2)}\cos i + 2R_d \tag{2.12}$$

with *disturbing function*

$$R_d = \mu\left(\frac{1}{||\, r - r_2||} - \frac{\mathbf{r}\cdot\mathbf{r}_2}{r_2^3}\right) \tag{2.13}$$

To obtain the keplerian elements of the orbit, the relations 2.8 and 2.9 could be used. These express the position r of the satellite with respect to the first primary (which is the center of the frame) and the relative position r' with respect to the second primary. The following relations are obtained projecting these position vectors in the inertial coordinate system.

$$\begin{cases} x = r_\rho \cos(\theta + \tau) \\ y = r_\rho \sin(\theta + \tau) \\ z = z \end{cases} \tag{2.14}$$

$$\begin{cases} x' = (r_\rho - \cos\theta)\cos(\theta + \tau) - \sin\theta \sin(\theta + \tau) \\ y' = (r_\rho - \cos\theta)\sin(\theta + \tau) + \sin\theta \cos(\theta + \tau) \\ z' = z \end{cases} \tag{2.15}$$

So, the velocity in the desired frame simply derive from these ones.

$$\begin{cases} \dot{x} = \dot{\rho}\cos(\theta+\tau) - r_\rho \sin(\theta+\tau)\left(1+\dot{\theta}\right) \\ \dot{y} = \dot{\rho}\sin(\theta+\tau) + r_\rho \cos(\theta+\tau)\left(1+\dot{\theta}\right) \\ \dot{z} = \dot{z} \end{cases} \tag{2.16}$$

It is now possible to use routine *rv2equinoctial* (seen in chapter 1), using as input position and velocity in the Cartesian inertial frame and getting as outputs the keplerian elements, with the possibility of verifying the Jacobi constant with equation 2.12.

The following system of equations for velocity is also derived from the previous ones.

$$\begin{cases} \dot{x'} = \dot{\rho}\cos(\theta+\tau) - r_\rho \sin(\theta+\tau)\left(1+\dot{\theta}\right) + \sin\tau \\ \dot{y'} = \dot{\rho}\sin(\theta+\tau) + r_\rho \cos(\theta+\tau)\left(1+\dot{\theta}\right) - \cos\tau \\ \dot{z'} = \dot{z} \end{cases} \tag{2.17}$$

In reality, velocity relative to the second primary could be expressed also subtracting $-\sin\tau$ e $\cos\tau$ (which are the components of the velocity of the second primary in the ecliptic plane of the inertial frame centered in the first primary) to velocities of equation 2.16.

2.2.4 From keplerian elements to curvilinear coordinates

A way to transform keplerian elements into curvilinear coordinates is to do it passing through position and velocity in the inertial frame centered in the first primary (RV).

Using *equinoctial2rv* with the keplerian elements as input, position and velocity (RV) could be get as output. Finally, curvilinear coordinates could be computed simply by reversing equations 2.14 and 2.16, with $\tau = 0$ when computing the initial conditions of the problem.

In this way the correct curvilinear initial coordinates could be obtained. In fact, results are almost identical to the ones obtained in the previous chapter and Jacobi remains fixed, as will be shown below.

2.3 Comparison between curvilinear and Cartesian

As was done in chapter 1, all trajectories were studied with the same initial conditions, using the relations above to transform them in curvilinear ini-

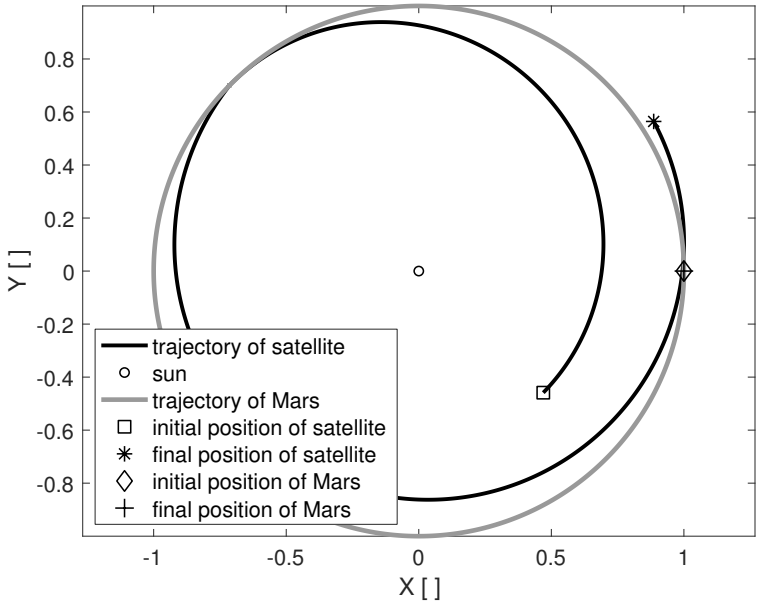

Figure 2.2: Motion of the satellite and of Mars in the inertial frame centered in the Sun, in the case of external flyby.

tial conditions. Here, only one example will be shown to demonstrate the matching with the results found out previously.

2.3.1 External flyby at Mars

In the case of external flyby at Mars with $\alpha_{min} = 0.14$, the initial conditions are exactly the same presented in the previous chapter. The trajectory and the detail of the passage near the planet are shown in figures 2.2 and 2.3.

The conservation of Jacobi constant is respected, because the maximum variation is in the order of magnitude of 10^{-12}. In figure 2.4,its variation during a period of the orbit is shown for both equation 2.10 and 2.12. The first one is the equation which uses curvilinear coordinates to compute Jacobi constant, the second one is the one that uses orbital parameters, as introduced in the previous chapter. Results are clearly coincident.

In addition to the same trajectory, this procedure gives the same keplerian elements obtained for the orbits after the gravity assists for this external flyby and for all the orbits in the different planetary systems discussed in chapter 1. All these results are not presented here for conciseness.

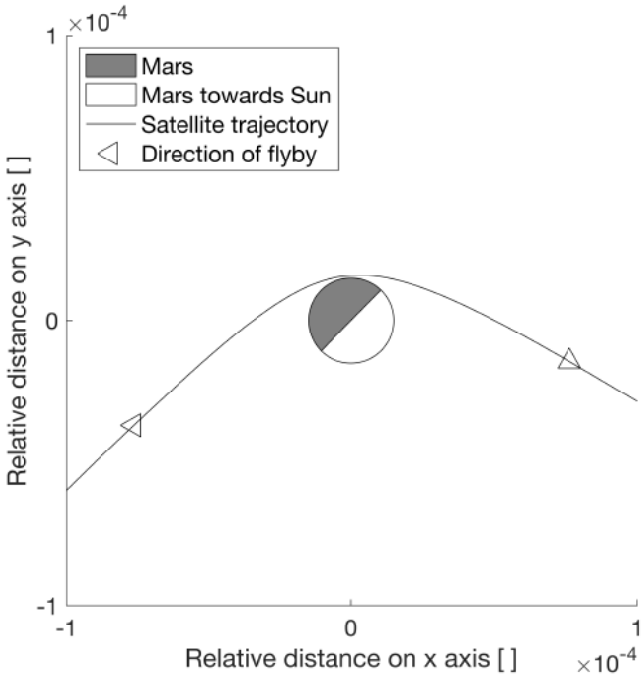

Figure 2.3: Detail of the external flyby.

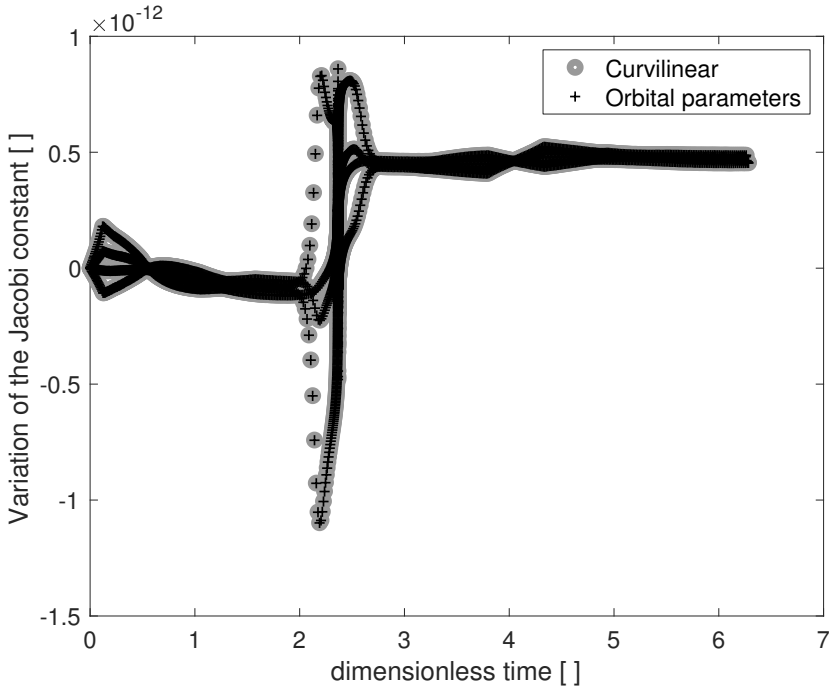

Figure 2.4: Variation of the Jacobi constant during a period of the orbit of the satellite, in the case of external flyby. Results given by equations 2.10 and 2.12 are shown here. The value of the constant is $C_J = 2.987953$.

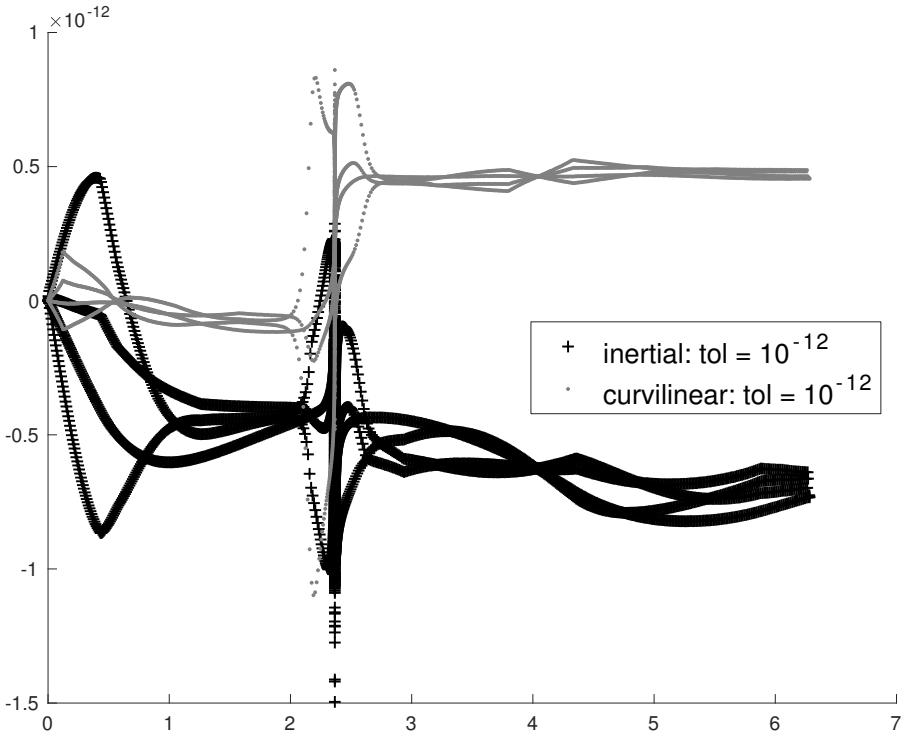

Figure 2.5: Comparison of the Jacobi constant in the two coordinate systems analyzed.

2.3.2 Jacobi in curvilinear and Cartesian coordinates

In figure 2.5 results obtained in curvilinear and Cartesian coordinates are compared and, thanks to this, it will be clear which one is the more precise.

The conclusion is that the two methods of propagation obviously coincide, but curvilinear coordinates give a slightly better precision, even though the variation of the constant is in the same order of magnitude.

Chapter 3

Definition of ballistic capture

After the introduction of the rotating frame in curvilinear coordinates for CRTBP and the evaluation of its precision (higher than inertial frame in Cartesian coordinates), only this preferable system of reference will be used for propagation. In some cases, also the inertial frame will be analyzed afterwards for its more recognizable representation axes.

In this chapter the keplerian energy (kinetic plus potential) will be introduced in the inertial reference frame. This could be computed with respect to the first primary or to the second primary. Obviously, the last one will be considered to analyze the capture of the body by the planet. Conditions for the ballistic capture will be briefly discussed and, finally, some examples regarding these capture will be given.

3.1 Keplerian energy from Vis Viva equation

Orbital keplerian energy could be obtained from the sum between kinetic and potential energy of a body. This must be done in a dimensionless form coherently to all the computations seen so far, considering parameters evaluated in an inertial frame centered in a primary.

First of all, keplerian energy with respect to the first primary will be studied, using Vis Viva equation with dimensional parameters. The following equation is called Vis Viva and contains the first term which is the kinetic one proportional to v^2 and the second term which represents the gravitational potential. This one depends on μ, the gravitational constant of the first primary, and r, the relative distance between the body and the primary.

$$\varepsilon = \frac{v^2}{2} - \frac{\mu}{r} \tag{3.1}$$

3.1.1 Keplerian energy with respect to the second primary

Making dimensionless the previous equation 3.1 and considering the parameters relative to the second primary, it becomes

$$\varepsilon = \frac{v'^2}{2} - \frac{\mu}{r'} \tag{3.2}$$

where r' and v' are the norm of, respectively, the vector of position and velocity of the satellite relative to the second primary in the inertial frame centered in the same second primary (system of equations 2.15 and 2.17) and μ is the mass ratio given in equation 2.1 (already referred to m_2).

3.1.2 Keplerian energy with respect to the first primary

Making dimensionless the previous equation 3.1 with parameters relative to the first primary, it becomes

$$\varepsilon = \frac{v^2}{2} - \frac{1-\mu}{r} \tag{3.3}$$

where r and v are the norm of, respectively, the vector of position and velocity of the satellite relative to the first primary in the inertial frame centered in the same first primary (system of equations 2.14 and 2.16) and μ is the mass ratio given in equation 2.1 ($1-\mu$ could also be arranged as $\frac{m_1}{m_1+m_2}$).

3.2 Conditions of the ballistic capture

In this section, the method implemented in this work to measure the time spent in a ballistic capture is briefly discussed and is shown in a couple of examples that are displayed at the end of this chapter.

Using the relations already introduced, the main criterion is to identify the moments when the keplerian energy with respect to the second primary is null. These moments will be considered as transitions between the ballistic capture of a body (when keplerian energy with respect to the planet is negative) and escape trajectories or classic orbits around the first primary (for example, flybys and gravity assist).

Another criterion, of less importance and used only when the first is devious, employs the distance from the planet exploiting the peculiarity of

the value of the Hill radius r_{Hill}.

$$r_{Hill} = \left(\frac{\mu}{3}\right)^{\frac{1}{3}} \tag{3.4}$$

This parameter is defined as the distance from the second primary where the influence of the planet itself is as important as the one of the first primary. However, even if the satellite is more distant than a Hill radius, it could be affected by a non negligible influence determining a temporary capture. If this distance is of less than 4 Hill's radii and it is maintained for a long time, the orbit will be considered captured. It must be underlined that this criterion is not used in this work and for this reason has not been further analyzed.

Instead, as it will be shown in next chapters, sometimes even a trajectory which spends a brief time with negative keplerian energy with respect to the second primary and quite near to it (distant less than 2 Hill's radii) could not be in a capture at all.

3.3 Examples of ballistic captures

For all the configurations analyzed in chapter 1, the study of the keplerian energy parameter was developed at this point. Variations of this energy will be shown in a couple of examples, illustrating two cases: the first one of a mere flyby; the second of a real ballistic capture.

3.3.1 Example of external flyby at Mars

In this section, the case of external flyby at Mars, analyzed also in the previous chapter, will be studied in figures 3.1 and 3.2, showing the characteristics of the keplerian energy with respect to the second primary.

Figure 3.2 in particularly represents this feature and it could be noted that the value of the energy never reaches zero, hence it is never negative. This indicates that this trajectory is a mere flyby, as it has been called since the beginning. In other words, it is a gravitational assist that passes near the planet with a hyperbolic orbit. In fact, in these kind of orbits the energy is always positive. Even if the satellite gets in the Hill's sphere, there is no ballistic capture.

Finally, in figure 3.3 is shown the trend of the other energy, the one relative to the first primary. Even this one changes over time and its variation is focused in the instant of the gravity assist. Indeed, the energy increases

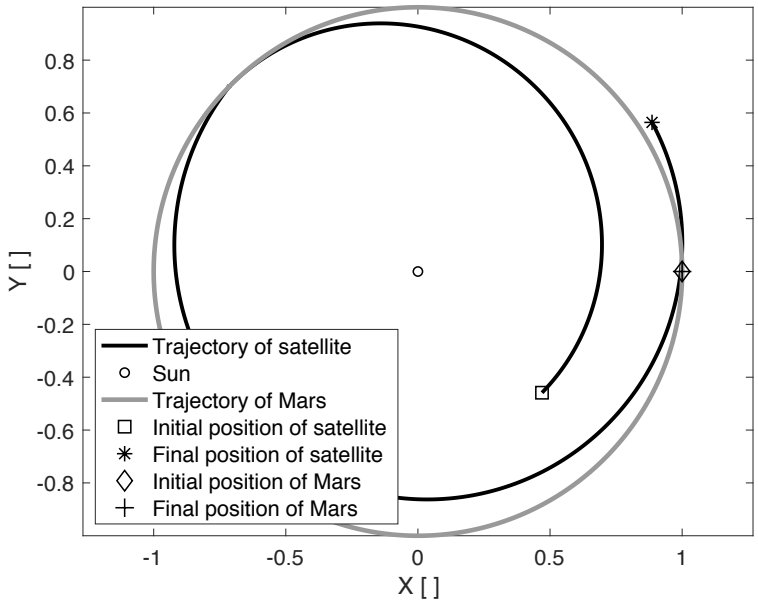

Figure 3.1: Trajectory of the flyby orbit at Mars and of the planet itself. The value of the Jacobi constant is $C_J = 2.987978$.

after this moment indicating that the orbit after this event is less strongly linked to the Sun.

3.3.2 Example of ballistic captured trajectory

Here will be shown an example of ballistic capture found with the method discussed in the next chapter. This trajectory takes place in the Sun-Jupiter system.

The simulation of this example begins in the moment when the keplerian energy relative to the second primary is null. The trend of the energy could be seen in figure 3.4, where it goes negative indicating a ballistic capture long almost 2 Jupiter's years. The motion of the satellite in the synodic reference frame is represented in figure 3.5, while in figure 3.6 the system of reference is the inertial one still centered in the Sun. The movement of the satellite and of the planet are both represented because Jupiter is not fixed in this last frame. It is important to underline that *zero velocity curves* (ZVC) are not present in this particular trajectory because the Jacobi constant is too low for them to appear. They will be introduced in the next chapters.

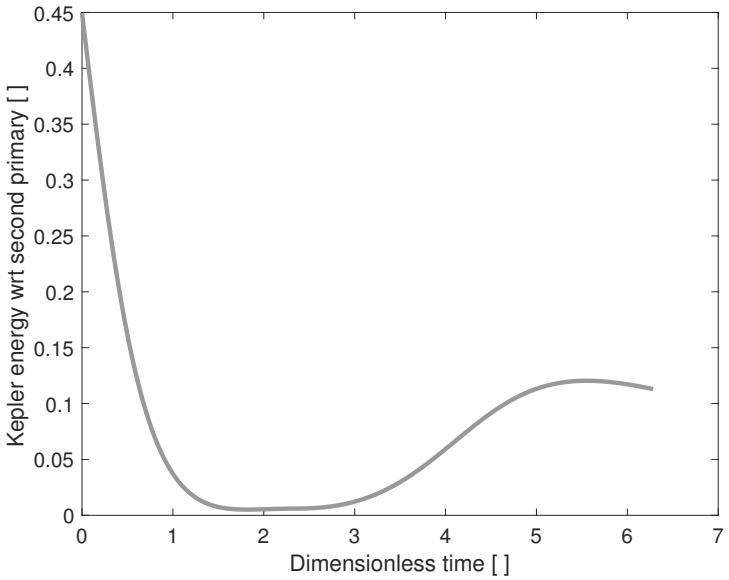

Figure 3.2: Keplerian energy with respect to (wrt) the second primary in the case of flyby orbit at Mars. The satellite is in the Hill's sphere in the dimensionless time interval τ: [2.3232, 2.4078].

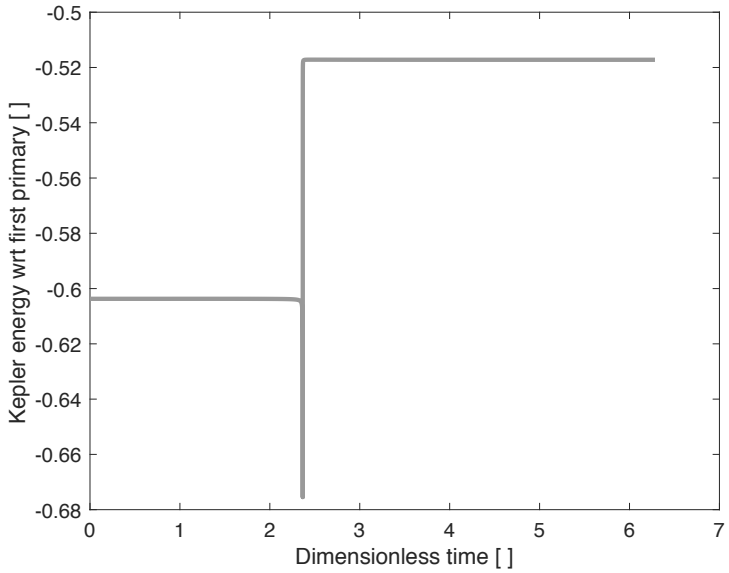

Figure 3.3: Keplerian energy with respect to (wrt) the first primary in the case of flyby orbit at Mars.

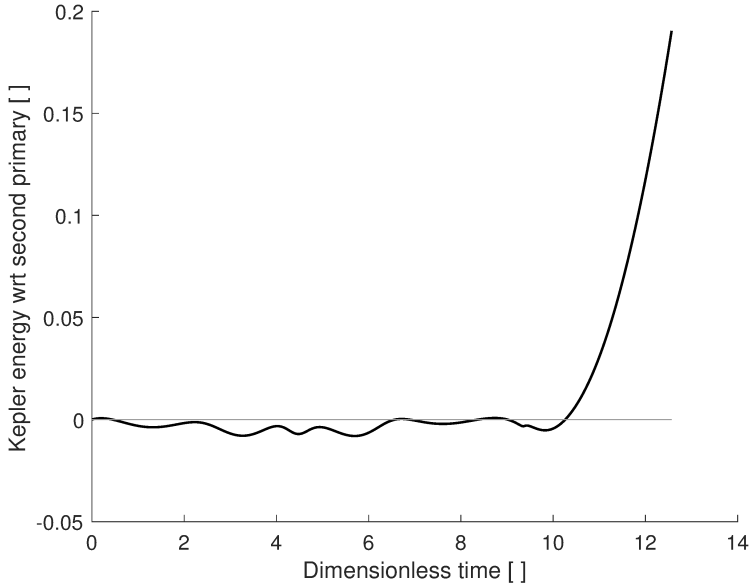

Figure 3.4: Keplerian energy with respect to (wrt) the second primary for a typical ballistic capture.

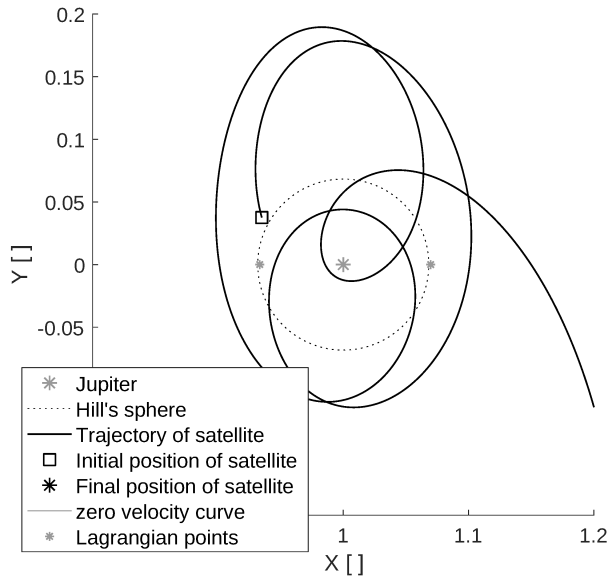

Figure 3.5: Motion of the satellite in the synodic reference frame for a typical ballistic capture. Hill's sphere and Lagrangian points are tracked, but *zero velocity curves* are not because the Jacobi constant is too low for them to appear.

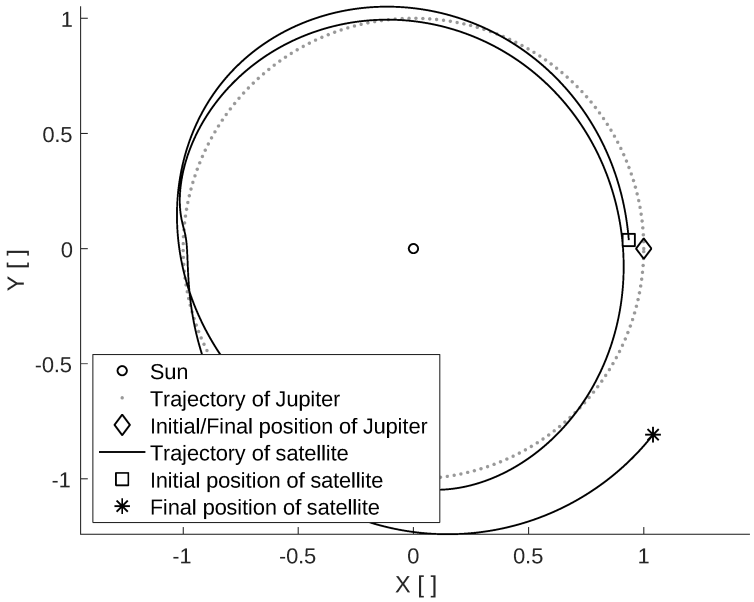

Figure 3.6: Motion of the satellite and of the planet in the inertial reference frame for a typical ballistic capture.

Chapter 4

Search algorithm for ballistic captures

In the previous chapters the synodic frame in curvilinear coordinates for CRTBP was introduced, validation of its better accuracy than Cartesian coordinates was developed and keplerian energy in the inertial frame was introduced. This formula was used to define ballistic capture.

In this chapter, a huge amount of trajectories with different initial conditions will be analyzed in order to find ballistic captures of bodies by the second primary. Results presented here are for Sun-Jupiter system. Particular attention will be paid to the features linked to the initial condition propagated and the peculiarity of the trajectory.

4.1 Zero velocity curves and Lagrangian points

Using the formulation for the Jacobi constant, *zero velocity curves* were implemented and displayed in every diagram for the trajectory in the synodic frame. This is a locus of points having null velocity for a fixed Jacobi constant. It represents the contour of the accessible zone with a limited energy, while the zones beyond these curve can not be reached with this energy and are called "forbidden regions".

It is important to remind that low energy is directly linked to a high Jacobi constant. Typical values for this constant will be given in the next section. Examples of *zero velocity curves* could be seen in figures 4.1 and 4.2. Zones prohibited to the motion for a fixed Jacobi constant always include triangular Lagrangian points L4 and L5. They are always represented in figures too and are computed using well-known formulas [6].

4.2 Jacobi constant in Lagrangian points

Here, equations for the calculus of Jacobi constant in the Lagrangian points and their results will be shown. Afterwards, values could be considered correct: they are very precise and a minute correction (using trial and error search) will be used only in the generatrix trajectory (section 5.5).

In increasing order of energy in the synodic frame, therefore in decreasing order of Jacobi constant, the following results could be obtained for Sun-Jupiter system. Also the curvilinear coordinates of the Lagrangian points are shown.

$$\begin{cases} L1 : \rho = -0.0667, \quad \theta = 0; \quad C_{J,L1} \approx 3 + 9\left(\dfrac{\mu}{3}\right)^{\frac{2}{3}} - 10\left(\dfrac{\mu}{3}\right) = 3.0387 \\ L2 : \rho = +0.0698, \quad \theta = 0; \quad C_{J,L2} \approx 3 + 9\left(\dfrac{\mu}{3}\right)^{\frac{2}{3}} - 14\left(\dfrac{\mu}{3}\right) = 3.0375 \\ L3 : \rho = -0.0006, \quad \theta = \pi; \quad C_{J,L3} \approx 3 + \mu = 3.0010 \\ L4 : \rho = 0, \quad \theta = +\dfrac{\pi}{3}; \quad C_{J,L4} = 3 - \mu = 2.9990 \\ L5 : \rho = 0, \quad \theta = -\dfrac{\pi}{3}; \quad C_{J,L5} = 3 - \mu = 2.9990 \end{cases} \tag{4.1}$$

4.3 Examples of ballistic captures

During the development of this work for the implementation of an algorithmic search for ballistic captures, some examples of them were found. They are presented here in order to introduce their peculiarities. Various parameters were used to locate the initial conditions for these trajectories.

The first example was introduced also in the previous chapter in figures 3.4, 3.5 and 3.6. This is an orbit beginning at $1.1\, r_{Hill}$ of distance from Jupiter, with relative velocity relative to it $v_{2,0}$ such that the keplerian energy with respect to the planet is null. Initial position is located at 150° from x-axis (conjunction of both primaries, counterclockwise) and initial velocity relative to Jupiter $v_{2,0}$ is located in a direction at 125° in the same reference frame of position.

The second example is shown in figures 4.1, 4.2, 4.3 and 4.4. It was obtained for a initial position in $x_{2,0} = -0.117$ and $y_{2,0} = -0.004$. These coordinates are referred to the Cartesian inertial frame centered in the second

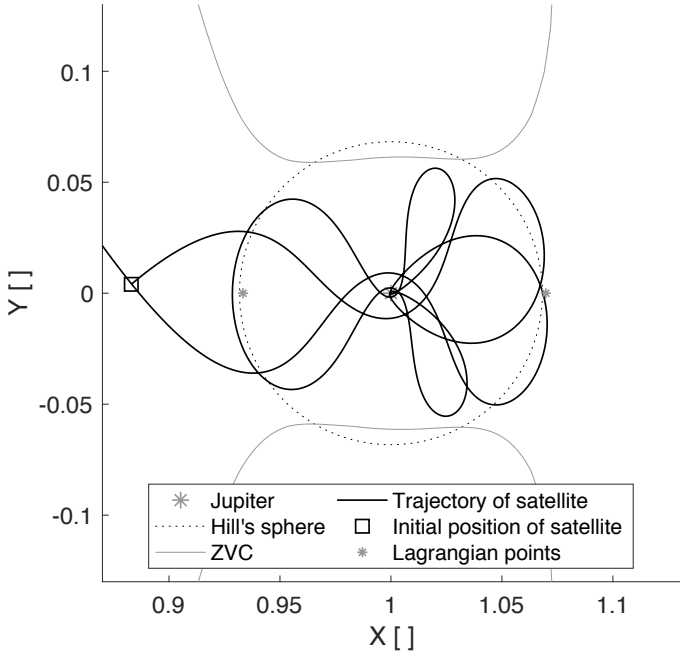

Figure 4.1: Motion of the satellite in the synodic frame around Jupiter. *Zero velocity curves* (ZVC) are present but they are not an essential limit to the motion of the satellite.

primary. Initial velocity is computed so that the Jacobi constant is equal to $C_J = 3.0274702$. All the characteristics introduced here will be further analyzed in the next chapters. Propagation time is of 5 Jupiter's years. In this example are present also *zero velocity curves* (ZVC) introduced in section 4.1.

4.4 Algorithm for the search of ballistic captures

The target is to find ballistic captures in any system composed by two celestial bodies.

Firstly, the Sun-Jupiter system will be considered, but then also other systems like Sun-Mars or Sun-Earth will be addressed. A satellite with initial keplerian energy null with respect to the second primary will be considered: in this way energy will only be able to raise, escaping the capture; or energy will diminish, sketching an orbit linked (and therefore near) to the planet. This last one is the scenario that will be searched.

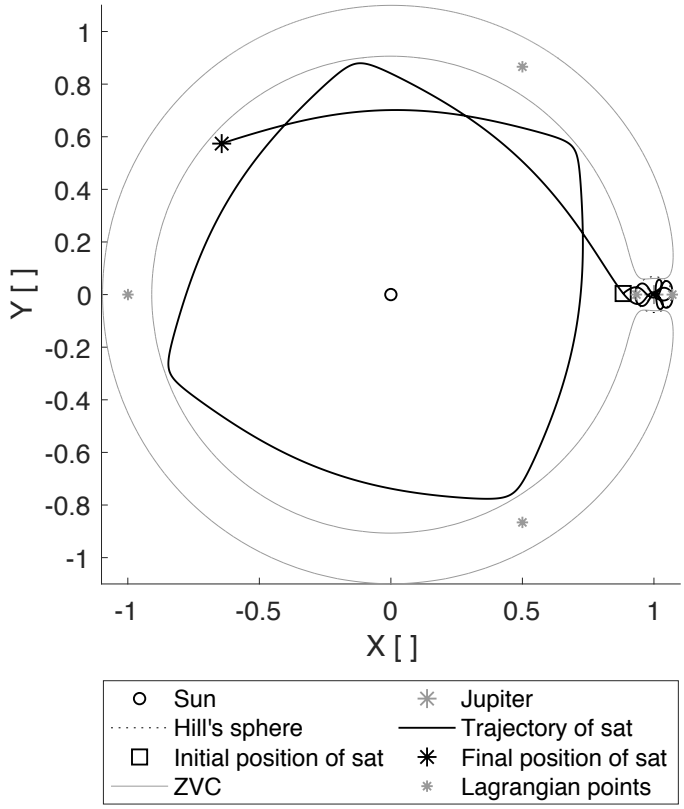

Figure 4.2: Motion of the satellite in the synodic frame in a whole view. Here ZVC are displayed in full.

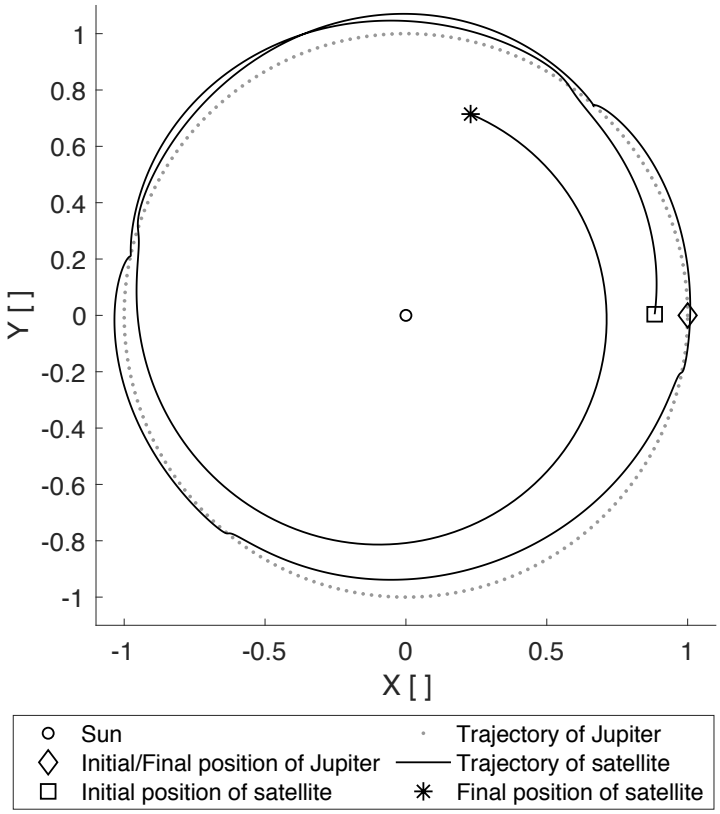

Figure 4.3: Motion of the satellite in the inertial frame centered in the Sun, where also Jupiter moves in a circular orbit.

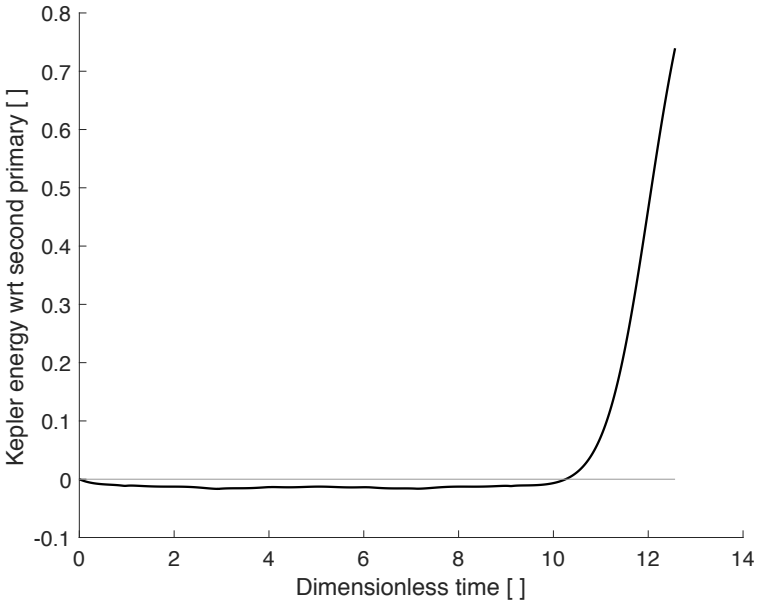

Figure 4.4: Keplerian energy with respect to (wrt)the second primary. Zoom in the first 2 years of propagation, where the ballistic capture takes place.

Here, the algorithmic definition will be exposed. An important feature of this work is that all the analysis are developed for a 2D space, therefore only the ecliptic plane of the orbit of the planet around the Sun will be studied. All variables along z axis are always null.

1. A fixed distance from the second primary $r_{2,0}$ is chosen (360° around the planet) using ψ variable. Depending on how many positions are to be considered, a variable number of ψ are contemplated. Successively, initial conditions are computed using simple trigonometric relations and transformed in Cartesian coordinates in the inertial system of the first primary and then also in curvilinear coordinates.

$$\begin{cases} x_{2,0} = r_{2,0} \cos \psi \\ y_{2,0} = r_{2,0} \sin \psi \end{cases} \tag{4.2}$$

$$\begin{cases} x_0 = x_{2,0} + 1 \\ y_0 = y_{2,0} \end{cases} \tag{4.3}$$

$$\begin{cases} \rho_0 = \sqrt{x_0^2 + y_0^2} - 1 \\ \theta_0 = \arctan\left(\dfrac{y_0}{x_0}\right) \end{cases} \tag{4.4}$$

2. Computation of the velocity of the body relative to the second primary in order to set the energy with respect to the same primary to null.

$$v_{2,0} = \sqrt{\frac{2\mu}{r_{2,0}}} \tag{4.5}$$

3. Transformed the velocity from the previous point in the current curvilinear frame, it will be pointed in all directions. Discretization is made using α, developing a vector of possible velocities in every direction, using a fixed number of alternative conditions. Initial velocities are computed in the Cartesian frame of the first primary and also in curvilinear coordinates using simple relations. In this way every initial positions considered has a large number of initial velocities which all guarantee that keplerian energy relative to the planet is null.

$$\begin{cases} \dot{x}_{2,0} = v_{2,0} \cos\alpha \\ \dot{y}_{2,0} = v_{2,0} \sin\alpha \end{cases} \tag{4.6}$$

$$\begin{cases} \dot{x}_0 = \dot{x}_{2,0} \\ \dot{y}_0 = \dot{y}_{2,0} + 1 \end{cases} \tag{4.7}$$

$$\begin{cases} \dot{\rho}_0 = \dot{x}_0 \cos\theta_0 + \dot{y}_0 \sin\theta_0 \\ \dot{\theta}_0 = \dfrac{\dot{y}_0 \cos\theta_0 - \dot{x}_0 \sin\theta_0}{1 + \rho_0} - 1 \end{cases} \tag{4.8}$$

4. For every velocity in every point considered it must be verified that Jacobi constant is lower than its value in the Lagrangian point L1 $C_j < C_{j,L1}$. This means that the total energy is higher than the limit value when a trajectory can not pass from the area near a primary to the area near the other one. In this way the passage is open and ZVC do not contain at least the Lagrangian point L1. This relations was introduced previously in equation 2.10 and the successive one.

5. Propagation of the orbit with given initial conditions. Every orbit obtained is evaluated for 2 years in the future (forward propagation, FW) and 2 in the past (backward propagation, BW). In this way, it

could be verified if the trajectory is feasible or if it collides with a primary and it could be analyzed the origin of the orbits that lead to a ballistic capture.

6. Symmetries will be exploited to reduce the computational cost and for a better understanding of the problem. This study is developed in section 4.6. Thanks to this symmetry it is possible to propagate only half trajectories

7. For every trajectory the time spent with negative keplerian energy relative to the second primary is calculated, together with the time spent within 4 Hill's radii of distance from the planet. In every case, the criterion of negative energy is much more important, as described in section 3.2.

8. Using an *event function* integrated in the *ode function* it is possible to consider also collisions with the planet, while collisions with the first primary are not important for this study. When the distance from the second primary is lower than the radius of the planet, the simulation is interrupted and all parameters are saved in order to be catalogued as collisions and represented coherently in the results.

4.5 Preliminary results

A simulation was developed using an angle spacing of 1/6 degrees (0.167°) for both discretizations of position and velocity. Results are shown in figures 4.5 and 4.6, where in the vertical axis represents the duration time of the capture up to a maximum of 2 years. In the horizontal plane are present the discretizations mentioned previously. Figures are obtained exploiting the symmetry discussed in section 4.6, therefore using only the first 180° in the discretization of the position and developing two separated diagrams respectively for a forward (FW) propagation and for a backward (BW) propagation.

4.6 Symmetry of the problem

Study of the presence of symmetries verified afterwards. The following symmetry property was expected, being based on the equations of motion.

$$\left(\rho, \theta, \dot{\rho}, \dot{\theta}, t\right) \rightarrow \left(\rho, -\theta, -\dot{\rho}, \dot{\theta}, -t\right).$$

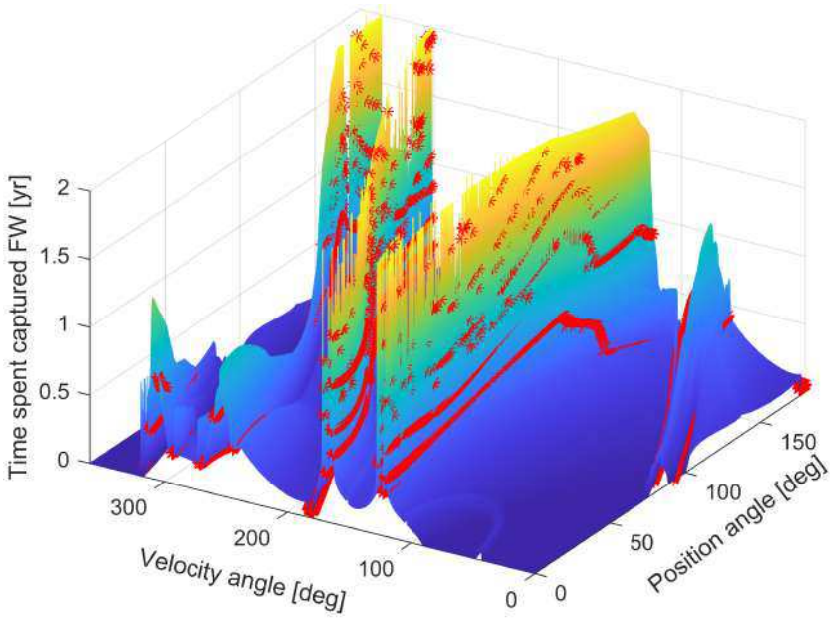

Figure 4.5: Results of the forward (FW) simulation for the search of ballistic captures with an initial position distant $1.1\,r_{Hill}$ from Jupiter. Horizontal axis represent the angles analyzed in position and velocity and are measured in degrees starting from the x-axis of the inertial frame centered in the Sun which connects the two primaries. In the vertical axis is represented the total time spent with negative keplerian energy relative to Jupiter, with an overall simulation time of 2 years. Red stars indicate collisions with the planet.

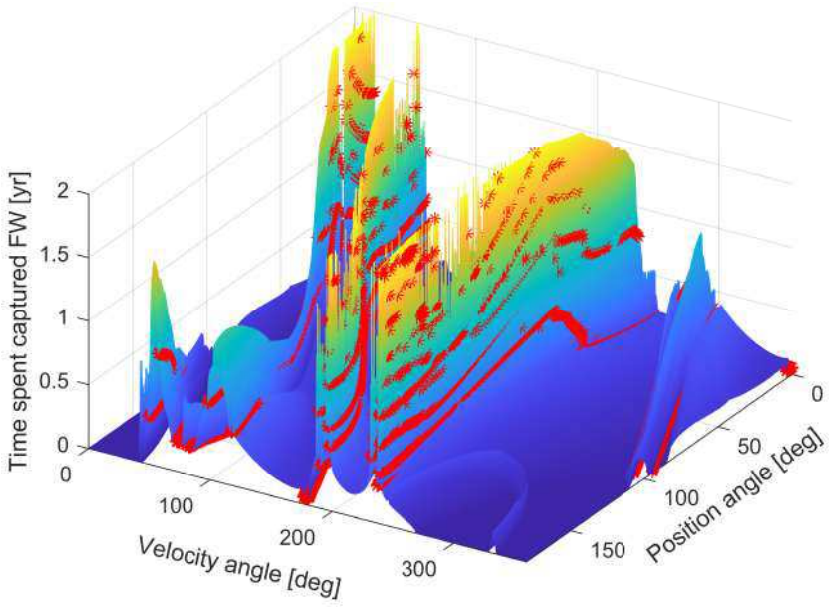

Figure 4.6: Results of the backward (BW) simulation for the search of ballistic captures with an initial position distant $1.1\, r_{Hill}$ from Jupiter. Horizontal axis represent the angles analyzed in position and velocity and are measured in degrees starting from the x-axis of the inertial frame centered in the Sun which connects the two primaries. In the vertical axis is represented the total time spent with negative keplerian energy relative to Jupiter, with an overall simulation time of 2 years. Red stars indicate collisions with the planet.

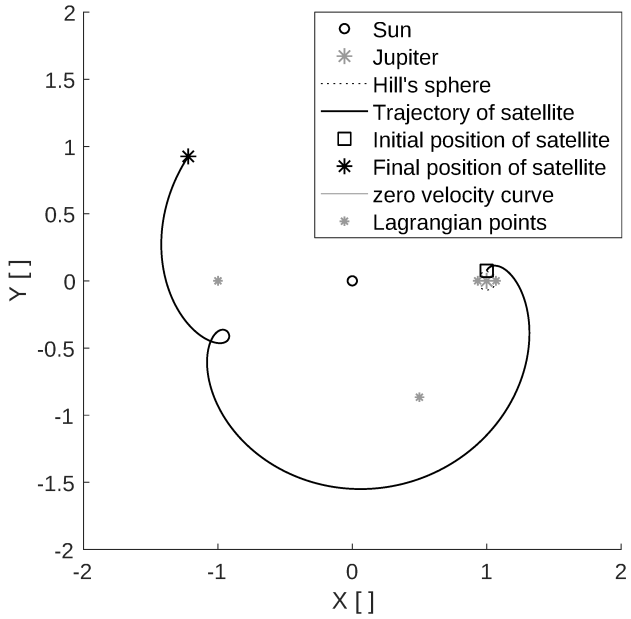

Figure 4.7: Trajectory in the synodic reference frame for FW propagation of the symmetric orbit.

This relations highlight the specularity of positions relative of the x-axis of the synodic frame (conjunction of the primaries), of velocities in the y-axis and of time, as illustrated in figures 4.7, 4.8, 4.9 and 4.10. This symmetry is actually an anti-symmetry, because it originates in the direction of the time propagation. Trajectories found with this property are identical, but symmetrical with respect to the x-axis of the synodic frame (conjunction of the primaries). In fact they are covered in the opposite way and in opposite time. For this reason the backward propagation was introduced.

Thanks to this property it is possible to develop the algorithm so that it halves the necessary propagation In fact, exploiting the symmetry it is possible to evaluate only half the initial positions (180° instead of 360°) in both FW and BW time. In this way, the range 0°-180° in BW propagation could be linked to the range 180°-360° not propagated for FW times. So it is clear the advantage of studying the possibility of capture trajectories and their origin with a lower computational cost.

Finally, it was verified this symmetry numerically. As it can be seen from the figures, it was verified that trajectories are perfectly symmetrical.

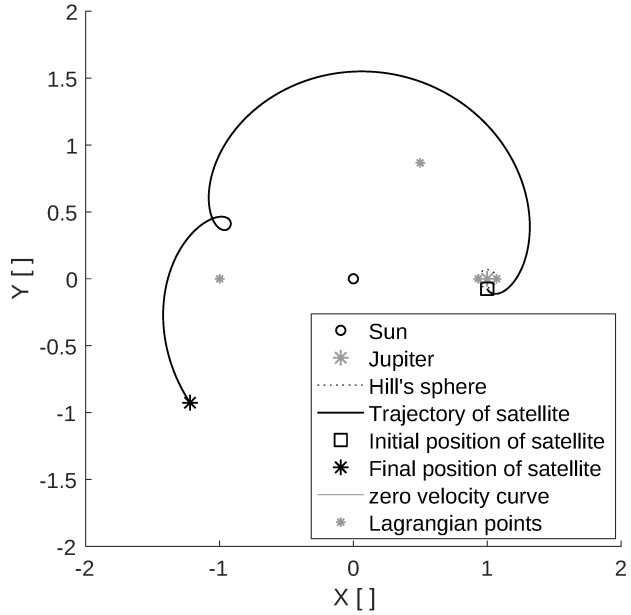

Figure 4.8: Trajectory in the synodic reference frame for BW propagation of the symmetric orbit.

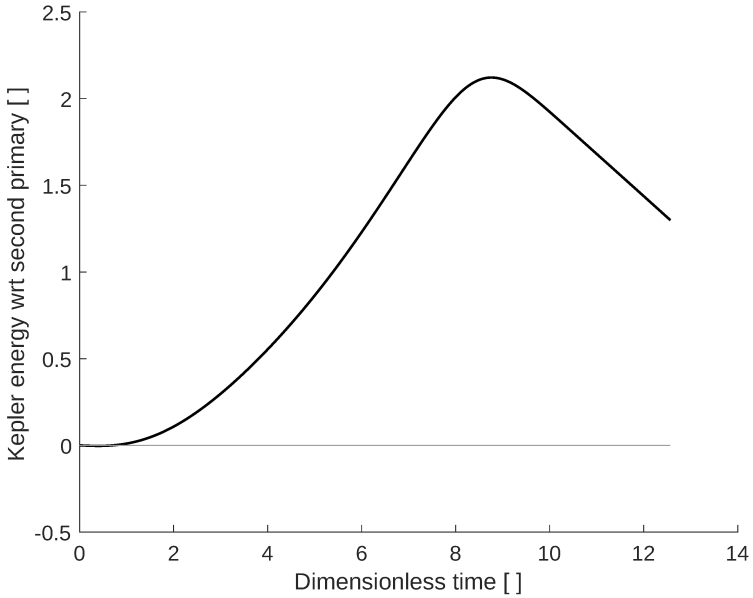

Figure 4.9: Keplerian energy relative to the second primary for FW propagation of the symmetric orbit.

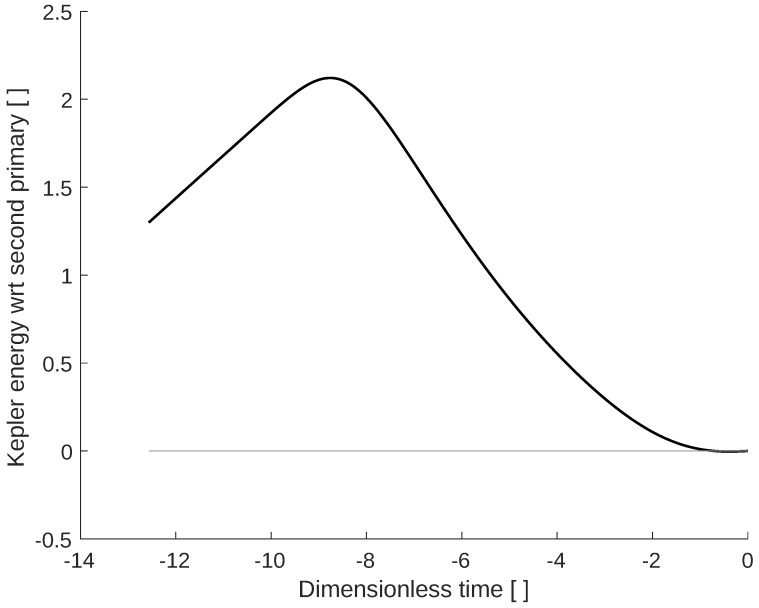

Figure 4.10: Keplerian energy relative to the second primary for BW propagation of the symmetric orbit.

4.6.1 Additional possible symmetry

An additional possible symmetry was observed in the parameters ρ e $\dot{\theta}$ and is also displayed in figures 4.11 and 4.12. Probably this is not analytical, because it was never found in this work a suitable relation for it. However, a future detailed study could be conducted for a better understanding of this phenomenon.

4.7 Relations between capture and initial velocity

A relation between the direction of the initial velocity and the derivative of the keplerian energy relative to the second primary was imagined. In fact, the proximity of the initial positions to the planet and the evaluation of the energy relative to it are clues to the fact that the influence of the first primary can have an effect on the change of the keplerian energy. This means that the perturbative body is now the Sun, while the planet is considered as the main body where the orbit stays around.

As an example, if the norm of the initial velocity relative to the planet is diminished by the perturbation of the Sun, it is probable that the energy

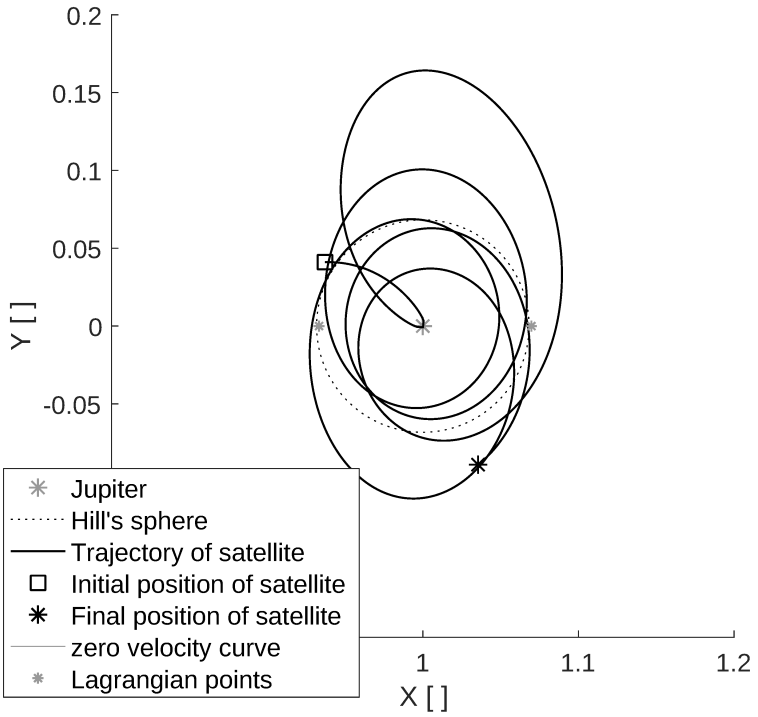

Figure 4.11: Trajectory in the synodic reference frame for FW propagation of the quasi-symmetric orbit.

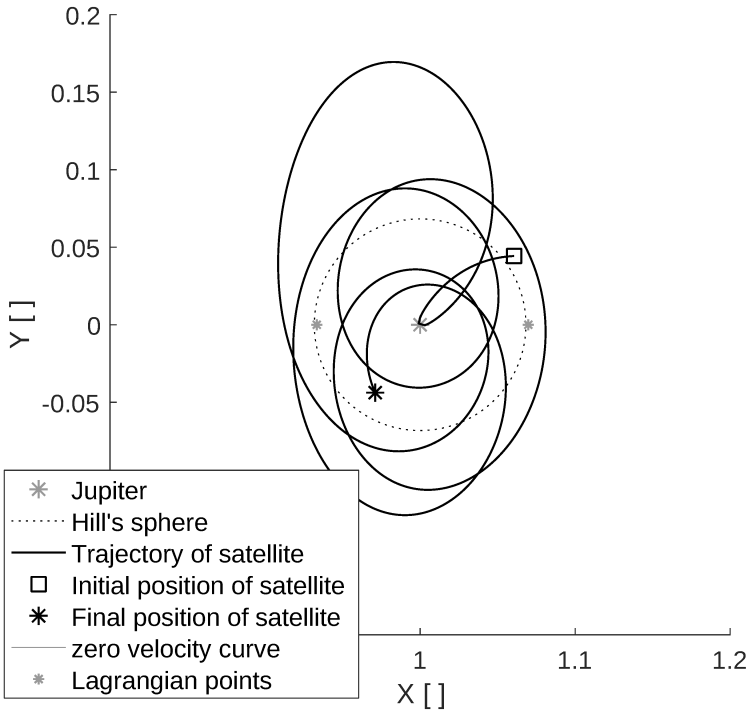

Figure 4.12: Trajectory in the synodic reference frame for BW propagation of the quasi-symmetric orbit..

will reduce and become negative, indicating a ballistic capture.

This analysis was examined but it did not conduct to any relevant result, even if some of them were promising. A further study of it is surely an important step for a future additional work.

Chapter 5

Ballistic captures for nearly closed ZVC in Jupiter

In addition to the algorithm defined in the previous chapter, here only initial conditions that guarantee a fixed Jacobi constant will be found and analyzed. All other aspects are unaltered.

In this way only some of the configurations will be analyzed, in particular the ones where ZVC (*zero velocity curves*) delimit clearly the accessible zone and the forbidden zones in the vicinity of the planet. ZVC will be considered quite closed in proximity of the Lagrangian points L1 and L2, making possible the evaluation of particular orbits that are stable and easily recognizable due precisely to the presence of forbidden zones which are a useful indicator for captures.

5.1 Definition of critical velocity, given a value of C_J

In this section the algorithm presented in the previous chapter will be integrated with the search of critical velocities. In other words, in addition to the norm of initial velocity making null the keplerian energy relative to the second primary, this initial velocity has to make the Jacobi constant equal to a wanted value. This is done by addressing the fixed value of the initial velocity in the right direction.

This last condition is linked also to the shape of ZVC and therefore to forbidden regions for the motion.

To do so, three systems of reference will be used: two of them are inertial Cartesian frames centered in both primaries and the third one is the synodic

frame in curvilinear coordinates.

5.1.1 New steps of the algorithm for critical velocities

Through the definition of the initial distance of the satellite from the second primary r_{20} and of the Jacobi constant, the following relations will be used. As said previously, it is important to underline that the Jacobi constant will be imposed with a value near the ones of $C_{J,L1}$ and $C_{J,L2}$, so that ZVC are partially or totally closed around the planet.

$$r_{2,0} = \sqrt{(r_\rho - \cos\theta)^2 + (\sin\theta)^2} \tag{5.1}$$

Therefore, the following steps are implemented next to the ones presented in section 4.4.

Primarily, it is important to note that the value for the Jacobi constant C_J is chosen arbitrarily as suggested above. Even more important is that now all the relations must be expressed in function of the parameter α, which indicates the direction of the velocity relative to the second primary $v_{2,0}$. In fact α will be exactly the unknown quantity to be obtained in this analysis.

1. Inserting the relations mentioned in the previous chapter in the relation for C_J and fixed a value for this parameter, α will be the only unknown in the following equation:

$$C_j = -2\left(\dot{\rho}^2 + \dot{\theta}^2 r_\rho^2 + z^2\right) + r_\rho^2 + 2\frac{1-\mu}{r} + 2R \tag{5.2}$$

   where

$$R = \frac{\mu}{r'} - \mu r_\rho \cos\theta \tag{5.3}$$

   is the "disturbing function".

2. It is obtained a value for α numerically using properly the *Symbolic Math Toolbox* of Matlab, as shown in the next section.

$$0 = -2\left(\dot{\rho}^2 + \dot{\theta}^2 r_\rho^2 + z^2\right) + r_\rho^2 + 2\frac{1-\mu}{r} + 2R - C_J \tag{5.4}$$

   And with initial position conditions set as $\rho = \rho_0$, $\theta = \theta_0$, $z = 0$ and

initial velocity $v_{2,0}$, the following relation is found.

$$\begin{aligned} 0 = -2\Bigg[\Big(v_{2,0}\cos\alpha\cos\theta_0 + (v_{2,0}\sin\alpha + 1)\sin\theta_0\Big) \\ +\Bigg(\frac{(v_{2,0}\sin\alpha+1)\cos\theta_0 - v_{2,0}\cos\alpha\sin\theta_0}{r_\rho} - 1\Bigg)^2 r_\rho^2\Bigg]^2 \\ +r_\rho^2 + 2\frac{1-\mu}{r} + 2R - C_J \end{aligned} \tag{5.5}$$

α angle computed with this procedure has two possible results, but in some cases no solutions could be extracted.

5.1.2 Analytical, simplified and numerical solution

From equation 5.5, using the *Symbolic Math Toolbox* of Matlab, the following simplification was obtained.

$$\begin{aligned} \big(1+\rho_0\big)^2 - \big(\rho_0 - \cos\theta_0 - \sin(\alpha-\theta_0)\,v_{2,0} + 1\big)^2 - C_J - \big(\sin\theta_0 + \cos(\alpha-\theta_0)\,v_{2,0}\big)^2 \\ -\frac{2(\mu-1)}{1+\rho_0} - \frac{2\mu(r_{2,0}\cos\theta_0 + r_{2,0}\rho_0\cos\theta_0 - 1)}{r_{2,0}} = 0 \end{aligned} \tag{5.6}$$

Given the complexity of this relation, it was reduced using general conditions adopted in this analysis which approximate well also all other solutions. In fact, the satellite could be found nearby the conjunction of the primaries. So it is possible to set $\theta_0 = 0$ and $\rho_0 < 0$ and at least an initial position will always be in this configuration. So equation 5.6 becomes

$$\big(1+\rho_0\big)^2 - C_J - \big(\rho_0 - \sin\alpha\; v_{2,0}\big)^2 - \frac{2(\mu-1)}{1+\rho_0} - \frac{2\mu(\rho_0^2+\rho_0+1)}{\rho_0} + \frac{2\mu\cos^2\alpha}{\rho_0} = 0 \tag{5.7}$$

and resolving for α the following relation could be obtained.

$$\sin\alpha = \frac{\sqrt{2}\left(C_J + 4\mu - 3\rho_0 + C_J\,\rho_0 + 4\mu\rho_0 + 2\mu\rho_0^2 - 2\rho_0^2 - 3\right)}{4\rho_0\sqrt{-\dfrac{\mu}{\rho_0}}\big(1+\rho_0\big)} \tag{5.8}$$

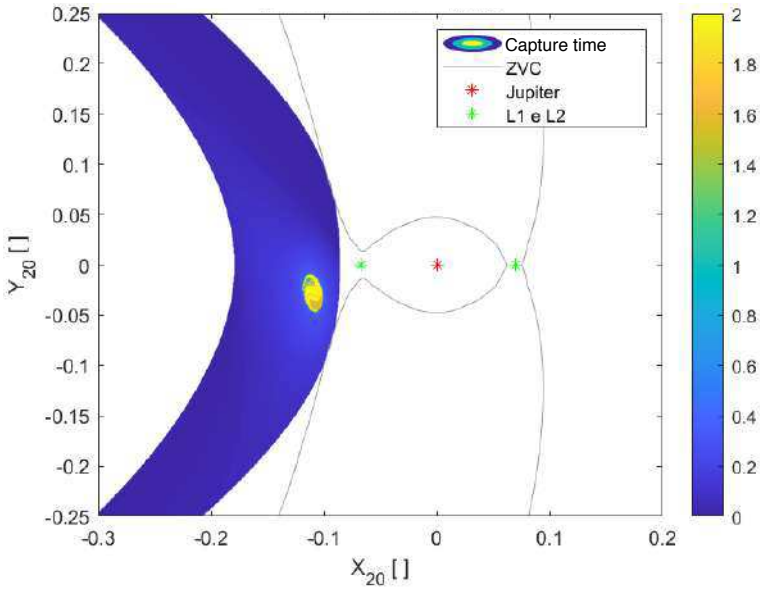

Figure 5.1: Morphology of solutions obtained with algorithm exposed in sections 4.4 and 5.1.1. As said previously, there are no acceptable initial conditions for this particular configuration near the gap of ZVC in L1. Solutions exist only for $x_{2,0} \leq -0.0858$. Besides, the domain of function 5.8 influences also the other acceptable initial positions, giving a shape of half moon colored in blue. For the most part of it there are no ballistic captures, except in a "bubble" colored in yellow, color that indicates a long time spent in capture.

In this way it is possible to solve analytically that for a value of $C_J \simeq 3.0378$ it is necessary that $\rho_0 \leq -0.0858$ in order to have real solutions. As a matter of fact, the domain of the function $\sin\alpha$ in equation 5.8 forces the condition given above.

In figure 5.1 is represented the morphology of possible solutions using the complete equation 5.6. For these configurations there are real solutions that corresponds to initial condition for which fixed Jacobi and null keplerian energy are respected. This solution is computed by the use of the aforementioned *Toolbox Matlab*, but it is not displayed here for brevity.

Given the shape of ZVC for high values of the Jacobi constant C_J it is clear that acceptable conditions exist only in the conjunction of the primaries of near there, but never in the regions at 90° and 270° from it (above and under the planet, where ZVC mark the forbidden regions).

Trajectory inside the colored region of figure 5.1 includes different kind of orbits. There are casual motions relative to the second primary, passages

Table 5.1: Approximated values of the Jacobi constant evaluated in the Lagrangian points. These are obtained by the previously introduced formulas 4.1

Lagrangian point	L1	L2	L3	L4	L5
Jacobi constant C_J [ ]	3.0387	3.0375	3.0010	2.9990	2.9990

in proximity of L1, fast captures that are more probably gravity assists and finally real captures. Respectively the colours are dark blue, light blue, green for the contour of the bubble and yellow for the bubble itself. Examples of everyone of them will be exposed in section 5.7.

It has to be underlined that equation 5.8 has always two solutions, when the domain is respected. The only exception is when the second term is exactly unitary. This takes the study to consider two initial velocities for every initial position. But in every case considered one of these solutions never conducts to capture, so all the following figures and results will be displayed for the "correct" velocity. This parameter is almost always the one obtained resolving "directly" the equation, in other words finding the value of α that stays in the first or fourth quadrant. The other possible solution for inverse function of sine and tangent is $\pi - \alpha$, which in the cases studied takes never to a ballistic capture, but it is a mere relative motion as in section 5.7.5.

Another noteworthy point is that there are no collisions with the planet when high Jacobi constant are considered, therefore with quite closed ZVC.

5.2 Results of the search for Jupiter

For a better understanding of the data and of results, table 5.1 is presented. It contains characteristic values of the Jacobi constant evaluated in the Lagrangian points.

The first simulation analyzed will be the one with a Jacobi constant equal to the mean value of the one in L1 and L2 $C_J = (C_{J,L1}+C_{J,L2})/2 =\simeq 3.0383$.

Research has been developed starting from an high number of initial conditions. In particular, the discretization grid was parameterized with the Cartesian coordinates relative to the second primary $x_{2,0}$ e $y_{2,0}$, as represented in figure 5.2. These parameters are then introduced in equation 5.9 (seen also in previous chapters), and finally using relations presented in section 5.1.1. Initial conditions for the propagation in curvilinear coordinates for the synodic system are obtained from this procedure.

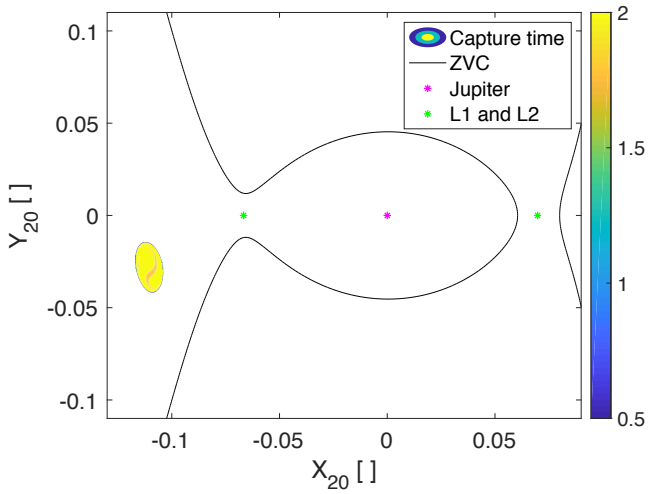

Figure 5.2: Results of the search for ballistic captures by Jupiter. The X_{20} - Y_{20} plane represented is referred to the Cartesian inertial frame centered in the second primary. All and only the capture are found in the yellow bubble, which includes the initial positions of trajectories that spend a long time with negative keplerian energy with respect to the planet. The measure of time is represented with the side "colorbar". On the contrary to figure 5.1, here all solutions with short or no capture were cut off. Only captures with duration of 0.5 Jupiter's years (6 Jupiter's months) or more are represented. In this graphic also ZVC (*zero velocity curves*) are present, evaluated for $C_J \simeq 3.0383$. They have a gap near L1 and are closed in proximity of L2, leaving no chance for the satellite to escape in this direction. Also position of Jupiter and Lagrangian points L1 and L2 are represented with stars.

$$
\begin{aligned}
r_{2,0} &= \sqrt{x_{2,0}^2 + y_{2,0}^2} \\
\rho_0 &= \sqrt{\left(1 + x_{2,0}\right)^2 + y_{2,0}^2} - 1 \\
\theta_0 &= atan2\left(y_{2,0}\,,\, 1 + x_{2,0}\right)
\end{aligned}
\tag{5.9}
$$

At the end, for every trajectory simulated various parameters are computed, such as the time the satellite spend being captured by the second primary (with negative relative energy or particularly near to it) and other parameters for the verification of the procedure. In this way it is possible to verify its correctness and extract data to plot figure 5.2.

The symmetry introduced in section 4.6 was used to simplify the simulation and solutions with positive keplerian energy relative to Jupiter were

cut off. This could be improved if an analytic relation could be determined to find out whether a direction conducts to capture or not.

5.3 Results obtained by varying Jacobi constant

Figure 5.3 contains different plots for initial conditions internal (between the primaries) and external (on the right of the planet in the synodic frame) evaluated with different Jacobi constants C_J. In order from left to right and from above to the bottom: $C_J = 3.0386$, $C_J = 3.0381$, $C_J = 3.0375$ and $C_J = 3.0370$. All and only the captures are found in the yellow area, which includes the initial positions of trajectories that spend a long time with negative keplerian energy with respect to the planet. The measure of time is represented with the side "colorbar". On the contrary to figure 5.1, here all solutions with short or no capture were cut off. Only captures with duration of 0.5 Jupiter's years (6 Jupiter's months) or more are represented. In this graphic also ZVC (*zero velocity curves*) are present, evaluated for the corresponding value of the Jacobi constant. Also position of Jupiter and Lagrangian points L1 and L2 are represented with stars.

From figure 5.3 it is clear that when C_J decreases the gaps of ZVC and as a consequence the bubble get bigger. Also the colour of this last one changes. For high Jacobi it is completely yellow indicating a long capture, while for lower values of the Jacobi constant it becomes mostly blue indicating shorter captures or even trajectories of flybys.

It is easy to find out that generally the more the gaps are closed, the longer are captures.

A particular case is found for the area with a shape of a drop inside the bubble for low Jacobi. A trajectory of this kind is shown in section 5.7.

5.4 Topology of the structures obtained

Bubbles obtained with this method have always an elliptic shape and it is interesting to analyze the change of this shape as a function of the Jacobi constant. This comparison in shown in figure 5.4, where all structures stretch out from a central point that is contained in all of them. Characteristics of the central point will be further analyzed in section 5.5.

For what concerns structures, they enlarge with the reduction of Jacobi constant and therefore with the increase of the gaps in the ZVC near Lagrangian points. This result is visible thanks to the fact that ZVC are plotted in the same colour of the bubble obtained with a fixed value of C_J.

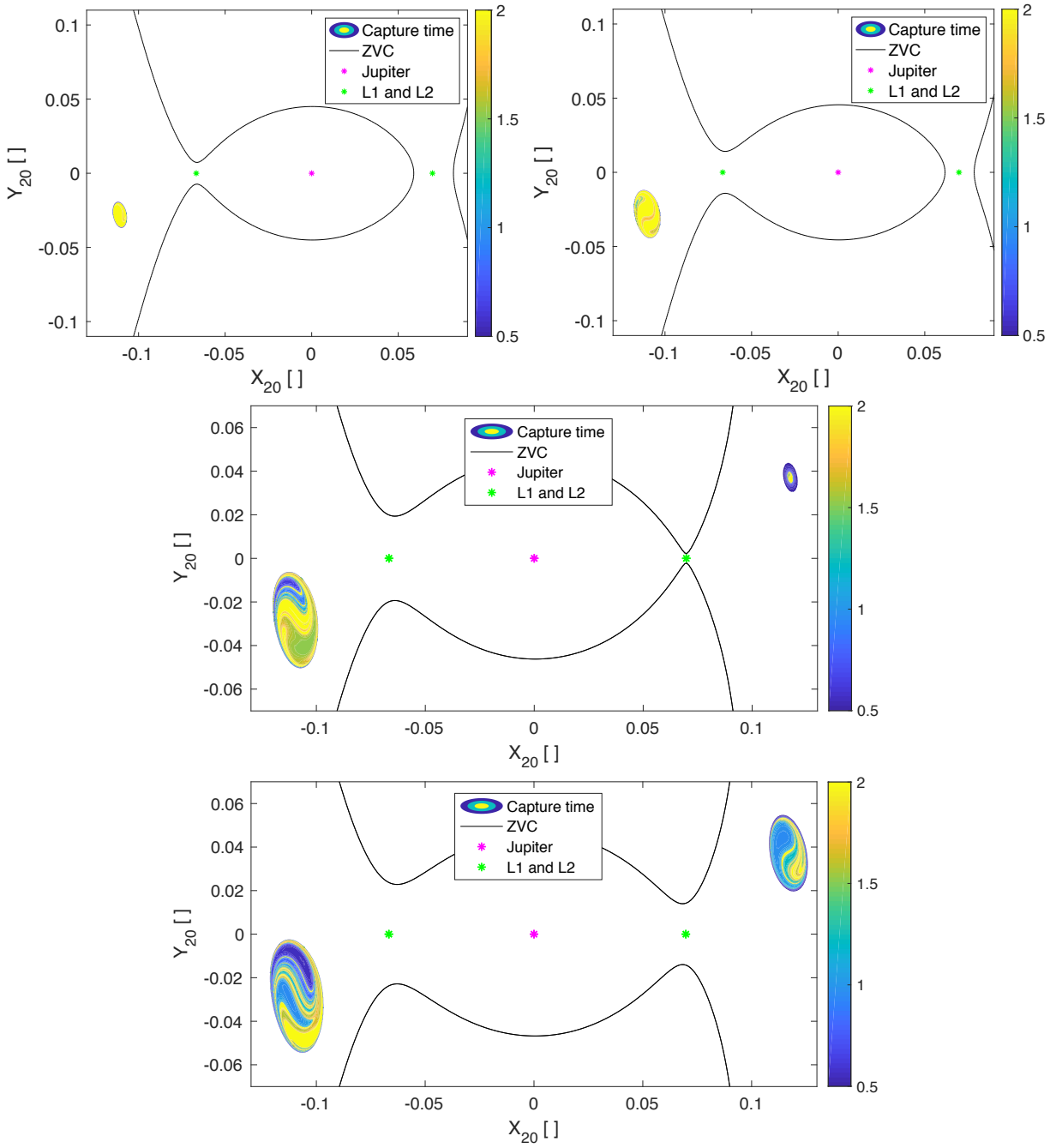

Figure 5.3: Results of the search for ballistic captures by Jupiter with different values of the Jacobi constant. The X_{20} - Y_{20} plane represented is referred to the Cartesian inertial frame centered in the second primary.

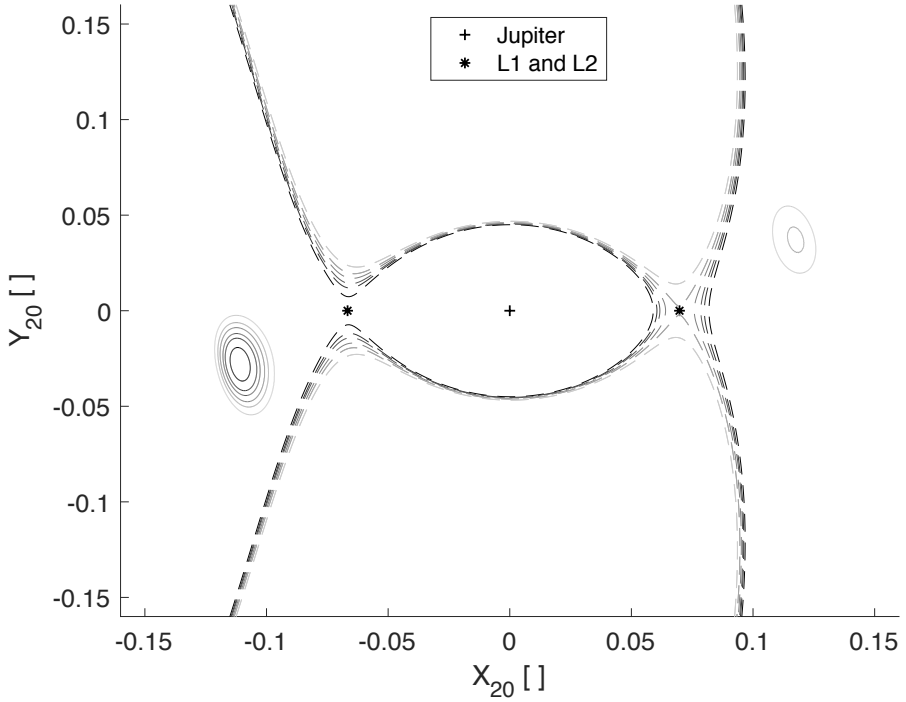

Figure 5.4: Analysis of the topology of "bubble" structures containing the initial positions that conducts to ballistic capture. Their dimensions increase and ZVC gaps grow bigger with the reduction of C_J. This trend is shown using the black colour fading into light gray. The gap of the ZVC in L2 opens up and the external bubbles appear only with the last two values of the Jacobi constant.

5.5 Analysis of generatrix orbits of the capture structures

An interesting study is to characterize the orbit that will be named "generatrix". This is the orbit obtained by finding the maximum value of C_J for which ZVC are still open. In this case ZVC will be almost closed, leaving only a little hole for the entrance in proximity of the second primary. This is obviously possible in both internal and external region, when the value of the Jacobi constant tends to $C_{J,L1}$ or $C_{J,L2}$ respectively. In this last case ZVC on the right will be almost closed, but on the left they will be completely open. However, this fact will not influence at all the analysis, because the region of interest is the one on the right near L2.

Table 5.2: Keplerian orbital elements (semi-major axis a, eccentricity e, perigee argument ω and true anomaly ν) of the internal and external generatrix orbits and relative numerical value of the Jacobi constant for these values.

	a [ ]	e [ ]	ω [ ]	ν [ ]	C_J [ ]
Internal orbit	0.7613758	0.1926487	-2.7509869	2.7195346	$C_{J,L1} + 0.0000129294$
External orbit	1.4339814	0.2338906	0.4655995	5.8508003	$C_{J,L2} + 0.0000126762$

Table 5.3: Initial coordinates used in Matlab simulations for internal and external generatrix orbits. On the left, the first two columns are taken in the inertial reference frame centered in the second primary. On the right, the following two columns are taken in the synodic frame in curvilinear coordinates. The last two columns are the distance of the initial point of these orbits from Jupiter, respectively dimensionless and measured in Hill's sphere radii.

	$X_{2,0}$ [ ]	$Y_{2,0}$ [ ]	ρ_0 [ ]	θ_0 [ ]	d_2 [ ]	d_2 [r_{Hill}]
Internal orbit	-0.111010	-0.027970	-0.110570	-0.031452	0.114479	1.6774
External orbit	0.117475	0.037130	0.118092	0.033214	0.123203	1.8052

5.5.1 Method and initial parameters

The keplerian orbital elements summarized in table 5.2 (together with the relative value of the Jacobi constant used in the Matlab scripts) are evaluated in the inertial reference frame of the first primary. They are the elements of the orbit around the Sun in the instant when the satellite is captured by Jupiter, hence the keplerian energy relative to the planet is null.

In table 5.3 initial coordinates used in Matlab simulations for the generatrix orbits are shown. These coordinates are taken in the inertial system of reference centered in the second primary or in the synodic centered in the first primary for both internal and external case. In this case and in the research previously exposed *Ode113* was used due to its lighter computations (as shown in chapter 1) with absolute and relative tolerances set to 10^{-12}. Other parameters (masses and reference radius) used in the simulations are summarized in table 5.4.

- It has to be underlined that the orbit presented here is the one obtained not considering (only in this moment) the gravitational attraction given by Jupiter. Obviously, the propagation on the whole requires this contribution to find the moment when the ballistic capture begins.

Table 5.4: Parameters used in the simulations for Jupiter: mass of the Sun M_{Sun}, mass of Jupiter M_{Jup} and radius of its orbit around the Sun R_{ref}.

M_{Sun} [kg]	M_{Jup} [kg]	R_{ref} [km]
$1.988499251 \cdot 10^{30}$	$1.898190000 \cdot 10^{27}$	$778.4 \cdot 10^{6}$

However, in this way results represent only conditions at the instant of beginning of the capture, not the effective provenience of the trajectory, which is deflected also before this moment. In the next sections this point will be discussed separately for internal and external orbits.

- Being in a planar case it is not useful to consider right ascension of ascending node Ω and inclination i of the orbits, so they will be considered always null. In the results only the other four parameters will be shown.

- In this particular case the conditions of capture are particularly strict and only a representative orbit will be analyzed. Regardless how much the value of $C_{J,L1}$ is accurate, there are always infinite orbits all concentrated around a single point.

  The distinctive feature used to show the resulting characteristics is that everyone of the infinite orbits obtained has the same parameters of the one displayed in the following section, that is with an accuracy up to the seventh decimal point.

5.5.2 Diagrams and duration of the internal generatrix orbit

In this section interesting figures and parameters for the internal generatrix orbit will be shown. The initial conditions for this orbit were presented in tables 5.2 and 5.3.

In figure 5.5 it is represented the keplerian energy relative to Jupiter for a time span of 50000 Jupiter's years. All along this energy is negative and this indicates a very important capture, longer than 50000 years. That could be explained by considering the very small gap existing in the ZVC, which quite impede to enter or exit from the area in proximity of the planet. To propagate this huge time span, a diminution of integration tolerances to 10^{-10} is fundamental. In this way the necessary accuracy for the computation of the trajectory could be lost. In fact, the error in the propagation (measured with the absolute variation of the Jacobi constant) increases up to 10^{-5}, as shown in figure 5.6.

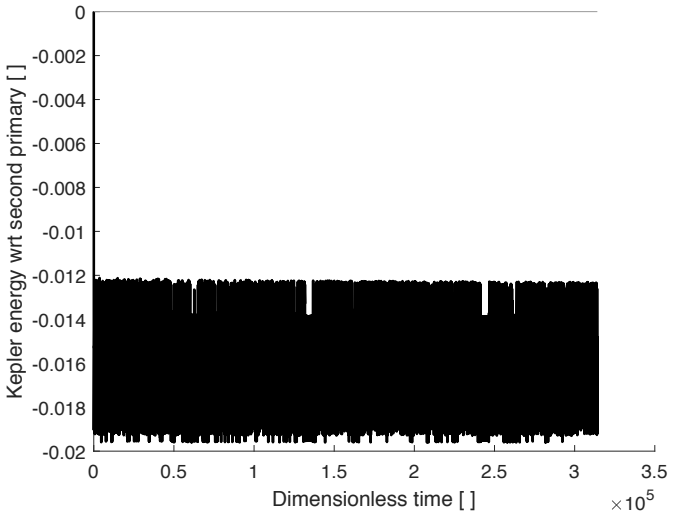

Figure 5.5: Internal generatrix Keplerian energy with respect to the planet for a time span of 50000 Jupiter's years from the beginning of the capture. The dimensionless energy is computed in the inertial reference frame centered in the second primary and it remains negative for the whole duration of the simulation

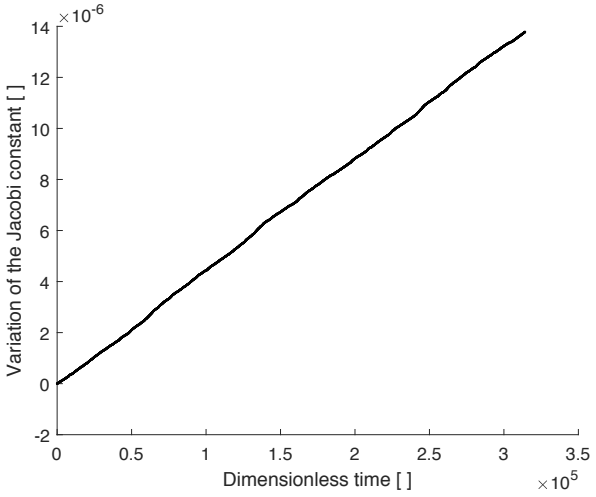

Figure 5.6: Internal generatrix variation of the Jacobi constant for a time span of 50000 Jupiter's years from the beginning of the capture. Despite the use of integration tolerances of 10^{-10}, the variation of the constant in the huge time span accumulates a notable error, in the order of magnitude of 10^{-5}.

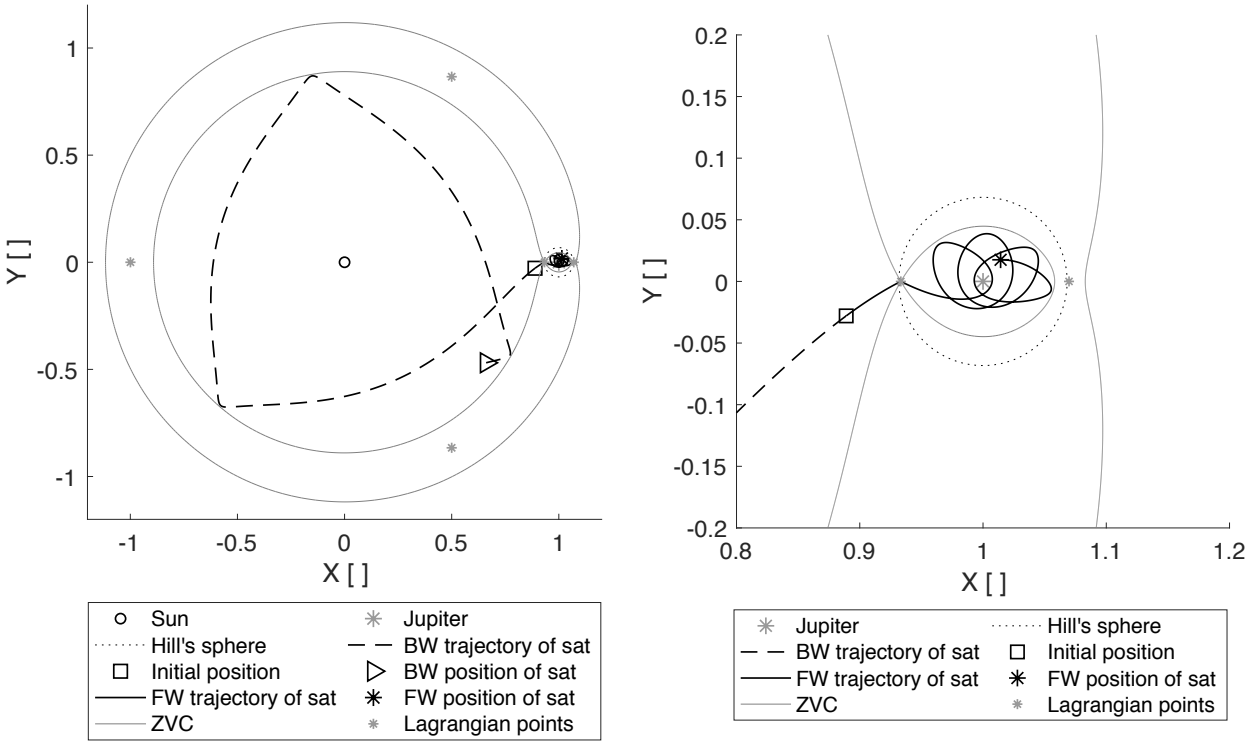

Figure 5.7: Internal generatrix trajectory in the synodic reference frame centered in the Sun. On the left, the overall view; on the right, a zoom of the area containing Jupiter. The trajectory propagated backward in time (BW) is dashed and the trajectory propagated forward in time (FW) is solid. They are linked in the initial point of the propagation (square).

In figures 5.7, 5.8, 5.9 and 5.10 is represented the trajectory of this peculiar orbit. First two figures (5.7 e 5.8) are taken in the synodic frame: the first is a complete view and a zoom around the planet; the second shows a detail of the passage of the trajectory near the gap at L1 and an ulterior zoom of the gap. The last two figures (5.9 e 5.10) represent the orbit in the Cartesian inertial reference frame centered respectively in the first and the second primary.

Total duration of the simulation is 4 years, 2 in backward propagation (BW) and 2 in forward propagation (FW).

The transition to entry in the area near the planet lasts about a Jupiter's year. This feature is particularly visible in figure 5.10, where the trajectory covers quite an entire circle near the Hill's sphere. Here relative velocities are

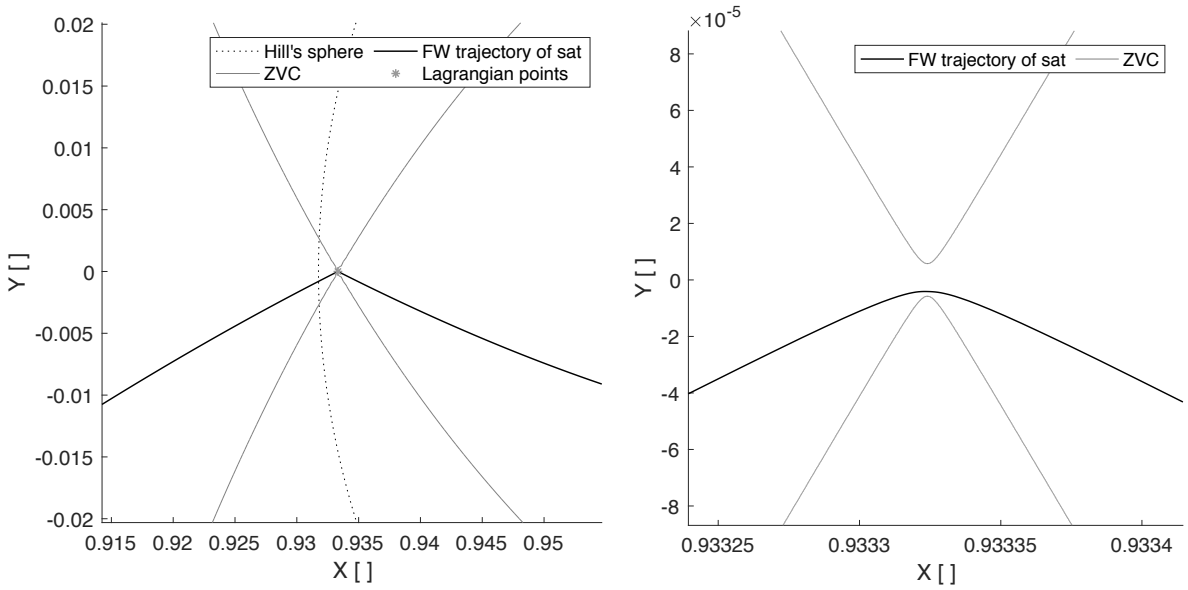

Figure 5.8: Internal generatrix trajectory in the synodic frame centered in the Sun. From left to right, detail and additional zoom of the passage between the ZVC near L1.

very small and for this reason in the synodic frame the trajectory is almost still in proximity of the Lagrangian point L1.

In the inertial frame centered in the Sun (figure 5.9) this feature is visible between the square of the initial position and the moment when the trajectory begins to be diverted by the planet. In fact, between these two moments there is an entire circle in which the orbit slowly gets nearer to Jupiter's orbit.

5.5.3 Variation of orbital elements for internal generatrix

In figures 5.11, 5.12 and 5.13 orbital elements a, e and ω are presented as a function of the distance of the body from the second primary. Besides, here semi-major axis a, eccentricity e and perigee argument ω are given for the internal generatrix orbit: $a = 0.7412$, $e = 0.1918$ and $\omega = -2.9259$. These values are taken in the figures mentioned above, where the plotted parameters tend to be steady. They have a modest difference with the ones presented in table 5.2 obtained in the instant of beginning of the capture. Since they continuously change, they can not be considered reference parameters for the analysis, if not when some criteria are specified.

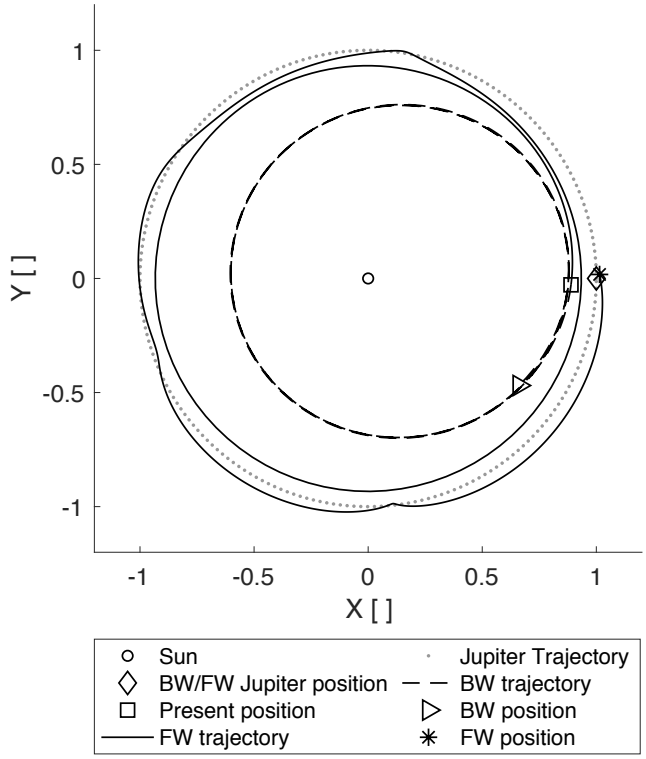

Figure 5.9: Internal generatrix trajectory in the inertial frame centered in the Sun.

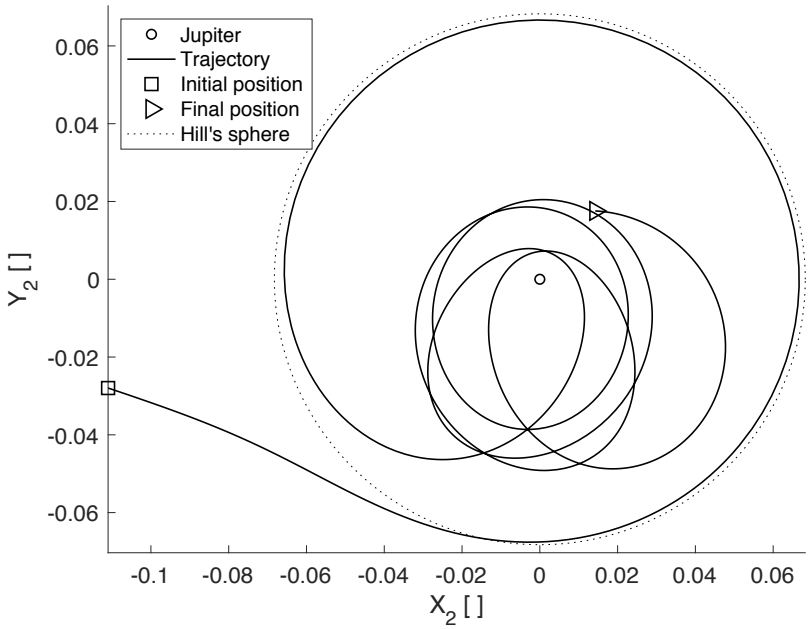

Figure 5.10: Internal generatrix trajectory in the inertial frame centered in Jupiter.

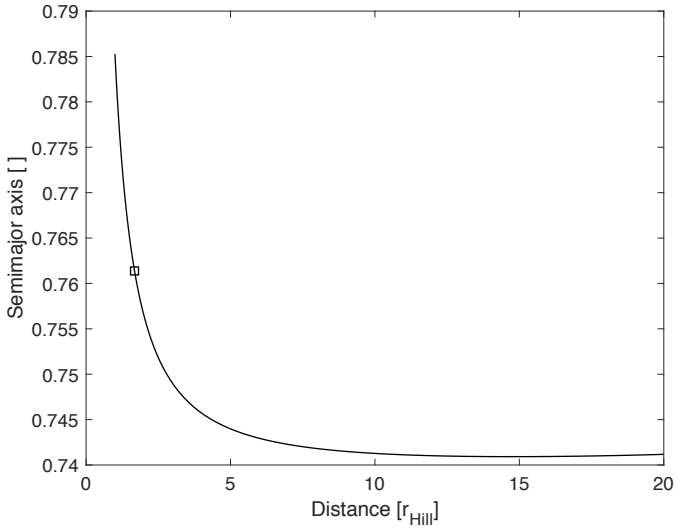

Figure 5.11: Semi-major axis of the internal generatrix computed in the inertial system of reference centered in the Sun. Its variation is shown as a function of the distance from the second primary in Hill's radii. The square indicates the moment when the capture begins. On its left there are the values for the FW propagation, nearer to the second primary; on the right there are the values for the BW propagation, where the body gets further from the planet.

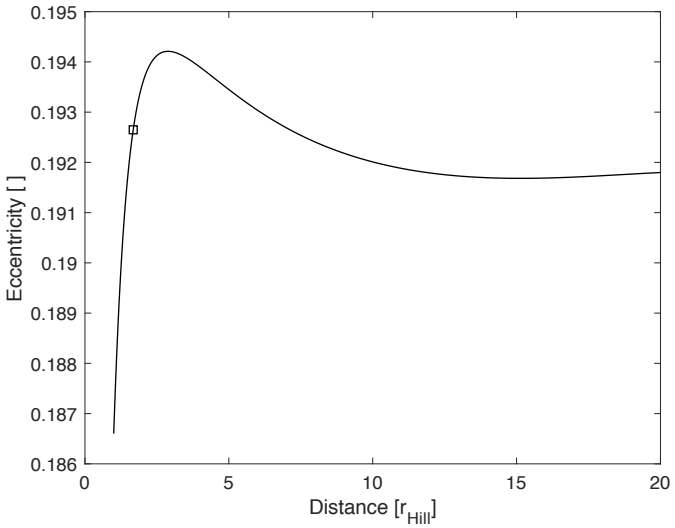

Figure 5.12: Eccentricity of the internal generatrix in the inertial system of reference centered in the Sun. Its variation is shown as a function of the distance from the second primary in Hill's radii. The square indicates the moment when the capture begins.

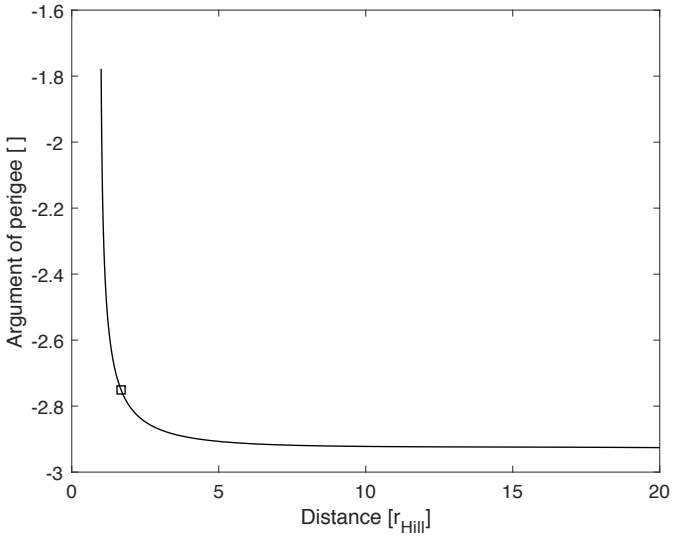

Figure 5.13: Perigee argument of the internal generatrix in the inertial reference centered in the Sun. Its variation is shown as a function of the distance from the second primary in Hill's radii. The square indicates the moment when the capture begins.

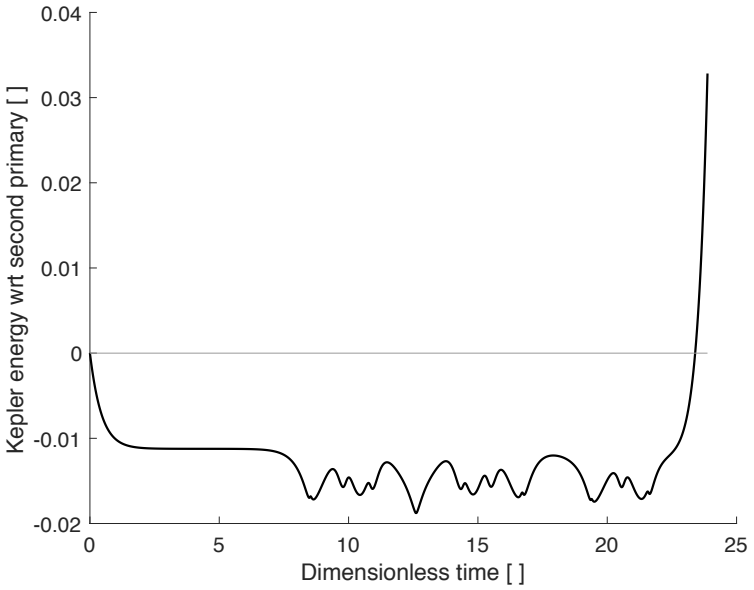

Figure 5.14: External generatrix Keplerian energy relative to the second primary for 3.8 Jupiter's years from the beginning of the capture.

5.5.4 Diagrams and duration of the external generatrix orbit

In this section interesting figures and parameters for the external generatrix orbit will be shown. The initial conditions for this orbit were presented in tables 5.2 e 5.3.

In figure 5.14 is represented the keplerian energy relative to Jupiter for a time span of 4 Jupiter's years. All along this energy is negative and this indicates a very important capture, long about 3.7 Jupiter's years. In figure is also shown the trajectory in the proximity of the planet with the detail of closed ZVC in L2 and wide open in L1.

In figures 5.16, 5.17, 5.18 and 5.19 is represented the trajectory of this peculiar orbit. First two figures (5.16 and 5.17) are taken in the synodic frame: the first is a complete view and a zoom around the planet; the second shows a detail of the passage of the trajectory near the gap at L2 and an ulterior zoom of the gap. The last two figures (5.18 and 5.19) represent the orbit in the Cartesian inertial reference frame centered respectively in the first and the second primary.

Total duration of the simulation is 4 years, 2 in backward propagation (BW) and 2 in forward propagation (FW).

The transition to entry in the area near the planet lasts about a Jupiter's

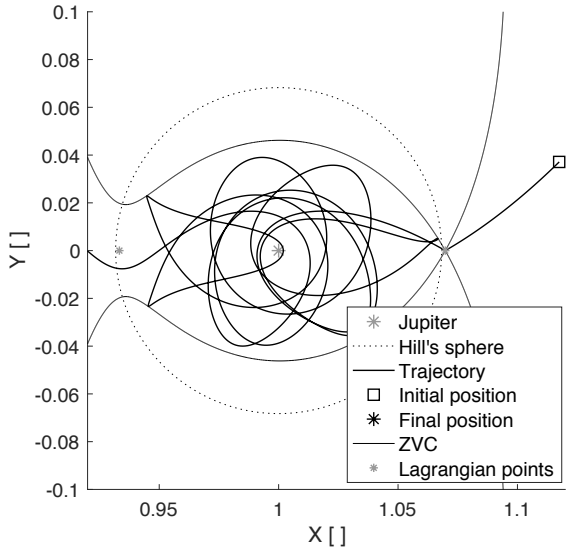

Figure 5.15: External generatrix trajectory in the synodic frame near to Jupiter. Capture lasts about 3.7 Jupiter's years and exits from the wider gap in L1.

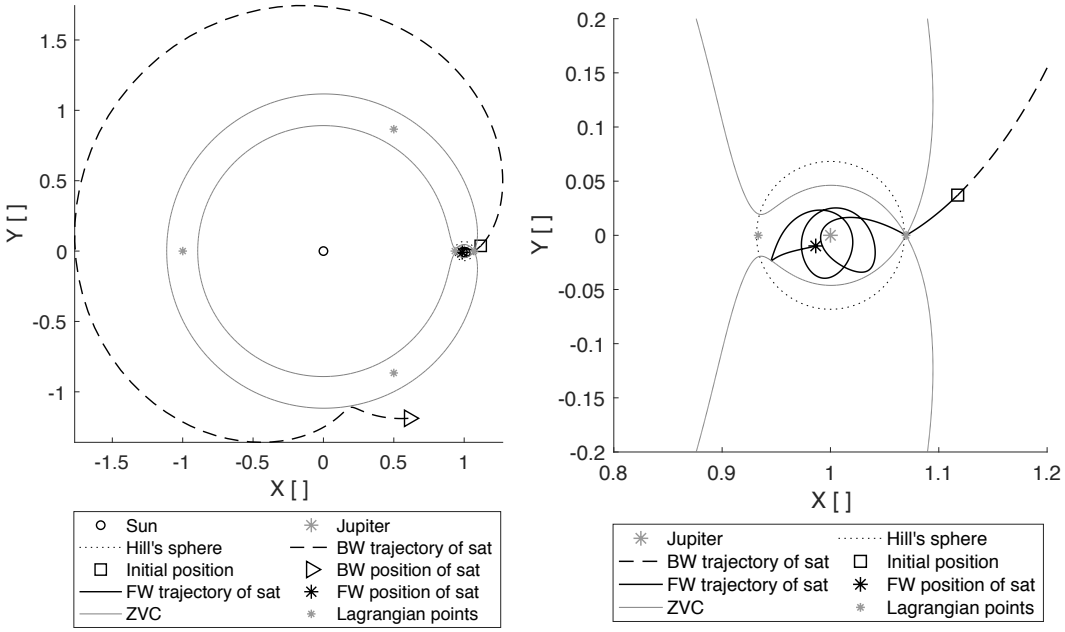

Figure 5.16: External generatrix trajectory in the synodic reference frame centered in the Sun. Left: overall view. Right: zoom on the area containing Jupiter.

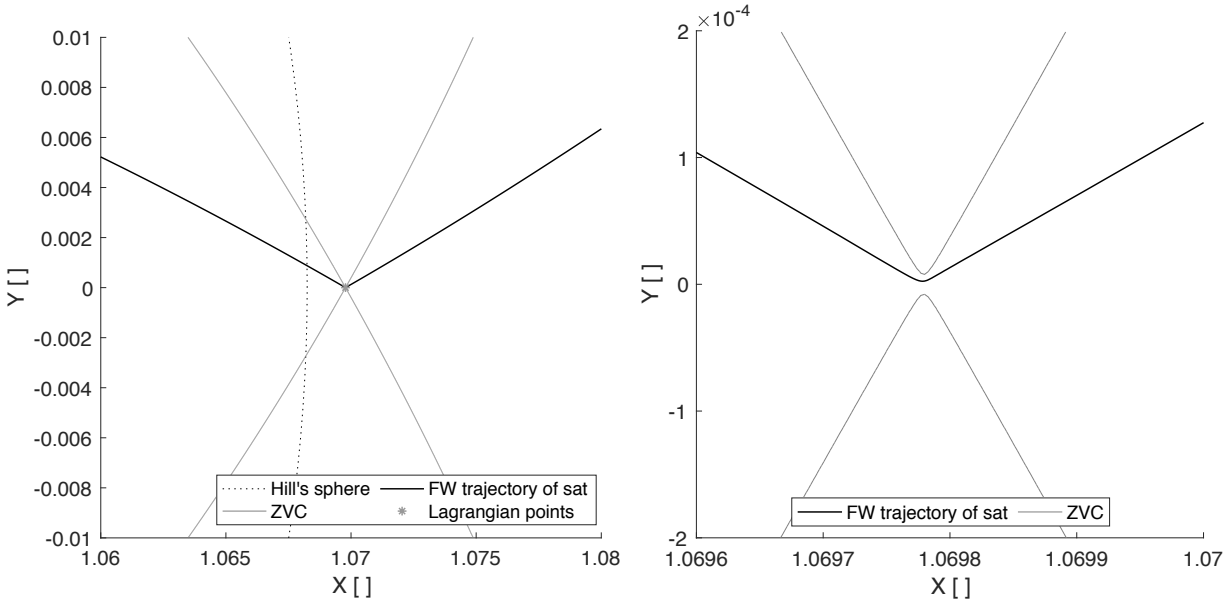

Figure 5.17: External generatrix FW trajectory of the satellite in the synodic reference frame centered in the Sun. From left to right, detail and additional zoom of the passage between the ZVC near L2.

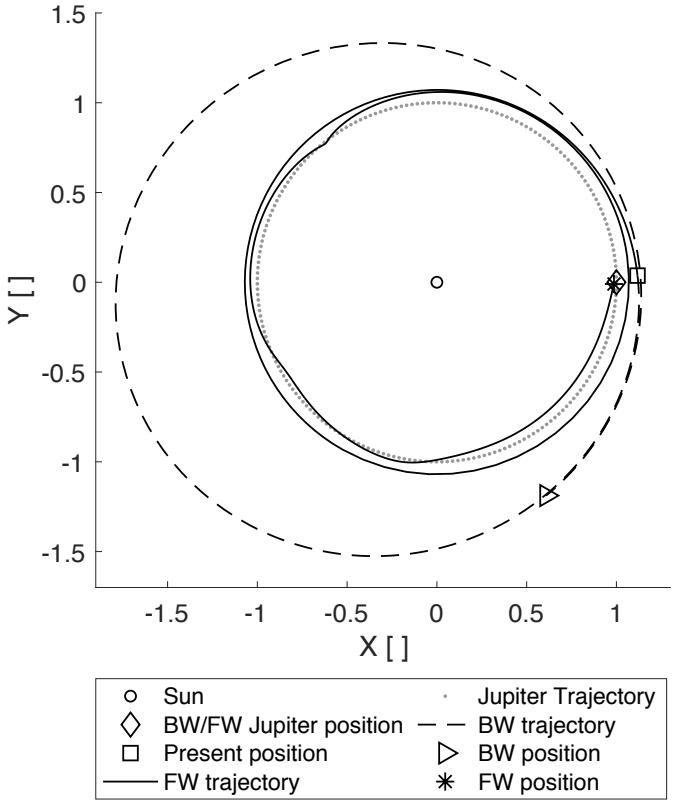

Figure 5.18: External generatrix trajectory of the satellite in the inertial reference frame centered in the Sun.

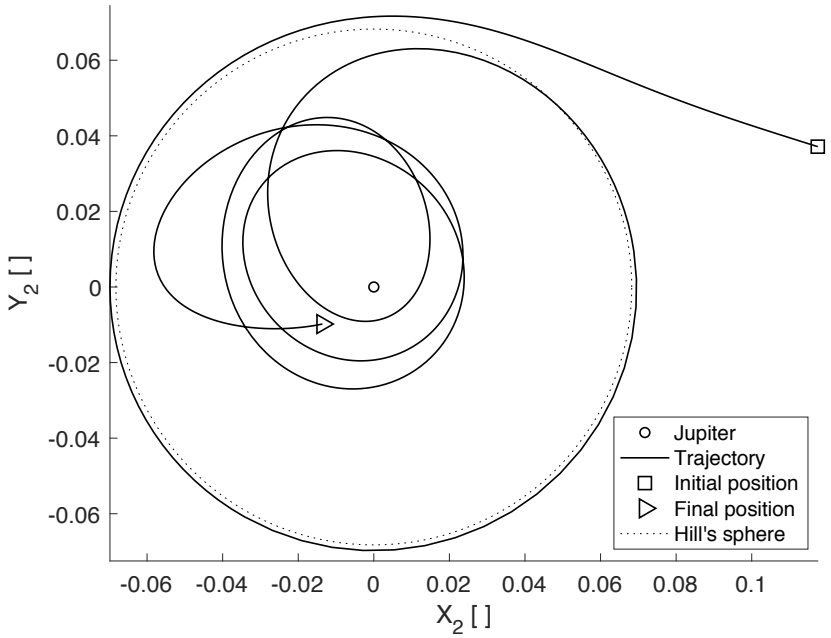

Figure 5.19: External generatrix trajectory in the inertial reference frame centered in Jupiter.

year. This feature is particularly visible in figure 5.19, where the trajectory covers quite an entire circle near the Hill's sphere. Here relative velocities are very small and for this reason in the synodic frame the trajectory is almost still in proximity of the Lagrangian point L2. In the inertial frame centered in the Sun (5.18) this feature is visible between the square of the initial position and the moment when the trajectory begins to be diverted by the planet. In fact, between these two moments there is an entire circle in which the orbit slowly gets nearer to Jupiter's orbit.

5.5.5 Variation of orbital elements for external generatrix

In figures 5.20, 5.21 and 5.22 the values of keplerian orbital elements a, e and ω are presented as a function of the distance of the body from the second primary. Besides, here semi-major axis a, eccentricity e and perigee argument ω are given for the external generatrix orbit: $a = 1.4695$, $e = 0.2308$ and $\omega = 0.2768$. These values are taken in the figures mentioned above, where the plotted parameters tend to be steady. They have a modest difference with the ones presented in table 5.2 obtained in the instant of

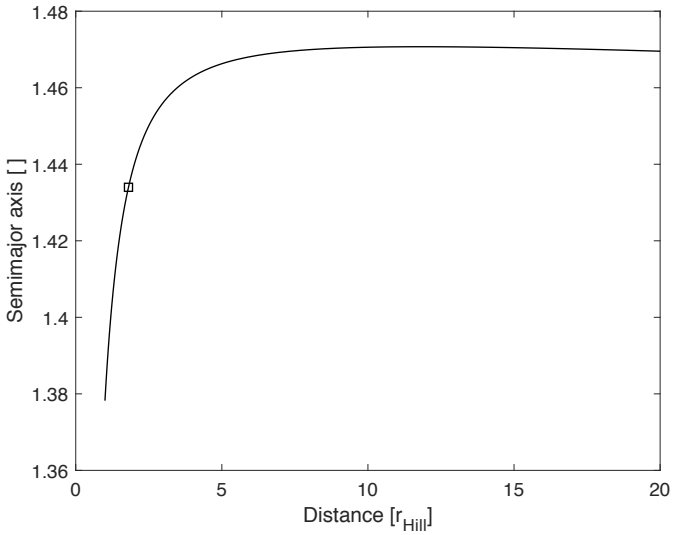

Figure 5.20: Semi-major axis of the external generatrix orbit computed in the inertial system of reference centered in the Sun. Its variation is shown as a function of the distance from the second primary in Hill's radii. The square indicates the moment when the capture begins. On its left there are the values for the FW propagation, nearer to the second primary; on the right there are the values for the BW propagation, where the body gets further from the planet.

beginning of the capture. It has to be highlighted that they continuously change and cannot be considered reference parameters for the analysis, if not when some criteria are specified.

5.6 Keplerian orbital elements in the capture structure

In the same way for keplerian orbital parameters of the generatrix orbits, in this section keplerian orbital elements for orbits in section 5.3 will be studied. For everyone on the captures inside the structures of figure 5.3, semi-major axis a, eccentricity e, perigee argument ω and true anomaly ν were computed. These results are shown in figures 5.23 and 5.24. The first one is for initial position between the primaries and $C_J = C_{J,L2} + 0.0003$, while the second is for external initial position and $C_J = C_{J,L2}$.

It has to be underlined that this second case reveals the approximation of the formulas for the Jacobi constant in the Lagrangian points. In fact, the

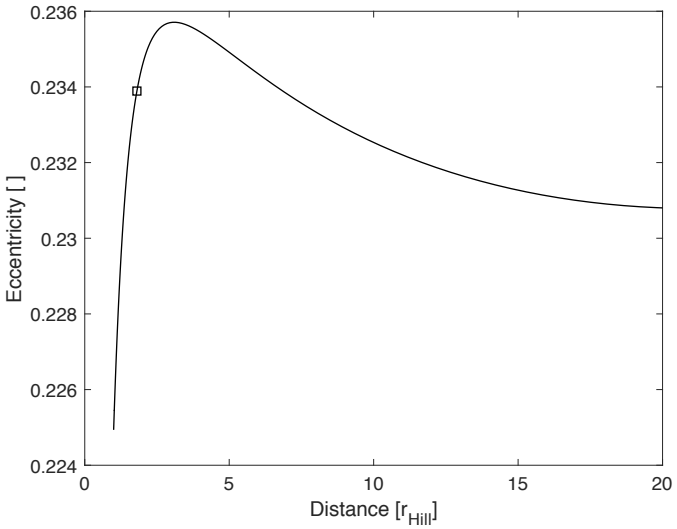

Figure 5.21: Eccentricity of the external generatrix orbit computed in the inertial system of reference centered in the Sun. Its variation is shown as a function of the distance from the second primary in Hill's radii. The square indicates the moment when the capture begins.

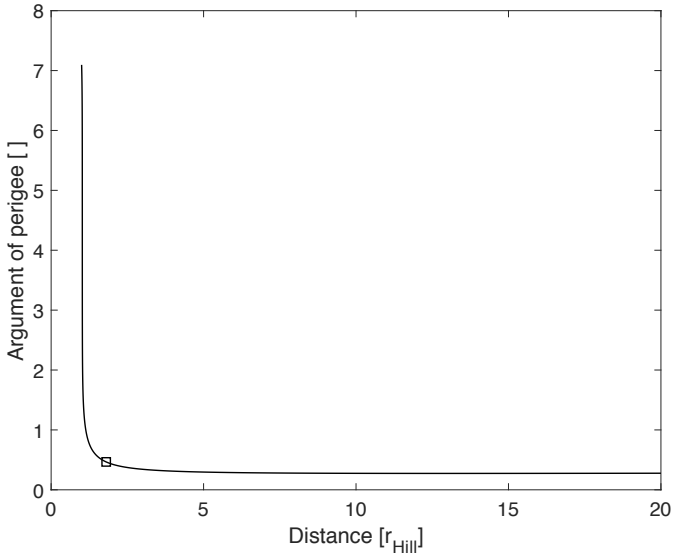

Figure 5.22: Perigee argument of the external generatrix orbit computed in the inertial system of reference centered in the Sun. Its variation is shown as a function of the distance from the second primary in Hill's radii. The square indicates the moment when the capture begins.

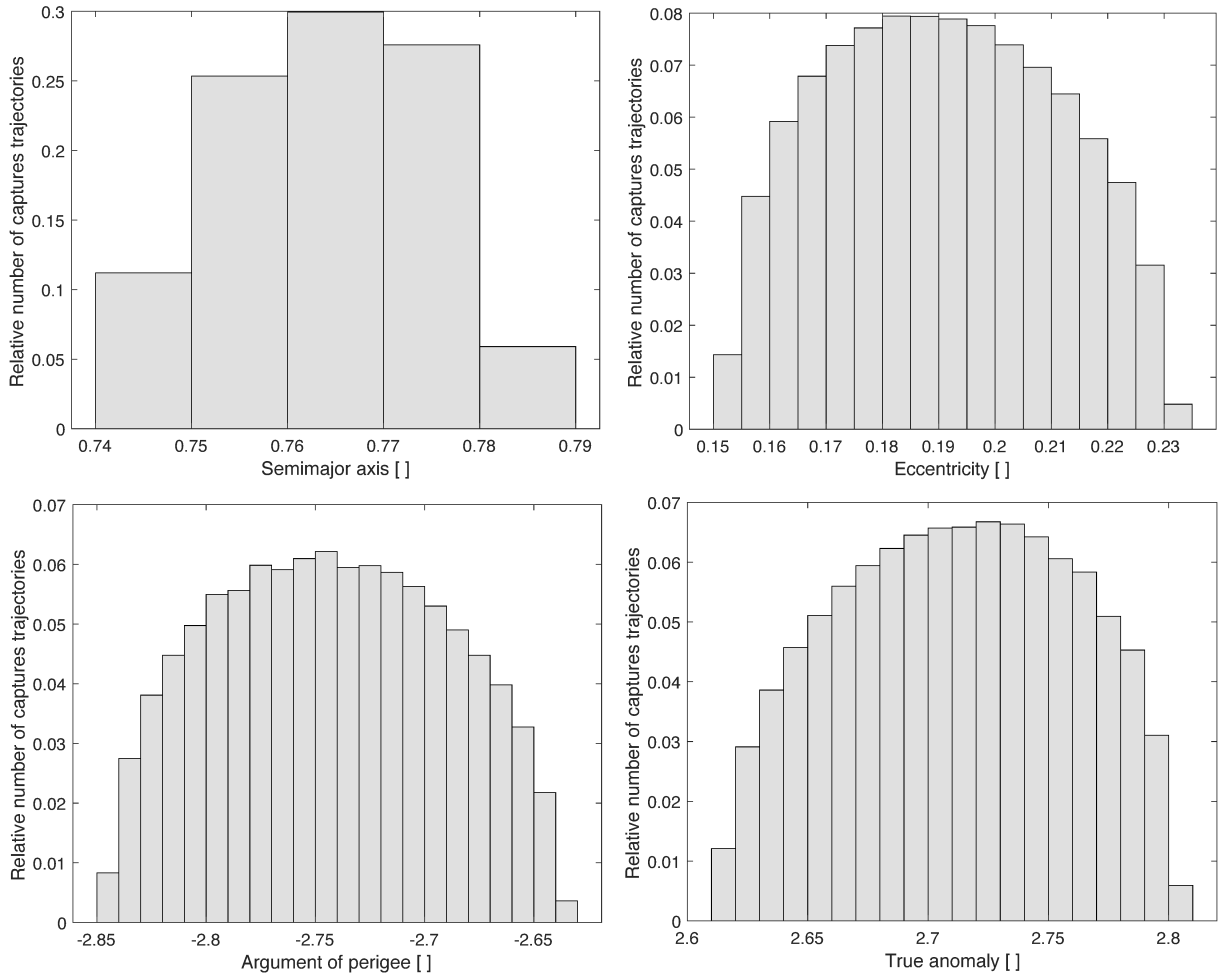

Figure 5.23: Keplerian orbital parameters for orbits inside the internal capture structure (or internal "bubble") for $C_J = C_{J,L2}+0.0003$. This values are distributed around the value of the internal generatrix orbits shown in table 5.2.

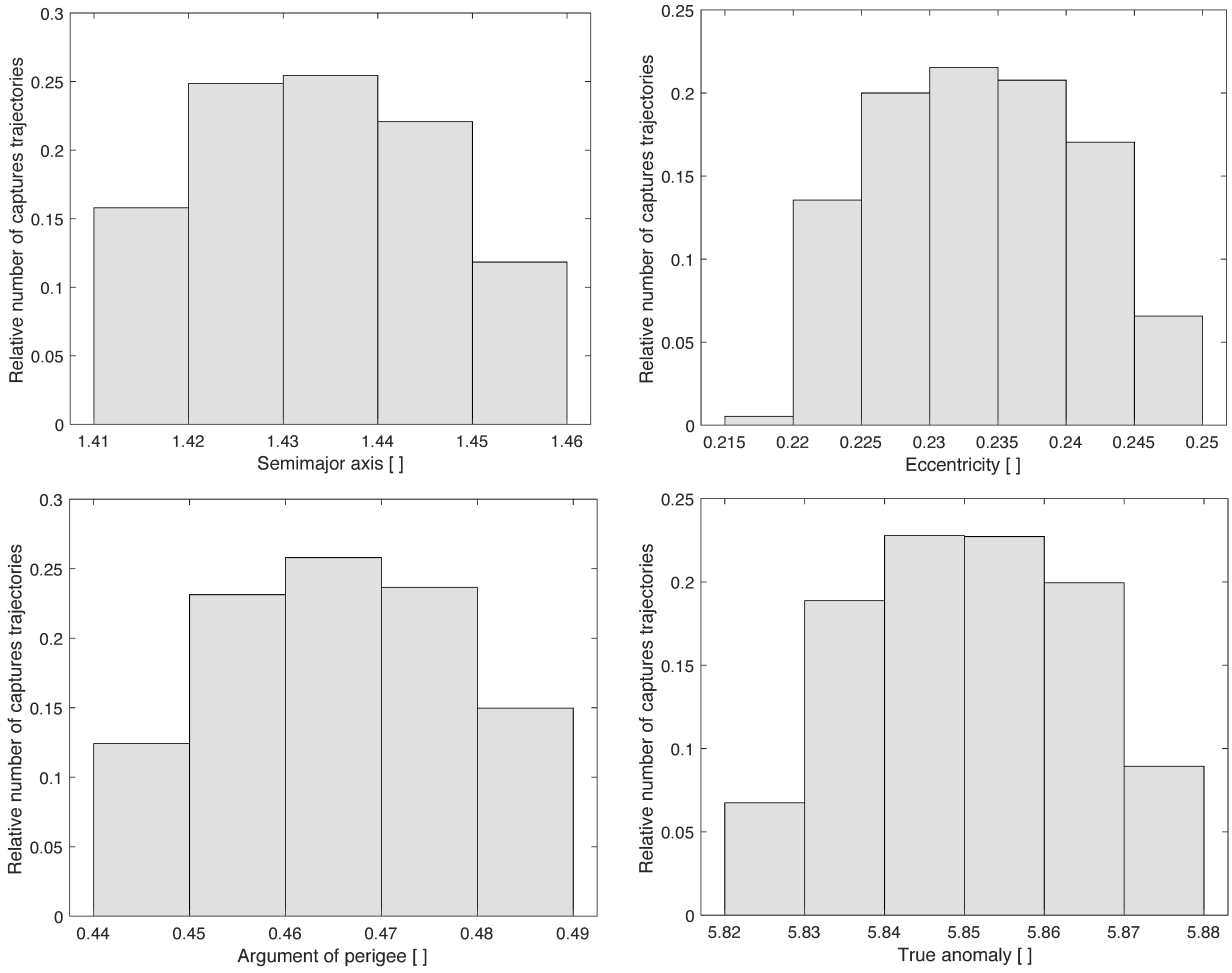

Figure 5.24: Keplerian orbital parameters for orbits inside the internal capture structure (or internal "bubble") for $C_J = C_{J,L2}$. This values are distributed around the value of the external generatrix orbits shown in table 5.2.

value used here is precisely the one computed in L2, but this underestimates the real value giving ZVC still slightly open and not closed as it would be expected to be with such a value.

It has to be noted that these values are equally distributed around the values given in table 5.2.

Besides, the elements of perigee argument and true anomaly are strictly linked between them for all the orbits. In the internal case ω and ν are quite opposites: it is the situation sketched in figure 5.25, where ballistic capture occurs usually when the satellite reaches about 25° before the apoapsis. In the external case ω and ν are quite explementary (the sum is slightly more than 360°): it is the situation sketched in figure 5.26, where ballistic capture occurs usually when the satellite reaches about 25° before the periapsis. Considerations made previously on computations of angles, semi-major axis and eccentricity are still valid.

These results are logical, but they highlight how the ballistic capture could take place only with these particular characteristics, which in all the cases analyzed diverge of only a few degrees from the configurations exposed here. In particular, a rotation of the red orbit in figure occurs, but the

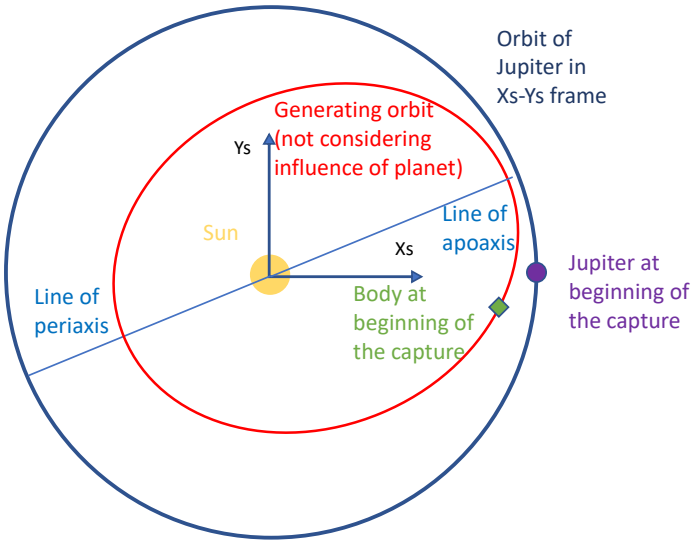

Figure 5.25: Schematic representation of the position of the body in its orbit around the Sun in the moment of the capture for the internal case. The red trajectory would be the one obtained not considering Jupiter's attraction. Coloured signs are linked to the sketched elements in the same colour.

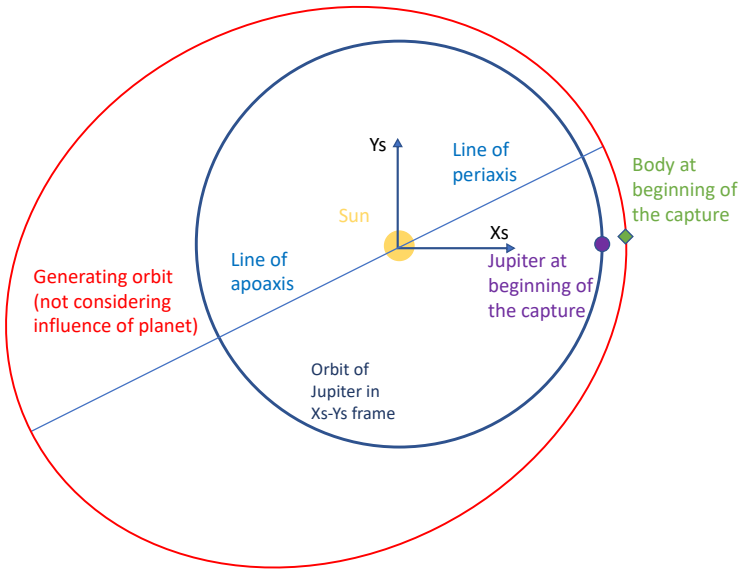

Figure 5.26: Schematic representation of the orbit around the Sun in the moment of the capture for the external case. The red trajectory would be the one obtained not considering Jupiter's attraction. Coloured signs are linked to the sketched elements in the same colour.

position of the beginning of the capture with respect to the apoapsis and periapsis remains substantially fixed.

Obviously, diminishing C_J and so enlarging ZVC and captures structures, the orbits get more variable but they remain meanly the ones analyzed previously. For example, it could be seen that in the internal case where there is a higher number of orbits propagated thanks to the higher dimensions of the gap in ZVC and therefore of the "bubble", also the orbital elements have a wider range of values.

Finally, it has to be underlined that as expected the initial position (where capture begins) for an internal orbit is delayed with respect to the planet. In fact, Jupiter is about 5° forward counterclockwise in the reference frame of the Sun. In addition, the velocity of the satellite is slightly lower (around 5%) than the one of the planet, but the minor length of the path will allow it to recover the lacking phase, entering in proximity of Jupiter. On the contrary, for external orbits initial position is in advance with respect to the planet of about 2° and this difference will be recovered when the keplerian energy relative to the second primary is already negative. The velocity of the satellite is slightly higher (around 5%) than the one of the planet, but

the advantage will be lost thanks to the longer path of the external orbit.

5.7 Examples of trajectories

As introduced at the end of section 5.1.1, in figure 5.1 and in section 5.3, there are different kinds of trajectories found with this search algorithm. Obviously, the most interesting ones are the one which spend a lot of time in capture. The capture structure, also named as "bubble", was computed by selecting only orbits that spend more than 6 Jupiter's months (0.5 years) captured.

5.7.1 Example of trajectory of a long capture

In this section an example of long capture is shown. It lasts about 8.6 Jupiter's years. In figure 5.27 are represented the trajectory in the synodic frame and the keplerian energy relative to the second primary.

5.7.2 Example of a capture exploiting symmetries

Another example of ballistic capture will be represented in figure 5.28, where the property of spatial and temporal symmetry introduced in section 4.6 will be exploited.

In this case, symmetry is applied to an initial position inside the yellow "bubble" of figure 5.3 for $C_J = 3.0378$. In this way it is obtained an initial position mirrored with respect to the x-axis and a reversed time. In other words, changing the sign of $y_{2,0}$ (coordinate of the initial point relative to the second primary) and propagating backwards, a perfectly symmetric orbits to the one with $y_{2,0}$ and forward propagation could be obtained. Therefore, in figure 5.28 the portion of trajectory near Jupiter is obtained by backward (BW) propagation, while the other branch departing from the initial position (square) is obtained by propagating forward (FW) in time. Initial position has $y_{2,0} > 0$.

So a symmetric trajectory (spatially and temporally) to the one in figure 5.28 will give a ballistic capture when propagated forward (FW) and will originate (BW) from a trajectory orbiting the first primary.

These symmetry properties are reminded here because they are considered important to compact the discussion and reduce importantly the number of trajectories to be computed. This halves the computational cost of the search, making possible to study both past and future behaviour of the body by studying a same number of simulation.

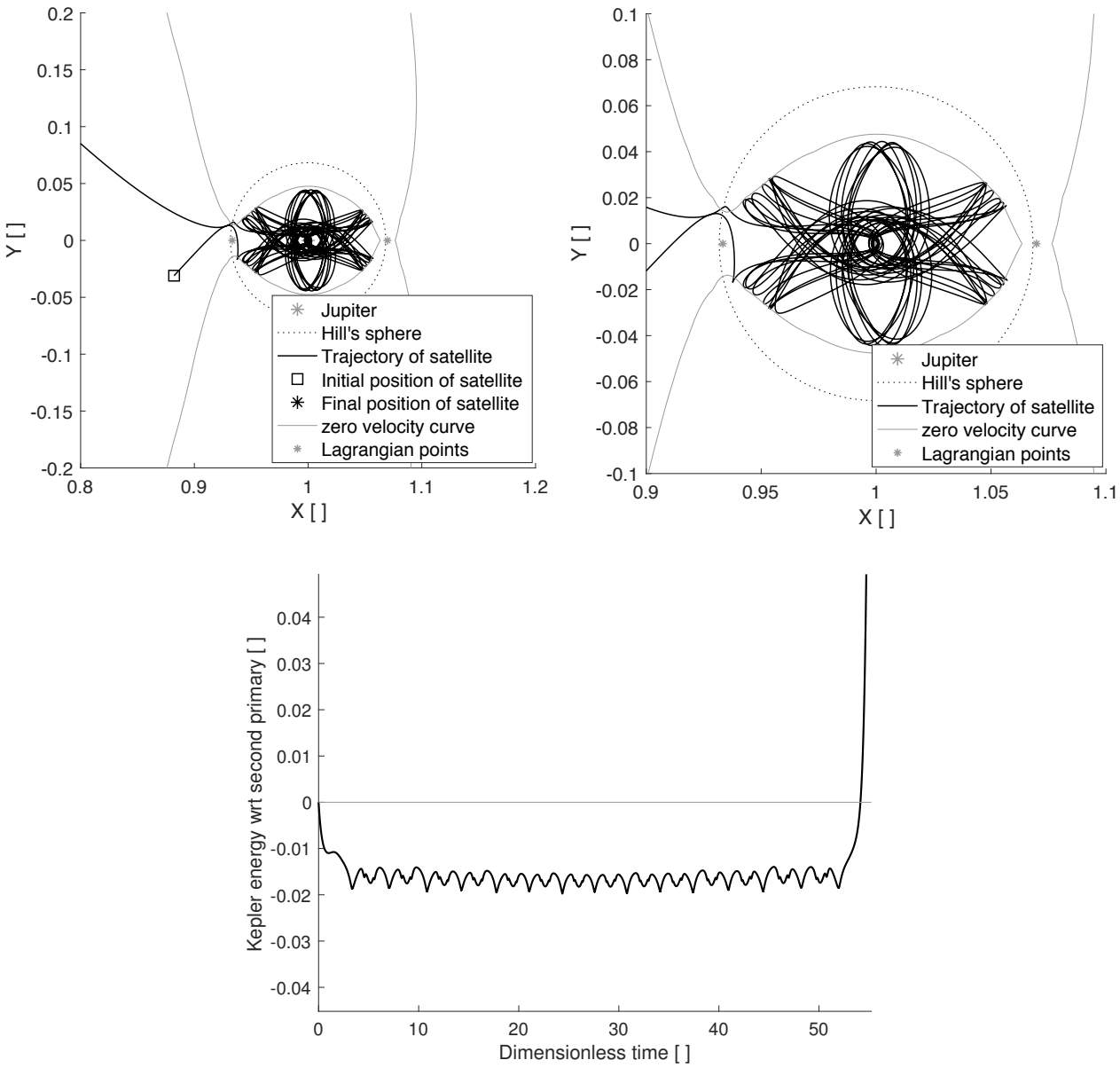

Figure 5.27: Example trajectory in the synodic reference frame where initial position is $x_{2,0} = -0.1178$ and $y_{2,0} = -0.031$. Upper left: trajectory with initial position outside the field of view. Upper right: zoom of the trajectory near the planet. Below: keplerian energy relative to the second primary, which remains negative for almost 8.6 years.

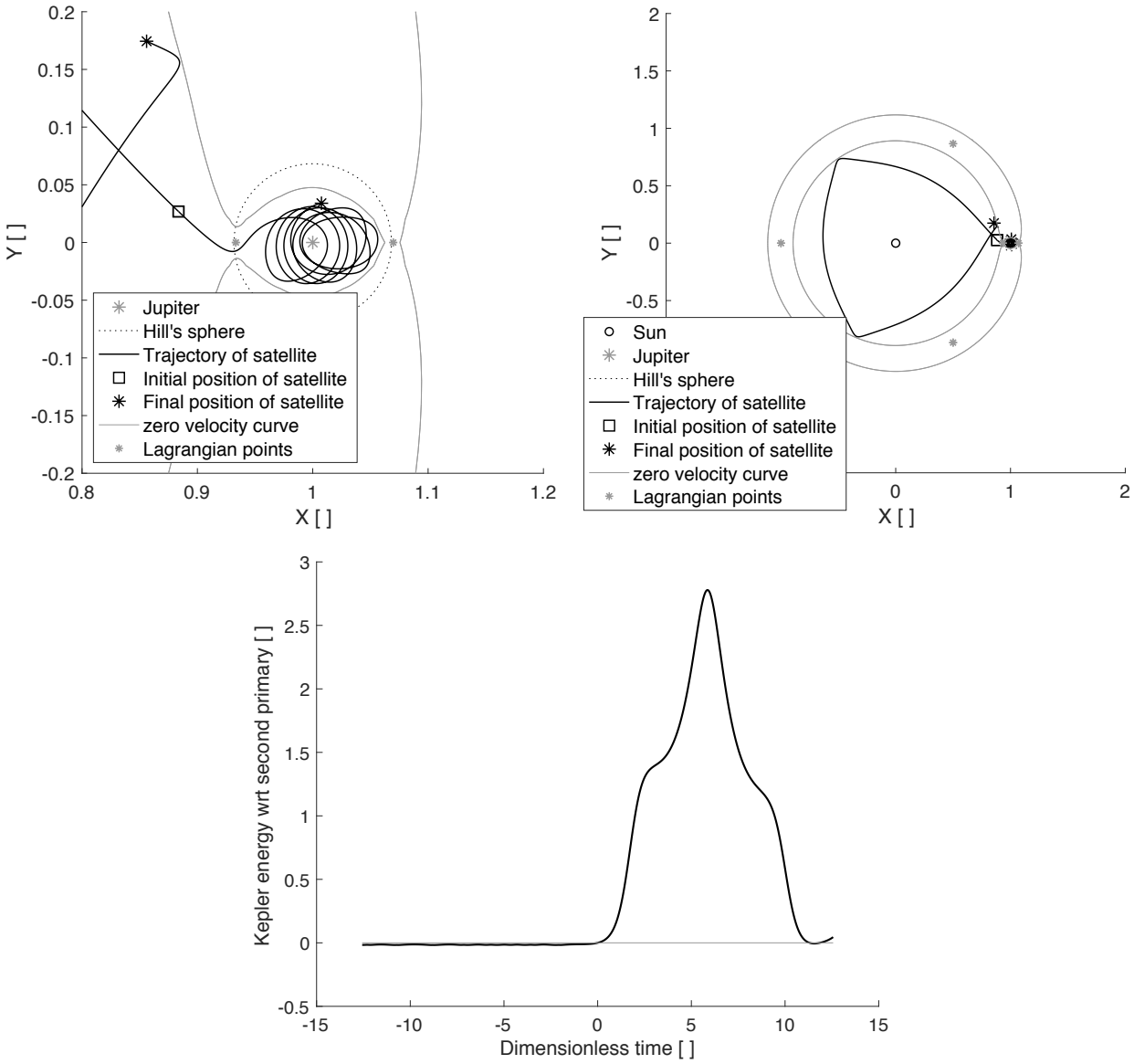

Figure 5.28: Example of symmetric properties. Upper left: detail of trajectory in the synodic frame near the planet. Upper right: overall view of the trajectory in the synodic frame. The branch going from the initial position towards left and orbiting the Sun is the one obtained with FW propagation. Below: keplerian energy relative to the second primary, which remains negative for more than 2 Jupiter's years in negative time. In the positive time it escapes from the capture and after 2 years it returns negative for a short time (relative motion that will be illustrated in the following examples).

5.7.3 Example of brief ballistic capture

An example of a brief ballistic capture is shown in figure 5.29 and it lasts 0.85 Jupiter's years. This trajectory enters the Hill's sphere and has negative keplerian energy with respect to the second primary, but only for a relatively short time. In this case, the orbit could be considered a mere flyby.

5.7.4 Example of relative motion around L1

An example of a very short capture is shown in figure 5.30 and it lasts 0.49 Jupiter's years. This trajectory barely enters the Hill's sphere and has negative keplerian energy with respect to the second primary, but only for a very short time. In fact, it makes only a revolution around L1 and immediately leaves, so it could be excluded from the ballistic captures. This is the reason why ballistic captures are found only for capture times higher than 0.5 years.

5.7.5 Example of relative motion distant from the planet

Another example of relative motion very brief is the one shown in figure 5.31 and it lasts only 0.24 Jupiter's years. Here the trajectory does not enter in the Hill's sphere, but it has negative keplerian energy relative to the planet for a very short time. In fact, it is a trajectory that has nothing to do with a ballistic capture, because the relative velocity is low only when the body is too far from the gaps in the ZVC near the Lagrangian points.

It is important to underline that this particular motion occurs also further away from the planet than represented here. The result is the one obtained in figure 5.1, where the majority of the half moon area is coloured in dark blue representing this kind of orbits.

5.7.6 Example of trajectory inside the drop of the "bubble"

An example of a trajectory beginning inside the capture structure (or "bubble") of figure 5.3 with $C_J = 3.0357$ (hence a low value of the Jacobi constant) is shown in figure 5.32.

This is a very short capture that lasts only 0.47 Jupiter's years. The trajectory enters Hill's sphere and has a negative keplerian energy relative to the planet, but only for a brief time span. In fact, it revolves only once around the planet in the synodic frame and it is immediately expelled. Hence, it is not considered in the ballistic capture found with the presented algorithm because it is under the imposed limit of 0.5 Jupiter's years.

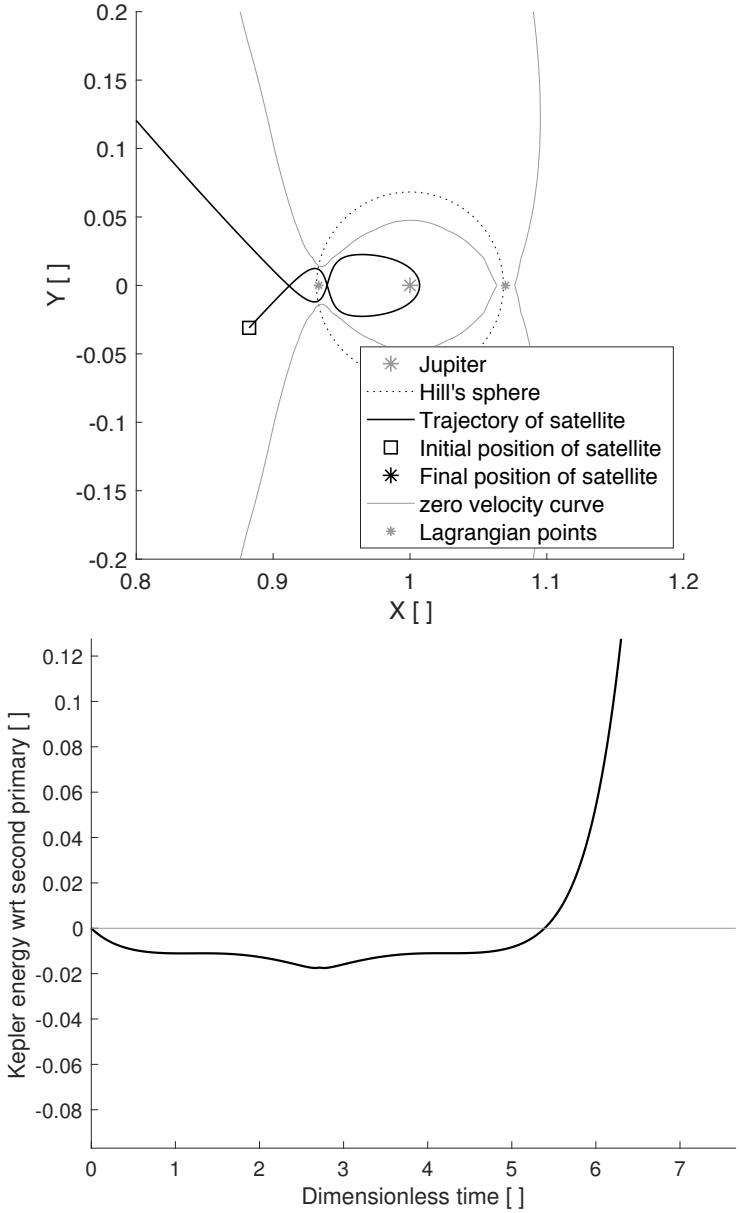

Figure 5.29: Example trajectory where ballistic capture is brief, of about 0.85 Jupiter's years. Above: detail of the trajectory near the planet with initial position, projection of the Hill's sphere, ZVC and Lagrangian points L1 and L2. Below: keplerian energy relative to the second primary.

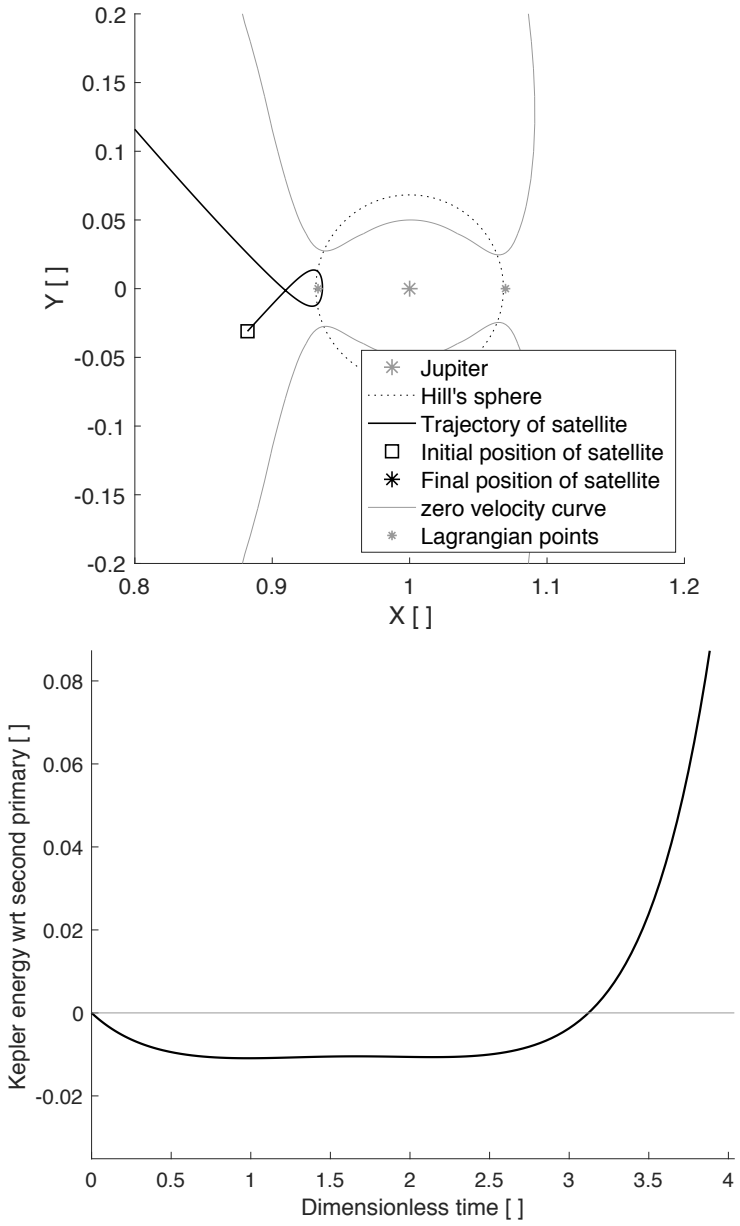

Figure 5.30: Example trajectory where ballistic capture is very short, of about 0.49 Jupiter's years. In fact it will not be considered as a ballistic capture, but a mere peculiar relative motion around L1. Above: detail of the trajectory near the planet with initial position, projection of the Hill's sphere, ZVC and Lagrangian points L1 and L2. Below: keplerian energy relative to the second primary.

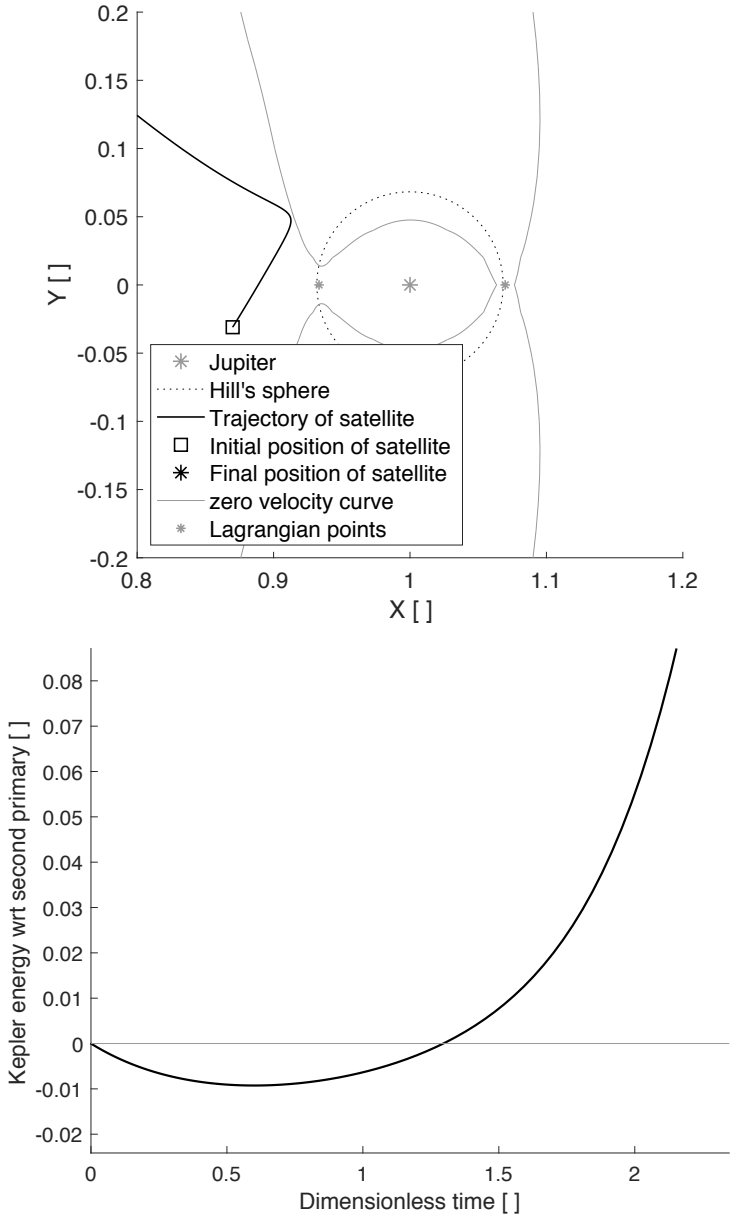

Figure 5.31: Example trajectory where keplerian energy lasts about 0.24 Jupiter's years. In fact it will not be considered a ballistic capture, but a mere relative motion far from the planet and its Hill's sphere. Above: detail of the trajectory near the planet with initial position, projection of the Hill's sphere, ZVC and Lagrangian points L1 and L2. Below: keplerian energy relative to the second primary.

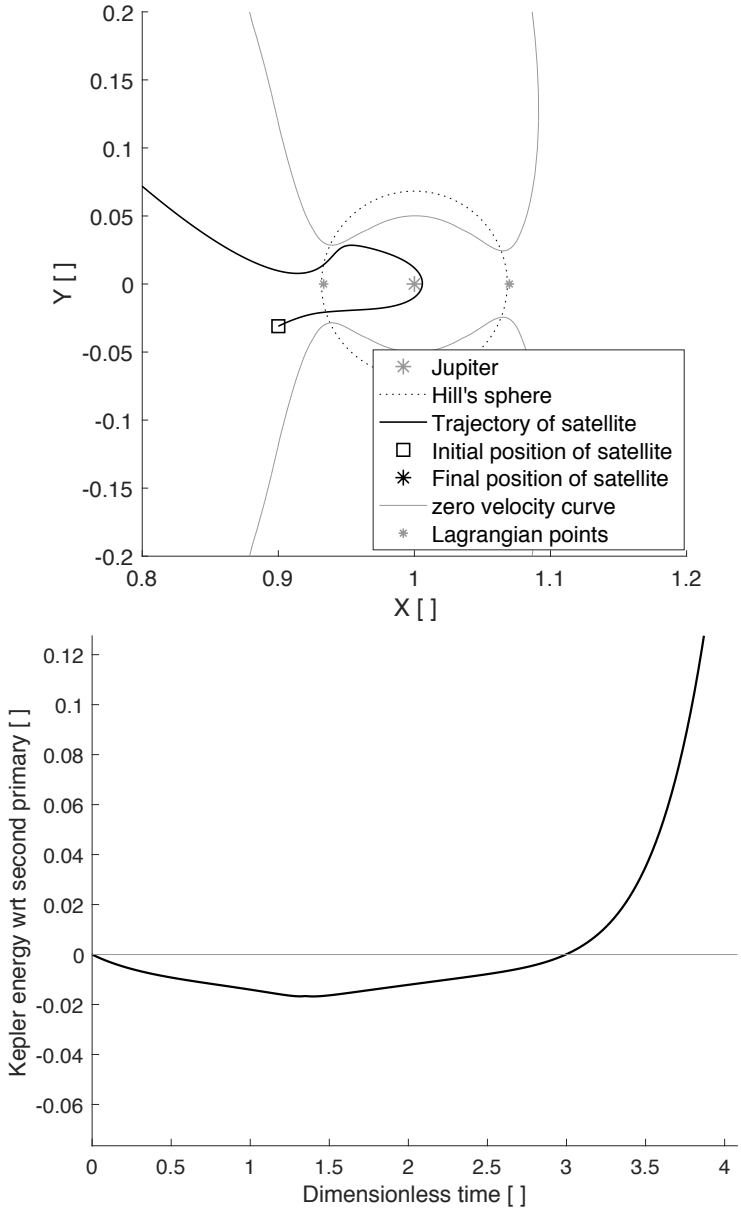

Figure 5.32: Example trajectory inside the capture structure ("bubble") of figure 5.3 where keplerian energy lasts about 0.47 Jupiter's years. In fact it will not be considered a ballistic capture, but a mere relative motion far from the planet and its Hill's sphere. Above: detail of the trajectory near the planet with initial position, projection of the Hill's sphere, ZVC and Lagrangian points L1 and L2. Below: keplerian energy relative to the second primary.

Chapter 6

Results of the search for Mars

In the same way as developed for the Sun-Jupiter system, in this chapter the Sun-Mars system will be analyzed.

For a better understanding of the search and of results obtained, table 6.1 is presented. It contains the values of the Jacobi constant in the Lagrangian points.

Analogously to Sun-Jupiter system, collisions are never found for high values of the Jacobi constant.

6.1 Capture structures for various values of high C_J

Diagrams for the search of the captures obtained with both internal and external initial position for different values of Jacobi constant C_J in figure 6.1 are ordered from left to right and from above to below: $C_J = 3.00020259 = C_{J,L1} - 10^{-7}$, $C_J = 3.00020228 = \frac{C_{J,L1} + C_{J,L2}}{2}$, $C_J = 3.00020196 = C_{J,L2} - 10^{-7}$ and $C_J = 3.00020156 = C_{J,L2} - 5\ 10^{-7}$. Last two values create both "bubbles" internal and external to the conjunction of the primaries.

From figure 6.1 it is clear that when C_J decreases the gaps of ZVC and as a consequence the bubble get bigger. Also the colour of this last one changes.

Table 6.1: Approximated values of the Jacobi constant in the Lagrangian points. Values are obtained with equation 4.1.

Lagrangian point	L1	L2	L3	L4	L5
Jacobi constant C_J [ ]	3.00020249	3.00020206	3.00000032	2.99999968	2.99999968

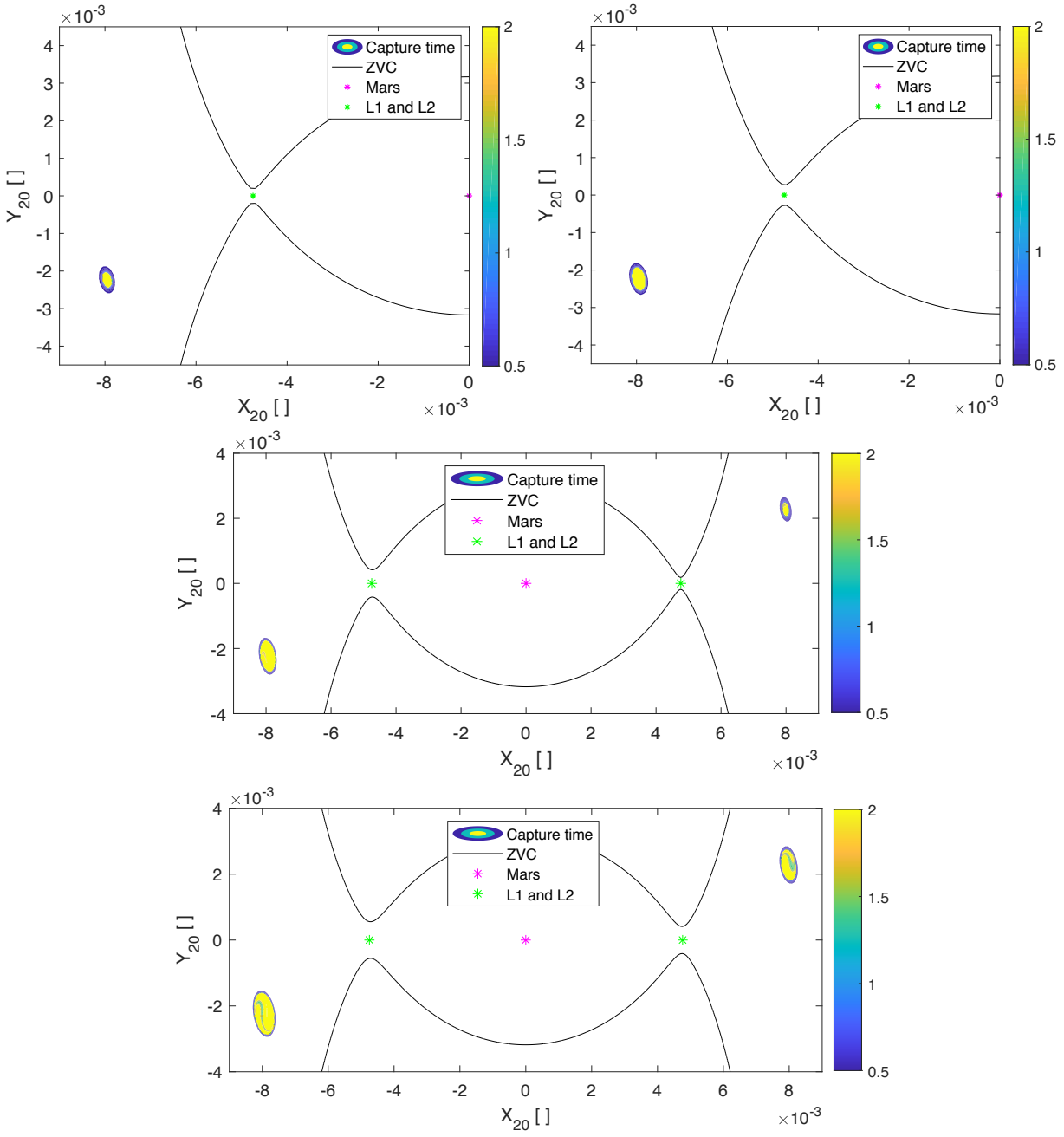

Figure 6.1: Results of the search for ballistic captures by Mars with different values of the Jacobi constant. The $X_{20} - Y_{20}$ plane represented is referred to the Cartesian inertial frame centered in the second primary

For high Jacobi it is completely yellow indicating a long capture, while for lower values of the Jacobi constant it becomes mostly blue indicating shorter captures or even trajectories of flybys.

6.2 Topology of the structures obtained

Bubbles obtained with this method have always an elliptic shape and it is interesting to analyze the change of this shape as a function of the Jacobi constant. This comparison in shown in figure 6.2, where all structures stretch out from a central point that is contained in all of them. Characteristics of the central point sill be further analyzed in section 6.3. For what concerns the structures, they enlarge with the reduction of the Jacobi constant and therefore with the increase of the gaps in the ZVC near the Lagrangian points. This result is visible thanks to the fact that ZVC are plotted in the same colour of the bubble obtained with the same value of C_J.

For what concerns the structures, they enlarge with the reduction of the Jacobi constant and therefore with the increase of the gaps in the ZVC near the Lagrangian points. This results is visible thanks to the fact that ZVC are plotted in the same colour of the bubble obtained with the same value of C_J.

6.3 Analysis of generatrix orbits of the capture structures

An interesting study is to characterize the orbit that will be named "generatrix". This is the orbit obtained by finding the maximum value of C_J for which ZVC are still open. In this case ZVC will be almost closed, leaving only a little hole for the entrance in proximity of the second primary. This is obviously possible in both internal and external region, when the value of the Jacobi constant tends to $C_{J,L1}$ or $C_{J,L2}$ respectively. In this last case ZVC on the right will be almost closed, but on the left they will be completely open. But this fact will not influence at all the analysis because the region of interest in the one on the right near L2.

6.3.1 Method and initial parameters

The keplerian orbital elements summarized in table 6.2 (together with the relative value of the Jacobi constant used in the Matlab scripts) are evaluated in the inertial reference frame of the first primary. They are the elements

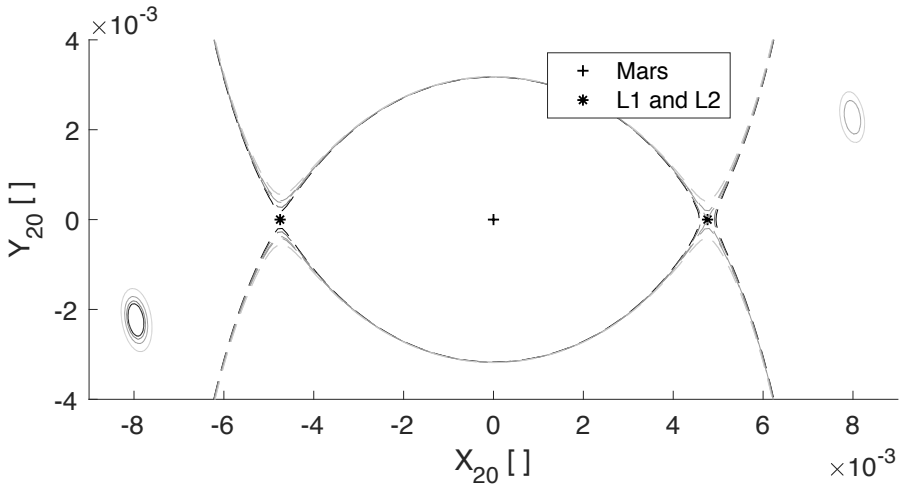

Figure 6.2: Analysis of the topology of "bubble" structures containing the initial positions that conducts to ballistic capture. Their dimensions increase and ZVC gaps grow bigger with the reduction of C_J. This trend is shown using the black colour fading into light gray. The gap of the ZVC in L2 opens up and the external bubbles appear only with the last two values of the Jacobi constant.

of the orbit around the Sun in the instant when the satellite is captured by Mars, hence the keplerian energy relative to the planet is null.

In table 6.3 initial coordinates used in Matlab simulations for the generatrix orbits are shown. These coordinates are taken in the inertial system of reference centered in the second primary or in the synodic centered in the first primary for both internal and external case. In this case and in the research previously exposed *Ode113* was used due to its lighter computations (as shown in chapter 1) with absolute and relative tolerances set to 10^{-12}. Other parameters (masses and reference radius) used in the simulations are

Table 6.2: Keplerian orbital elements (semi-major axis a, eccentricity e, perigee argument ω and true anomaly ν) of the internal and external generatrix orbits and relative numerical value of the Jacobi constant for these valued.

	a [ ]	e [ ]	ω [ ]	ν [ ]	C_J [ ]
Internal orbit	0.9790033	0.0146810	-2.7174643	2.7151963	$C_{J,L1} + 2\ 10^{-9}$
External orbit	1.0218821	0.0149045	0.4295923	5.8558549	$C_{J,L2} + 5\ 10^{-10}$

Table 6.3: Initial coordinates used in Matlab simulations for internal and external generatrix orbits. On the left, the first two columns are taken in the inertial reference frame centered in the second primary. On the right, the following two columns, are taken in the synodic frame in curvilinear coordinates. The last two columns are the distance of the initial point of these orbits from Mars, respectively dimensionless and measured in Hill's sphere radii.

	$X_{2,0}$ [ ]	$Y_{2,0}$ [ ]	ρ_0 [ ]	θ_0 [ ]	d_2 [ ]	d_2 [r_{Hill}]
Internal orbit	-0.00795	-0.00225	-0.008097	-0.002520	0.008477	1.78243
External orbit	0.00798	0.00228	0.007983	0.002262	0.008299	1.74506

Table 6.4: Parameters used in the simulations for Mars: mass of the Sun M_{Sun}, mass of Mars M_{Mars} and radius of its orbit around the Sun R_{ref}.

M_{Sun} [kg]	M_{Mars} [kg]	R_{ref} [km]
$1.988499251 \cdot 10^{30}$	$6.41714114 \cdot 10^{23}$	$227.9 \cdot 10^{6}$

summarized in table 6.4.

- It has to be underlined that the orbit presented here is the one obtained not considering (only in this moment) the gravitational attraction given by Mars. Obviously, the propagation on the whole requires this contribution to find the moment when the ballistic capture begins.

  But in this way results represent only conditions at the instant of beginning of the capture, not the effective provenience of the trajectory, which is deflected also before this moment. In the next sections this point will be discussed separately for internal and external orbits.

- Being in a planar case it is not useful to consider right ascension of ascending node Ω and inclination i of the orbits, so they will be considered always null. In the results only the other four parameters will be shown.

- In this particular case the conditions of capture are particularly strict and only a representative orbit will be analyzed. Regardless how much the value of $C_{J,L1}$ is accurate, there are always infinite orbits all concentrated around a single point.

  The distinctive feature used to show the resulting characteristics is that everyone of the infinite orbits obtained has the same parameters of the one displayed in the following section, that is with an accuracy up to the seventh decimal point.

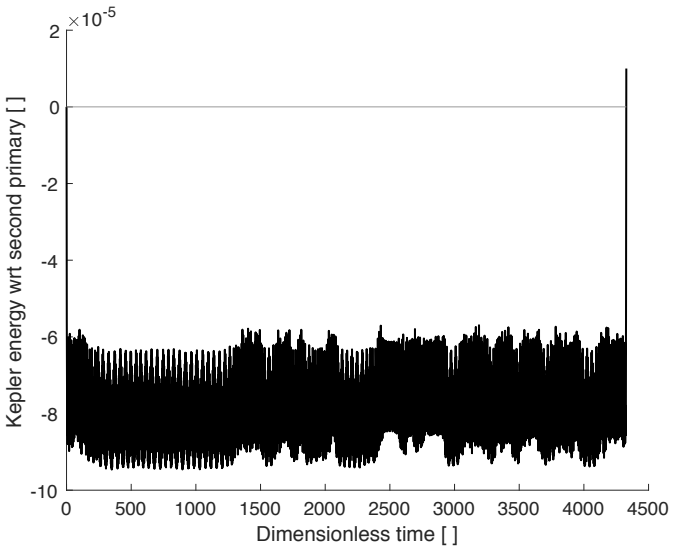

Figure 6.3: Internal generatrix Keplerian energy with respect to the planet for a time span of 689 Martian years from the beginning of the capture. The dimensionless energy is computed in the inertial reference frame centered in the second primary and it remains negative for the whole duration of the simulation

6.3.2 Diagrams and duration of the internal generatrix orbit

In this section interesting figures and parameters for the internal generatrix orbit will be shown. The initial conditions for this orbit were presented in tables 6.2 and 6.3.

In figure 6.3 it is represented the keplerian energy relative to Mars for a time span of 689 Martian years. All along this energy is negative and this indicates a very important capture, long about 689 years. That could be explained by considering the very small gap existing in the ZVC, which quite impede to enter or exit from the area in proximity of the planet.

In figures 6.4, 6.5, 6.6 and 6.7 is represented the trajectory of this peculiar orbit. First two figures (6.4 e 6.5) are taken in the synodic frame: the first is a complete view and a zoom around the planet; the second shows an additional zoom near the planet and a detail of the passage in the gap of L1. The last two figures (6.6 e 6.7) represent the orbit in the Cartesian inertial reference frame centered respectively in the first and the second primary.

Total duration of the simulation is 4 years, 2 in backward propagation (BW) and 2 in forward propagation (FW).

The transition to entry in the area near the planet lasts about 6 Martian

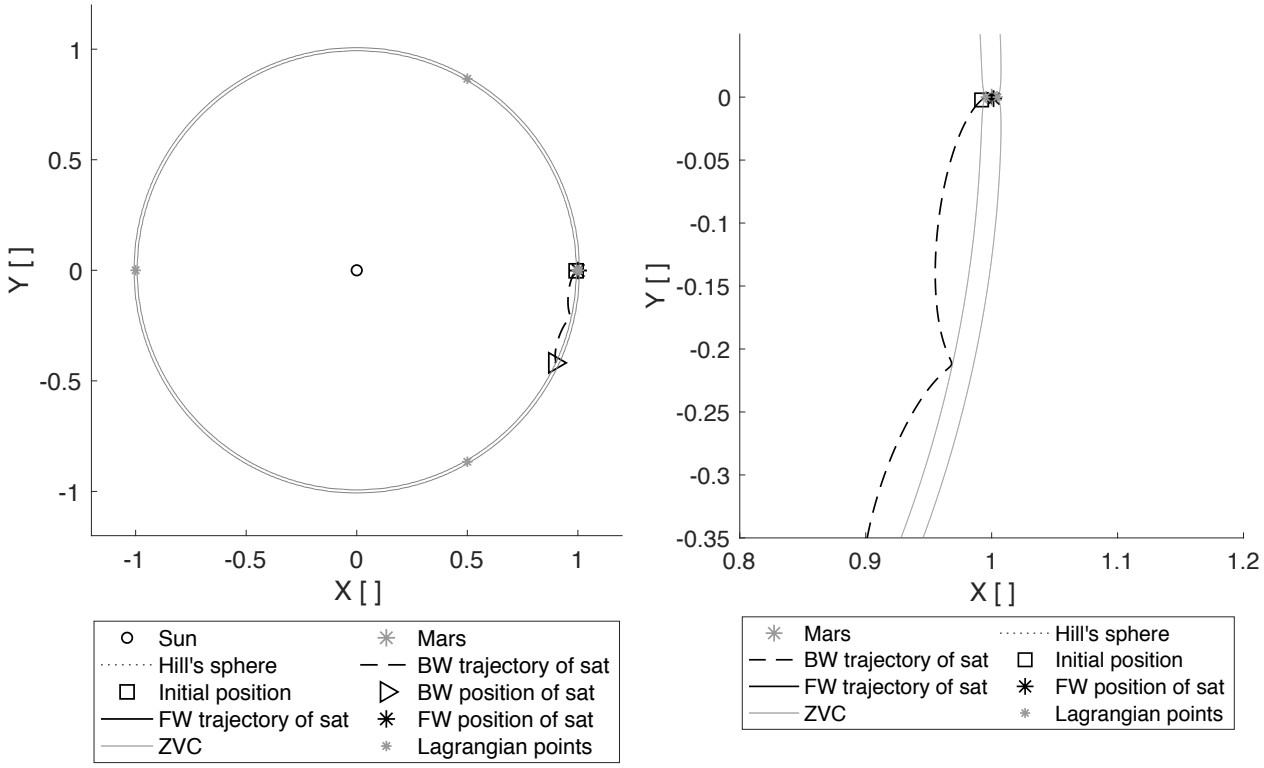

Figure 6.4: Internal generatrix trajectory of the satellite (sat) in the synodic frame centered in the Sun. On the left, the overall view; on the right, a zoom of the area containing Mars. The trajectory propagated backward in time (BW) is dashed. Initial point of the propagation is represented by a square.

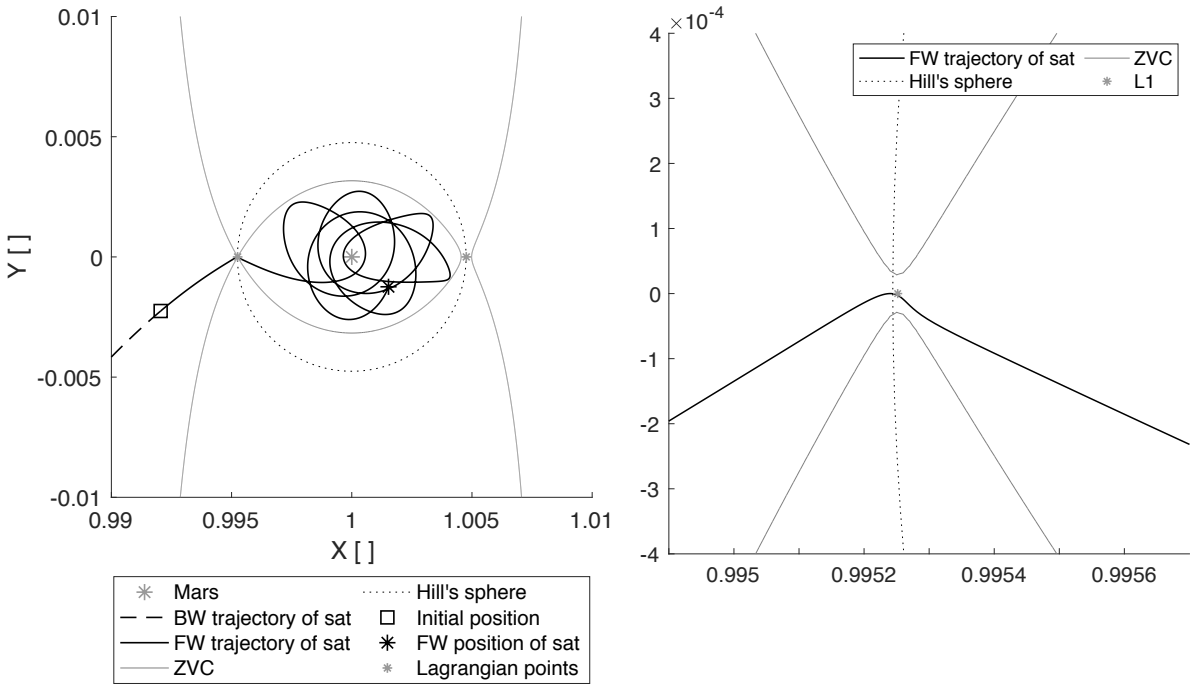

Figure 6.5: Internal generatrix trajectory in the synodic frame centered in the Sun. From left to right, additional zoom near planet and detail of the passage between the ZVC near L1.

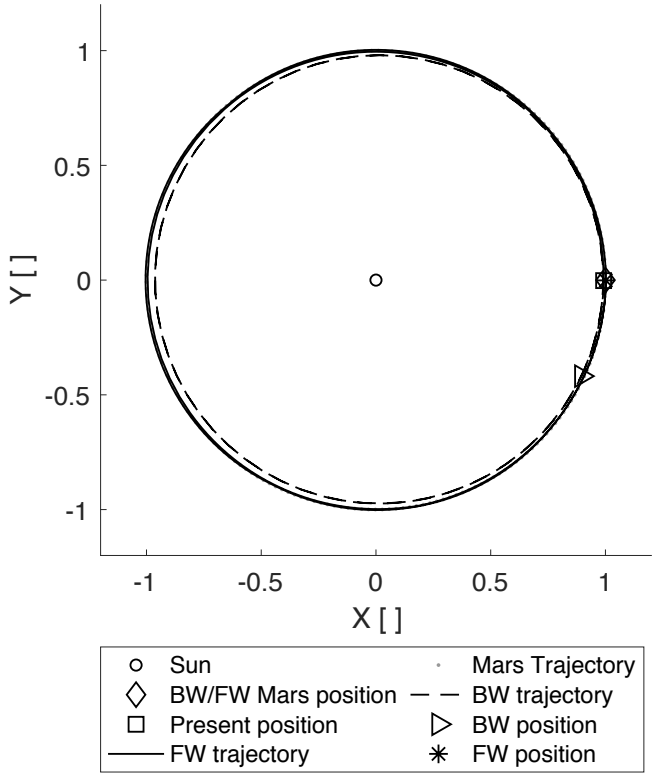

Figure 6.6: Internal generatrix trajectory in the inertial frame centered in the Sun.

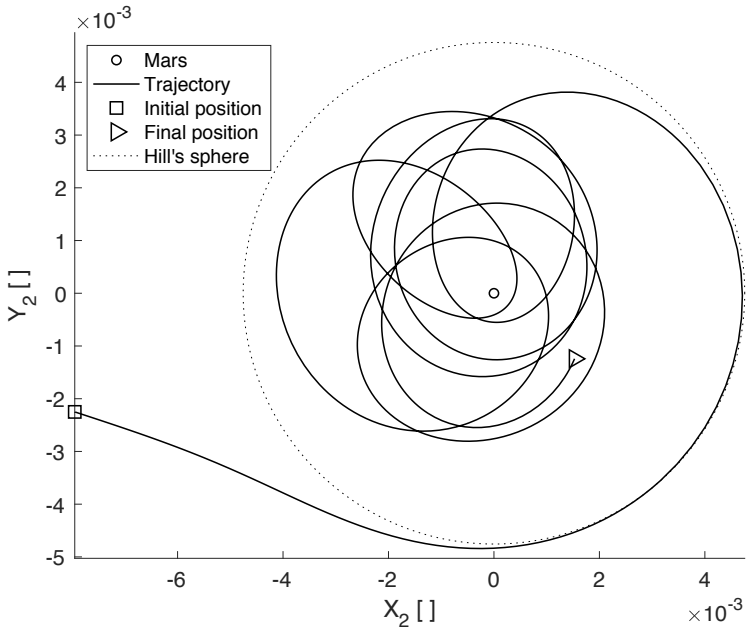

Figure 6.7: Internal generatrix trajectory in the inertial frame centered in Mars.

months. This feature is particularly visible in figure 6.7, where the trajectory covers quite half a circle near the Hill's sphere. Here relative velocities are very small and for this reason in the synodic frame the trajectory is almost still in proximity of the Lagrangian point L1.

In the inertial frame centered in the Sun (figure 6.6) this feature is visible between the square of the initial position and the moment when the trajectory begins to be diverted by the planet. In fact, between these two moments there is half circle in which the orbit slowly gets nearer to Mars' orbit.

Unfortunately, these details are barely visible in the case of Mars, because of the less importance in terms of mass of this second primary body. This feature takes to a packing of the characterising points near the planet and so they are not visible without any zoom in the diagrams.

6.3.3 Variation of orbital elements for internal generatrix

In figures 6.8, 6.9 and 6.10 the values of keplerian orbital elements a, e and ω are presented as a function of the distance of the body from the second primary. Besides, here semi-major axis a, eccentricity e and perigee

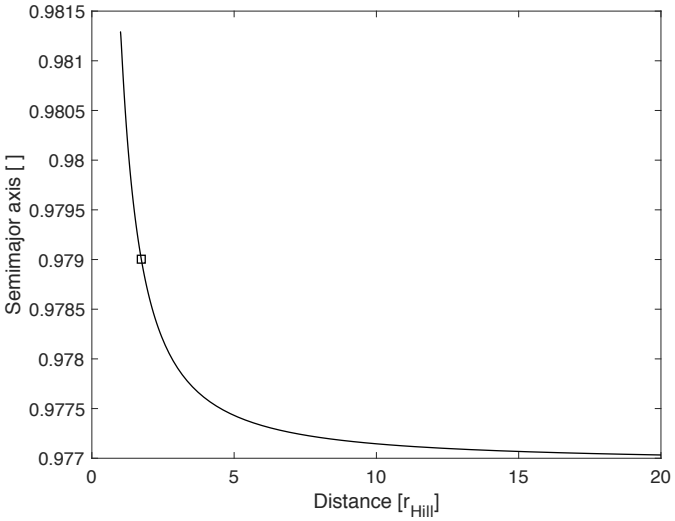

Figure 6.8: Semi-major axis of the internal generatrix computed in the inertial system of reference centered in the Sun. Its variation is shown as a function of the distance from the second primary in Hill's radii. The square indicates the moment when the capture begins. On its left there are the values for the FW propagation, nearer to the second primary; on the right there are the values for the BW propagation, where the body gets further from the planet.

argument ω are given for the internal generatrix orbit: $a = 0.97702$, $e = 0.01456$ and $\omega = -2.9048$. These values are taken in the figures mentioned above, where the plotted parameters tend to be steady. On the contrary to Jupiter's case, they have a negligible difference with the ones presented in table 6.2 obtained in the instant of beginning of the capture.

6.3.4 Diagrams and duration of the external generatrix orbit

In this section interesting figures and parameters for the external generatrix orbit will be shown. The initial conditions for this orbit were presented in tables 6.2 e 6.3.

In figure 6.11 is represented the keplerian energy relative to Mars for a time span of 26.5 Martian years. All along this energy is negative and this indicates a very important capture, long longer than 26 Martian years. In figure is also shown the trajectory in the proximity of the planet with the detail of closed ZVC in L2 slightly more open in L1.

The difference between the gap in L1 and the one in L2 depends on the mass ratio μ. In this case it is very small, hence this difference is very tiny.

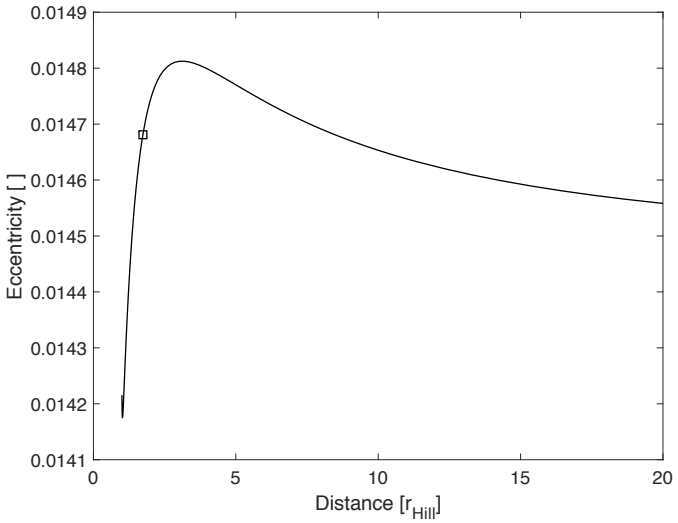

Figure 6.9: Eccentricity of the internal generatrix in the inertial system of reference centered in the Sun. Its variation is shown as a function of the distance from the second primary in Hill's radii. The square indicates the moment when the capture begins.

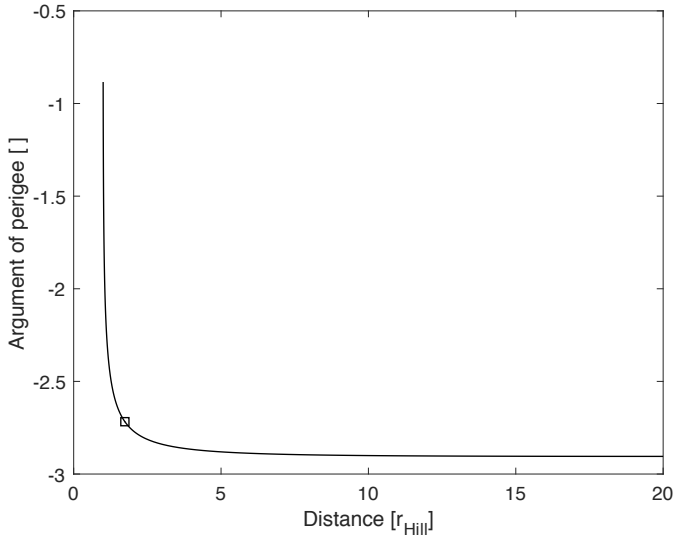

Figure 6.10: Perigee argument of the internal generatrix in the inertial reference centered in the Sun. Its variation is shown as a function of the distance from the second primary in Hill's radii. The square indicates the moment when the capture begins.

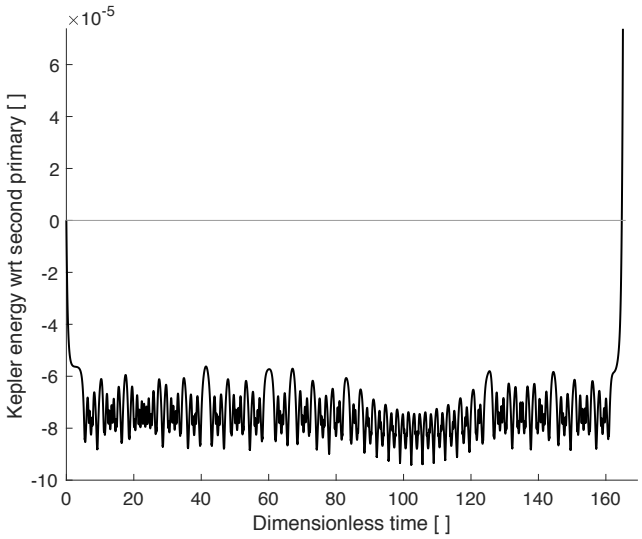

Figure 6.11: External generatrix Keplerian energy relative to the second primary for 26.5 Martian years from the beginning of the capture.

For this reason and thanks to the particular value of C_J studied, a trajectory entering by the gap of L2 stays longer in orbit near the planet. It is more difficult for it to exit from the narrow gap in L1.

In figures 6.12, 6.13, 6.14 and 6.15 is represented the trajectory of this peculiar orbit. First two figures (6.12 and 6.13) are taken in the synodic frame: the first is a complete view and a zoom around the planet; the second shows an additional zoom near the planet and a detail of the passage in the gap of L2. The last two figures (6.14 and 6.15) represent the orbit in the Cartesian inertial reference frame centered respectively in the first and the second primary.

Total duration of the simulation is 4 years, 2 in backward propagation (BW) and 2 in forward propagation (FW).

The transition to entry in the area near the planet lasts about half Martian year. This feature is particularly visible in figure 6.15, where the trajectory covers about half circle near the Hill's sphere. Here relative velocities are very small and for this reason in the synodic frame the trajectory is almost still in proximity of the Lagrangian point L2.

In the inertial frame centered in the Sun (6.14) this feature is visible between the square of the initial position and the moment when the trajectory begins to be diverted by the planet. In fact, between these two moments

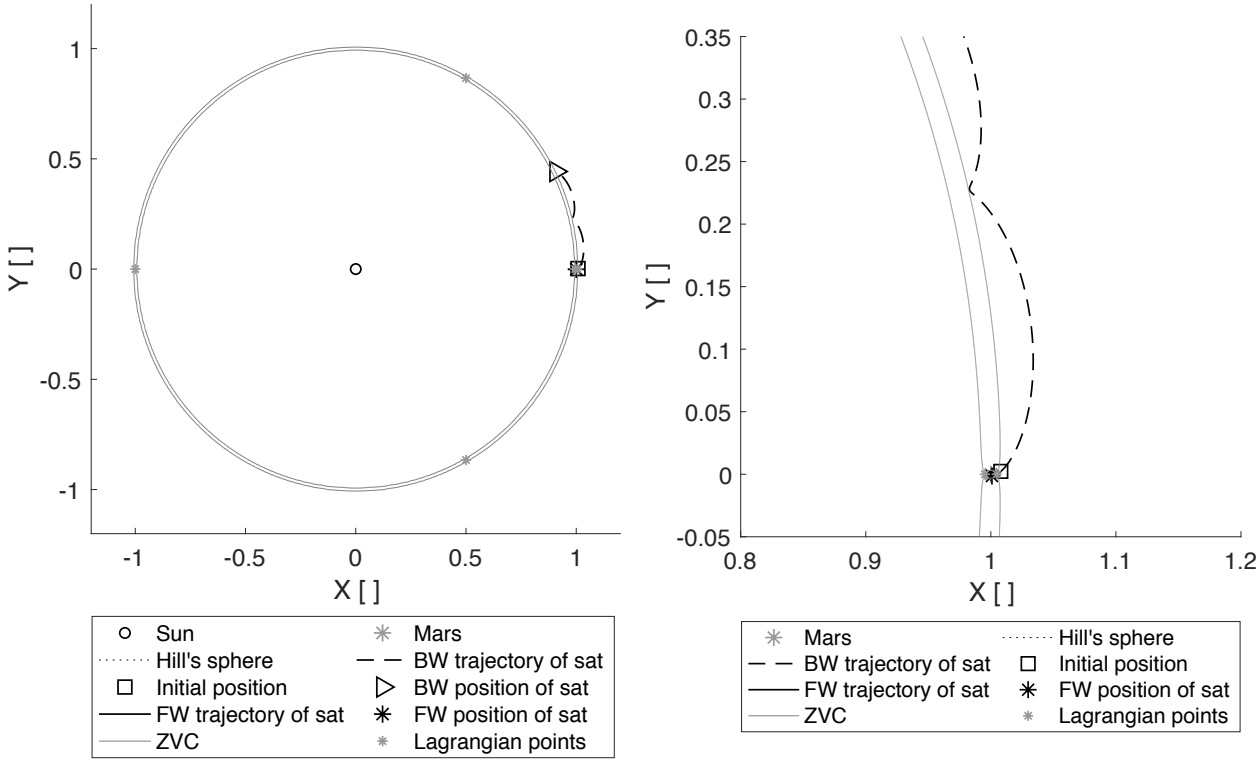

Figure 6.12: External generatrix trajectory of the satellite (sat) in the synodic reference frame centered in the Sun. On the left, the overall view; on the right, a zoom of the area containing Mars. The trajectory propagated backward in time (BW) is dashed. Initial point of the propagation is represented by a square.

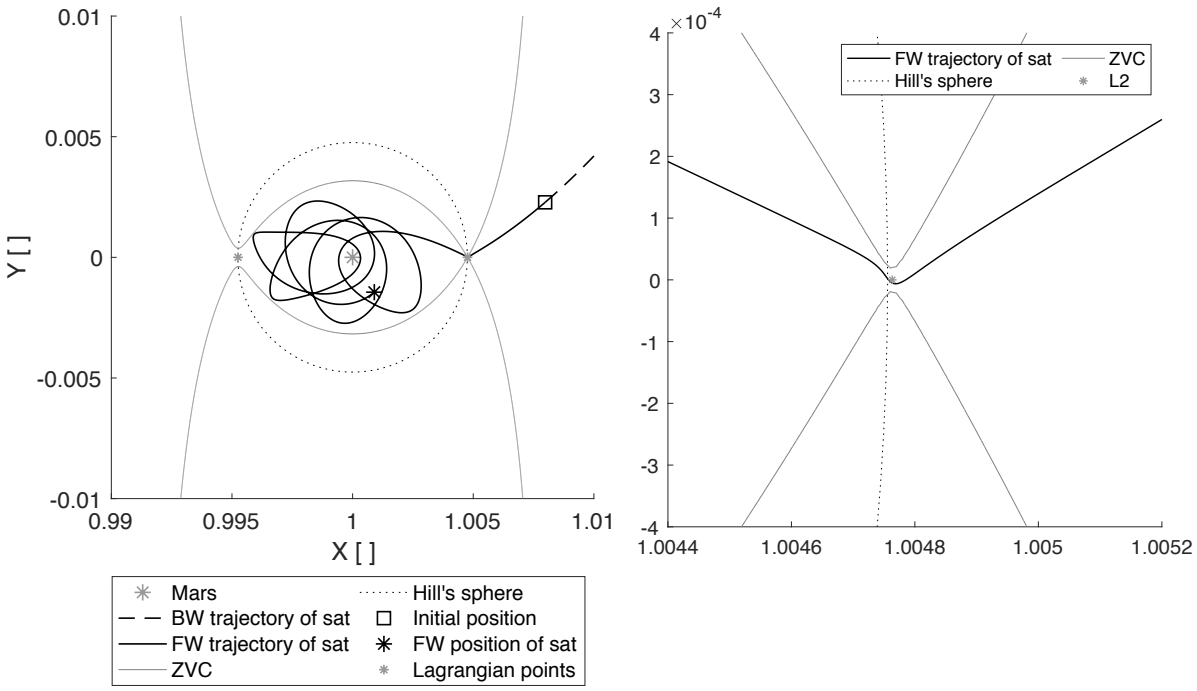

Figure 6.13: External generatrix trajectory in the synodic frame centered in the Sun. From left to right, additional zoom near Mars and detail of the passage between the ZVC near L2.

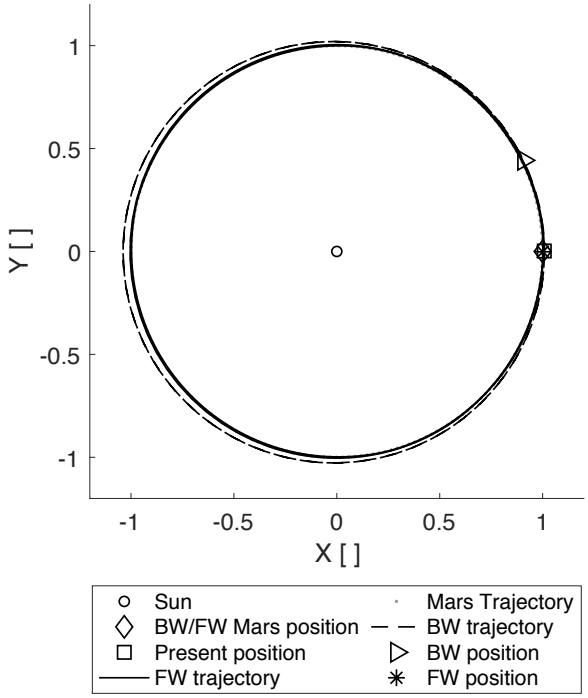

Figure 6.14: External generatrix trajectory in the inertial reference frame centered in the Sun.

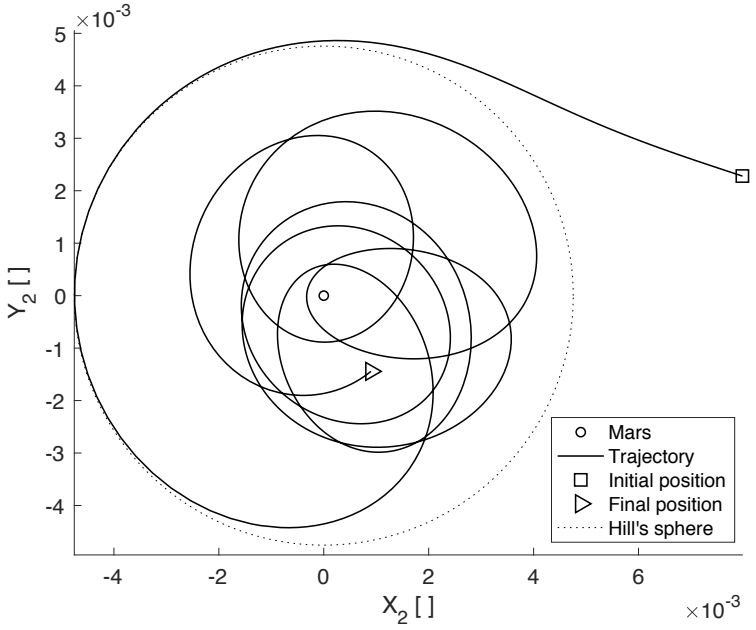

Figure 6.15: External generatrix trajectory in the inertial reference frame centered in Mars.

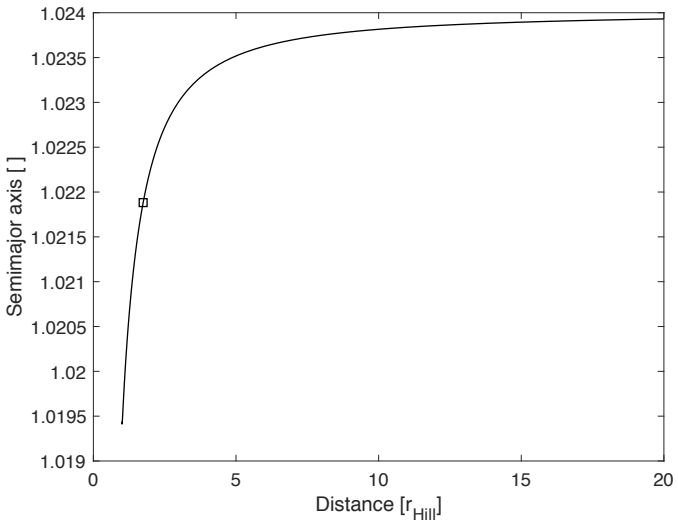

Figure 6.16: Semi-major axis of the external generatrix orbit computed in the inertial system of reference centered in the Sun. Its variation is shown as a function of the distance from the second primary in Hill's radii. The square indicates the moment when the capture begins. On its left there are the values for the FW propagation, nearer to the second primary; on the right there are the values for the BW propagation, where the body gets further from the planet.

there is half circle in which the orbit slowly gets nearer to Mars orbit.

Unfortunately, these details are barely visible in the case of Mars, because of the less importance in terms of mass of this second primary body. This feature takes to a packing of the characterising points near the planet and so they are not visible without any zoom in the diagrams.

6.3.5 Variation of orbital elements for external generatrix

In figures 6.16, 6.17 and 6.18 the values of keplerian orbital elements a, e and ω are presented as a function of the distance of the body from the second primary. Besides, here semi-major axis a, eccentricity e and perigee argument ω are given for the external generatrix orbit: $a = 1.0239$, $e = 0.0148$ and $\omega = 0.2414$. These values are taken in the figures mentioned above, where the plotted parameters tend to be steady. On the contrary to Jupiter's case, they have a negligible difference with the ones presented in table 6.2 obtained in the instant of beginning of the capture.

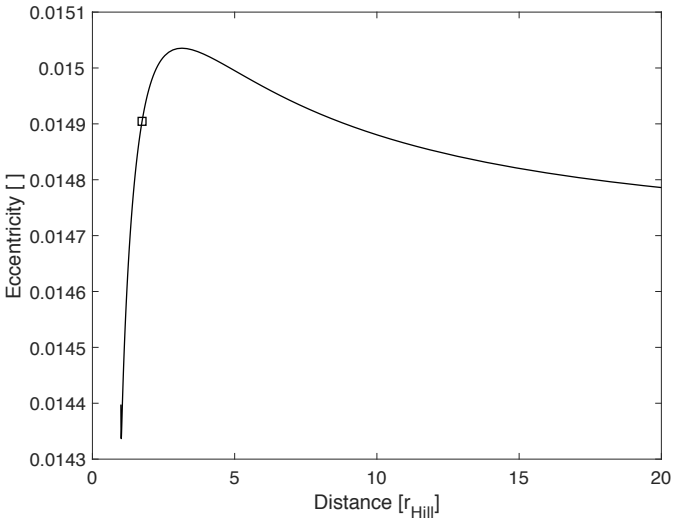

Figure 6.17: Eccentricity of the external generatrix orbit computed in the inertial system of reference centered in the Sun. Its variation is shown as a function of the distance from the second primary in Hill's radii. The square indicates the moment when the capture begins.

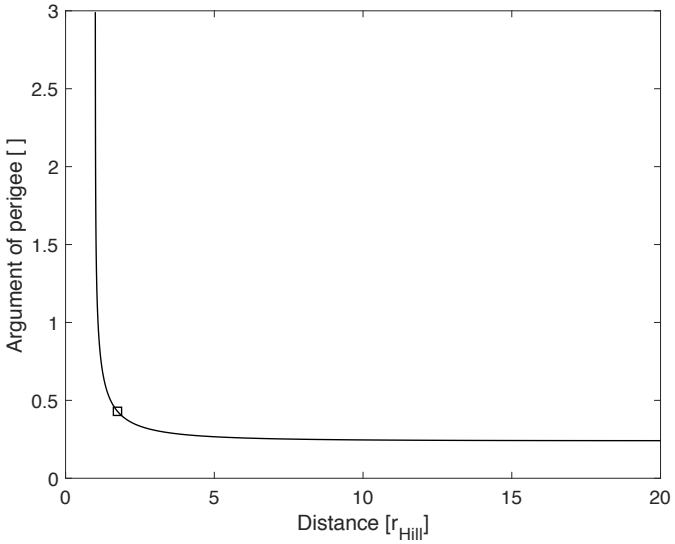

Figure 6.18: Perigee argument of the external generatrix orbit computed in the inertial system of reference centered in the Sun. Its variation is shown as a function of the distance from the second primary in Hill's radii. The square indicates the moment when the capture begins.

6.4 Keplerian orbital elements in the capture structure

In the same way for keplerian orbital parameters of the generatrix orbits, in this section keplerian orbital elements for orbits in section 6.1 will be studied. For everyone on the captures inside the structures of figure 6.1, semi-major axis a, eccentricity e, perigee argument ω and true anomaly ν were computed. These results are shown in figures 6.19 and 6.20. The first one is for initial position between the primaries and $C_J = 3.00020228 = \frac{C_{J,L1} + C_{J,L2}}{2}$, while the second is for external initial position and $C_J = 3.00020196 = C_{J,L2} - 10^{-7}$.

It has to be noted that these values are equally distributed around the values given in table 6.2.

Besides, the elements of perigee argument and true anomaly are strictly linked between them for all the orbits. In the internal case ω and ν are quite opposites: it is the situation sketched in figure 6.21, where ballistic capture occurs usually when the satellite reaches about 24.5° before the apoapsis. In the external case ω and ν are quite explementary (the sum is slightly more than 360°): it is the situation sketched in figure 6.22, where ballistic capture occurs usually when the satellite reaches about 24.5° before the periapsis. These results completely agree with the one found for Jupiter.

These results are also logical, but they highlight how the ballistic capture could take place only with these particular characteristics, which in all the cases analyzed diverge of only a few degrees from the configurations exposed here. In particular, a rotation of the red orbit in figure occurs, but the position of the beginning of the capture with respect to the apoapsis and periapsis remains substantially fixed.

Obviously, diminishing C_J and so enlarging ZVC and captures structures, the orbits get more variable but they remain meanly the ones analyzed previously. For example, it could be seen that in the internal case where there is a higher number of orbits propagated thanks to the higher dimensions of the gap in ZVC and therefore of the "bubble", also the orbital elements have a wider range of values.

Finally, it has to be underlined that as expected the initial position (where capture begins) for an internal orbit is delayed with respect to the planet. In fact, Mars is about 0.1° forward counterclockwise in the reference frame of the Sun. In addition, the velocity of the satellite is slightly lower than the one of the planet, but the minor length of the path will allow it to recover the lacking phase, entering in proximity of Mars. On the contrary,

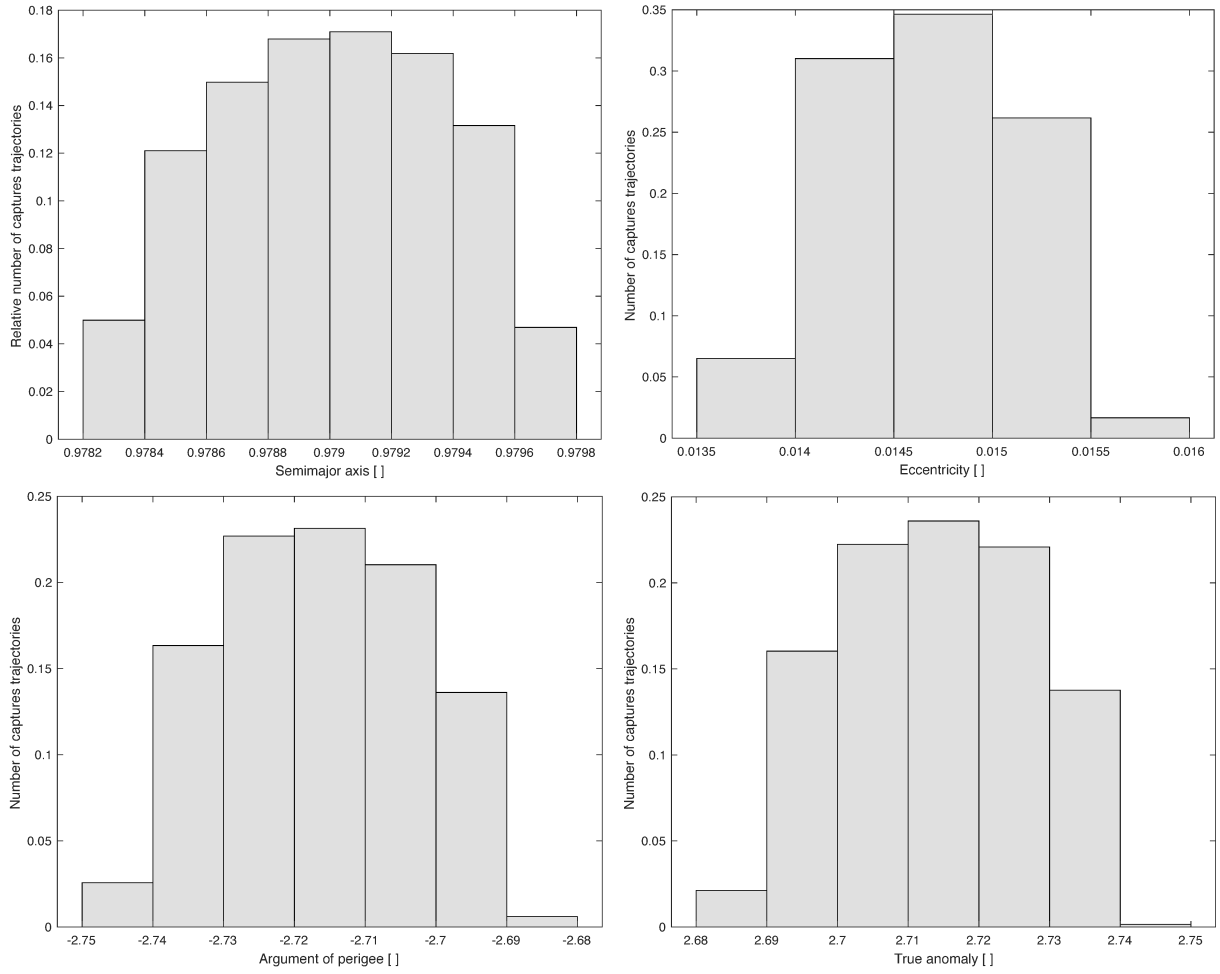

Figure 6.19: Keplerian orbital parameters for orbits inside the internal capture structure (or internal "bubble") for $C_J = C_{J,L1} + C_{J,L2}/2$. This values are distributed around the value of the internal generatrix orbits shown in table 6.2.

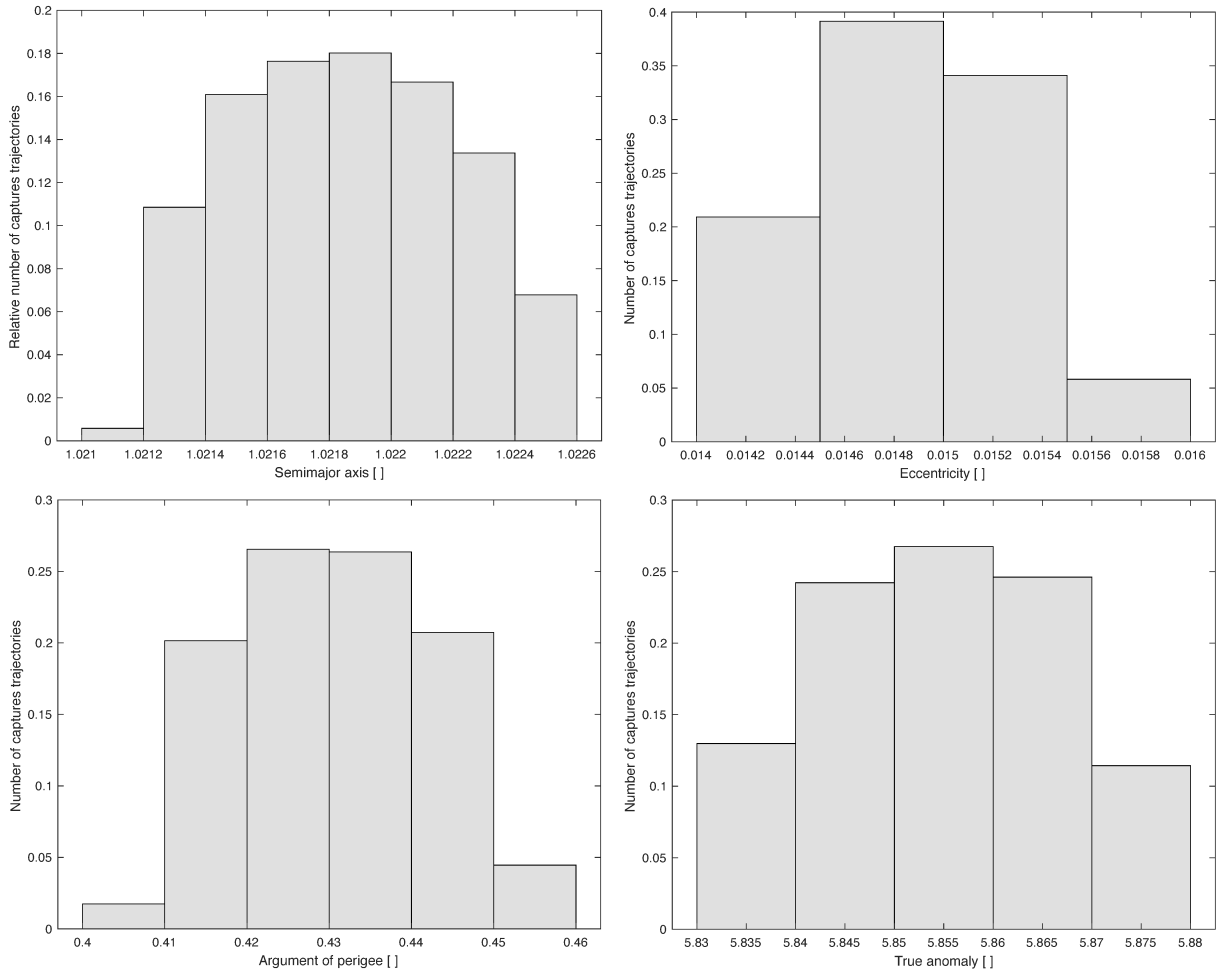

Figure 6.20: Keplerian orbital parameters for orbits inside the internal capture structure (or internal "bubble") for $C_J = C_{J,L2} - 10^{-7}$. This values are distributed around the value of the external generatrix orbits shown in table 6.2.

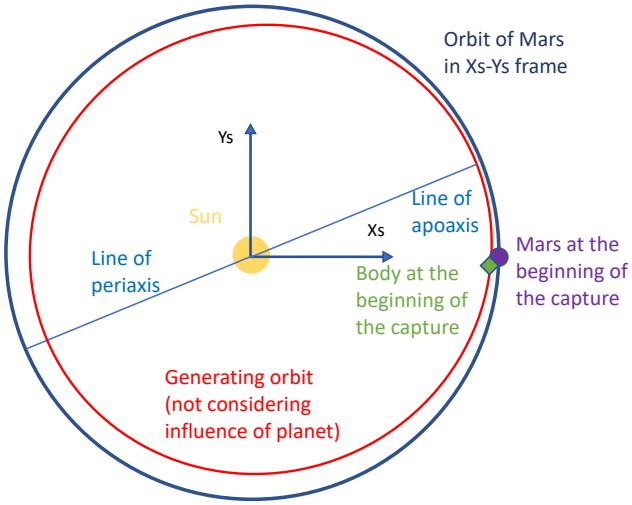

Figure 6.21: Schematic representation of the position of the body in its orbit around the Sun in the moment of the capture for the internal case. The red trajectory would be the one obtained not considering Mars attraction. Coloured signs are linked to the sketched elements in the same colour.

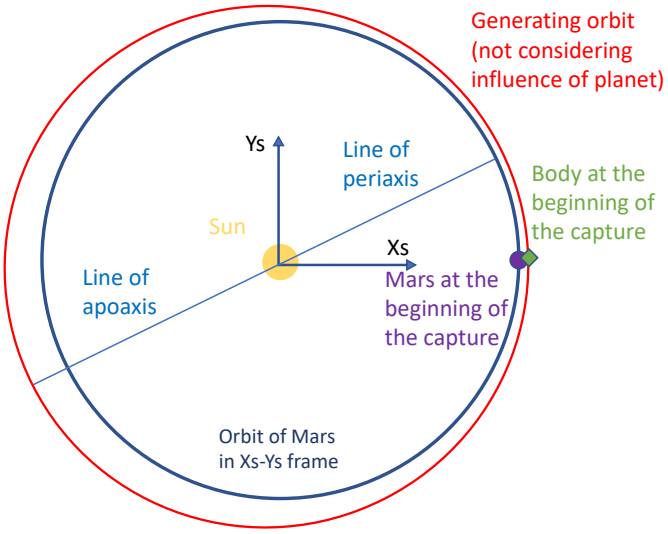

Figure 6.22: Schematic representation of the orbit around the Sun in the moment of the capture for the external case. The red trajectory would be the one obtained not considering Mars attraction. Coloured signs are linked to the sketched elements in the same colour.

for external orbits initial position is in advance of about 0.1° with respect to the planet and this difference will be recovered when the keplerian energy relative to the second primary is already negative. The velocity of the satellite is slightly higher than the one of the planet, but the advantage will be lost thanks to the longer path of the external orbit.

These characteristics are consistent with the ones observed in Jupiter case, but they present minor values for advance and delay. The reason is in the much lower mass ration, as indicated also previously.

6.5 Similarities and differences between Jupiter and Mars

The mass ratio μ for Mars is much lower than the one obtained considering Jupiter. This influences several aspects of the developed analysis.

- Jacobi constants of the Lagrangian points are more close to each other in Mars and also diagrams are more compact near Mars. Zooms will be needed to examine the behaviour for these cases.
- The previous point influences also capture structure. They are smaller, nearer to the planet and more influenced by a little change in the C_J.
- Also orbital keplerian elements are influenced. Semi-major axis and eccentricity are more modest (nearer respectively to 1 and 0), while angular parameters are less affected as they are similar to the ones obtained considering Jupiter. The only difference concerns the advance and the delay, which are considerably less important for Mars.
- The internal generatrix orbit for Mars is shorter and has a chaotic motion (see figure 5.10), but the external one lasts for a longer time then the one obtained with Jupiter. This is due to the fact that here the gap near L1 is less vast than the case studied considering Jupiter.
- Other features are consistent with the cases of Jupiter.

Chapter 7

Results of the search for Earth

In the same way as developed for the Sun-Jupiter and Sun-Mars system, in this chapter the Sun-Earth system will be analyzed.

For a better understanding of the search and of results obtained, table 7.1 is presented. It contains the values of the Jacobi constant in the Lagrangian points.

Analogously to Sun-Jupiter and Sun-Earth system, collisions are never found for high values of the Jacobi constant.

7.1 Capture structures for various values of high C_J

Diagrams for the search of the captures obtained with both internal and external initial position for different values of Jacobi constant C_J in figure 7.1 are ordered from left to right and from above to below: $C_J = 3.00088968 = C_{J,L1} - 10^{-6}$, $C_J = 3.00088868 = \frac{C_{J,L1} + C_{J,L2}}{2}$, $C_J = 3.00088568 = C_{J,L2} - 10^{-6}$ and $C_J = 3.00088168 = C_{J,L2} - 5\ 10^{-6}$. Last two values create both "bubbles" internal and external to the conjunction of the primaries.

From figure 7.1 it is clear that when C_J decreases the gaps of ZVC and as a consequence the bubble get bigger. Also the colour of this last one changes.

Table 7.1: Approximated values of the Jacobi constant in the Lagrangian points. Values are obtained with equation 4.1.

Lagrangian point	L1	L2	L3	L4	L5
Jacobi constant C_J [ ]	3.00089068	3.00088668	3.00000300	2.99999700	2.99999700

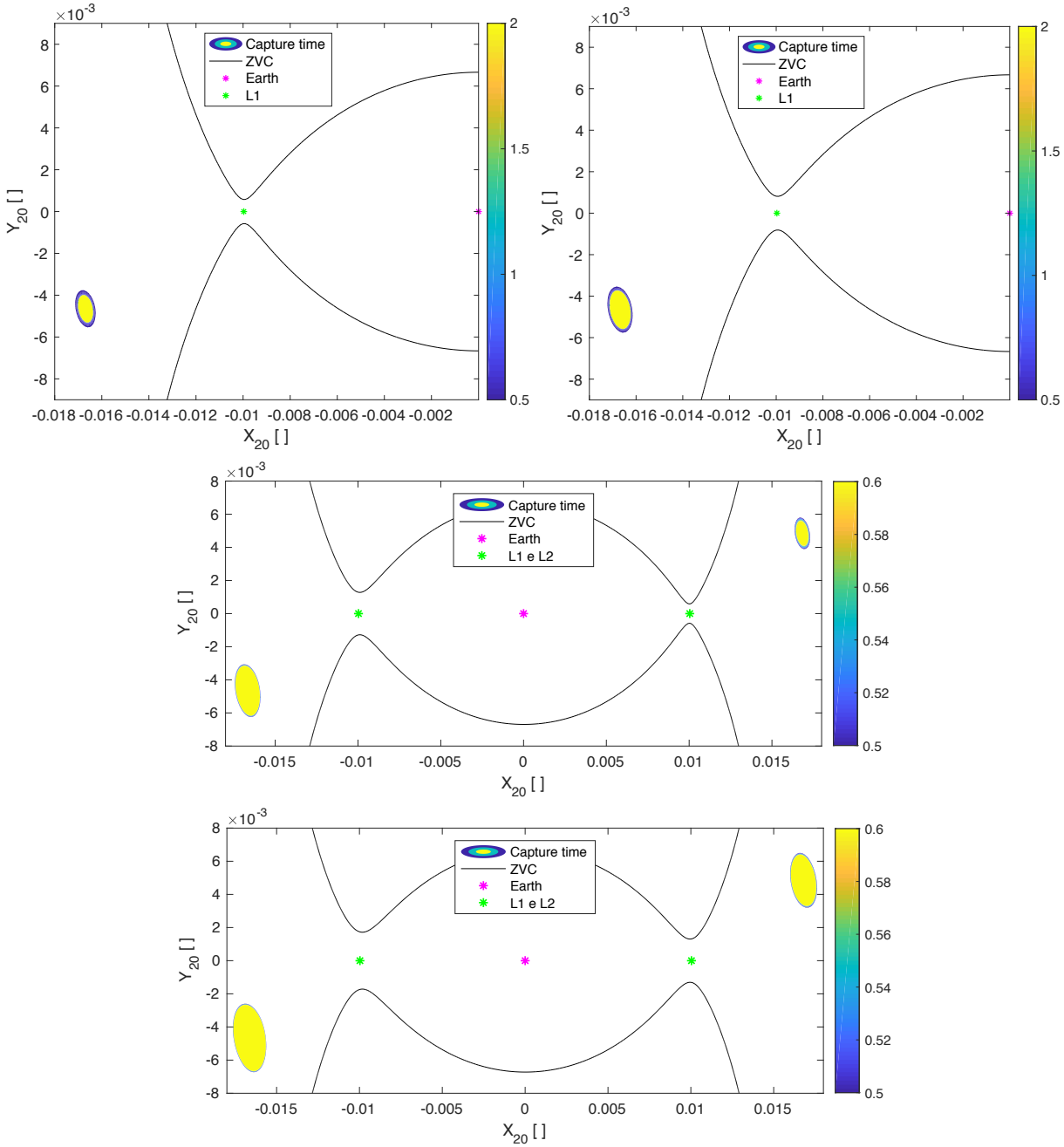

Figure 7.1: Results of the search for ballistic captures by Earth with different values of the Jacobi constant. The $X_{20} - Y_{20}$ plane represented is referred to the Cartesian inertial frame centered in the second primary

For high Jacobi it is completely yellow indicating a long capture, while for lower values of the Jacobi constant it becomes mostly blue indicating shorter captures or even trajectories of flybys.

7.2 Topology of the structures obtained

Bubbles obtained with this method have always an elliptic shape and it is interesting to analyze the change of this shape as a function of the Jacobi constant. This comparison in shown in figure 7.2, where all structures stretch out from a central point that is contained in all of them. Characteristics of the central point sill be further analyzed in section 7.3. For what concerns the structures, they enlarge with the reduction of the Jacobi constant and therefore with the increase of the gaps in the ZVC near the Lagrangian points. This result is visible thanks to the fact that ZVC are plotted in the same colour of the bubble obtained with the same value of C_J.

For what concerns the structures, they enlarge with the reduction of the Jacobi constant and therefore with the increase of the gaps in the ZVC near the Lagrangian points. This results is visible thanks to the fact that ZVC are plotted in the same colour of the bubble obtained with the same value of C_J.

7.3 Analysis of generatrix orbits of the capture structures

An interesting study is to characterize the orbit that will be named "generatrix". This is the orbit obtained by finding the maximum value of C_J for which ZVC are still open. In this case ZVC will be almost closed, leaving only a little hole for the entrance in proximity of the second primary. This is obviously possible in both internal and external region, when the value of the Jacobi constant tends to $C_{J,L1}$ or $C_{J,L2}$ respectively. In this last case ZVC on the right will be almost closed, but on the left they will be completely open. But this fact will not influence at all the analysis because the region of interest in the one on the right near L2.

7.3.1 Method and initial parameters

The keplerian orbital elements summarized in table 7.2 (together with the relative value of the Jacobi constant used in the Matlab scripts) are evaluated in the inertial reference frame of the first primary. They are the elements of

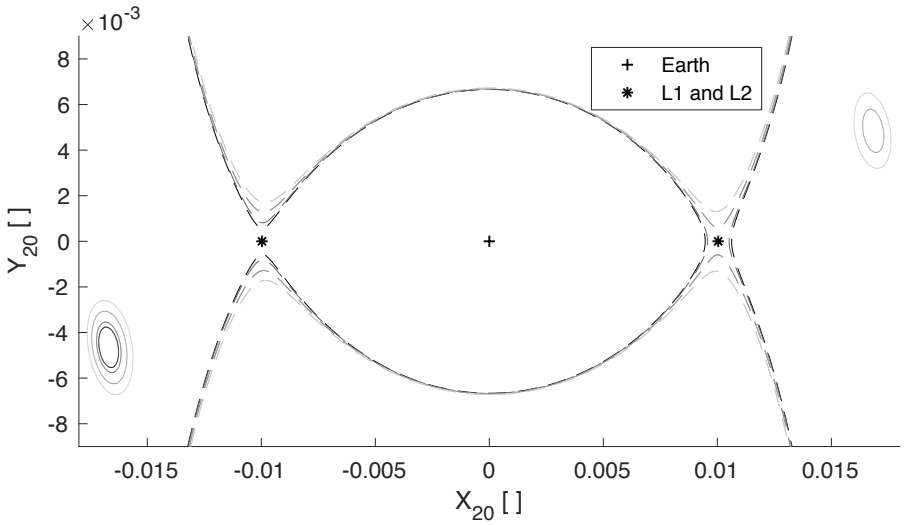

Figure 7.2: Analysis of the topology of "bubble" structures containing the initial positions that conducts to ballistic capture. Their dimensions increase and ZVC gaps grow bigger with the reduction of C_J. This trend is shown using the black colour fading into light gray. The gap of the ZVC in L2 opens up and the external bubbles appear only with the last two values of the Jacobi constant.

the orbit around the Sun in the instant when the satellite is captured by the Earth, hence the keplerian energy relative to the planet is null.

In table 7.3 initial coordinates used in Matlab simulations for the generatrix orbits are shown. These coordinates are taken in the inertial system of reference centered in the second primary or in the synodic centered in the first primary for both internal and external case. In this case and in the research previously exposed *Ode113* was used due to its lighter computations (as shown in chapter 1) with absolute and relative tolerances set to 10^{-12}. Other parameters (masses and reference radius) used in the simulations are summarized in table 7.4.

- It has to be underlined that the orbit presented here is the one obtained not considering (only in this moment) the gravitational attraction given by the Earth. Obviously, the propagation on the whole requires this contribution to find the moment when the ballistic capture begins.

  But in this way results represent only conditions at the instant of beginning of the capture, not the effective provenience of the trajectory, which is deflected also before this moment. In the next sections this point will be discussed separately for internal and external orbits.

Table 7.2: Keplerian orbital elements (semi-major axis a, eccentricity e, perigee argument ω and true anomaly ν) of the internal and external generatrix orbits and relative numerical value of the Jacobi constant for these valued.

	a [ ]	e [ ]	ω [ ]	ν [ ]	C_J [ ]
Internal orbit	0.9567533	0.0306770	-2.7194328	2.7147090	$C_{J,L1} + 9.4\ 10^{-9}$
External orbit	1.0470573	0.0315388	0.4333722	5.8545779	$C_{J,L2} + 9.3\ 10^{-9}$

Table 7.3: Initial coordinates used in Matlab simulations for internal and external generatrix orbits. On the left, the first two columns are taken in the inertial reference frame centered in the second primary. On the right, the following two columns, are taken in the synodic frame in curvilinear coordinates. The last two columns are the distance of the initial point of these orbits from the Earth, respectively dimensionless and measured in Hill's sphere radii.

	$X_{2,0}$ [ ]	$Y_{2,0}$ [ ]	ρ_0 [ ]	θ_0 [ ]	d_2 [ ]	d_2 [r_{Hill}]
Internal orbit	-0.016700	-0.004645	-0.016689	-0.004724	0.017334	1.73273
External orbit	0.016835	0.004845	0.016847	0.004765	0.017518	1.75115

- Being in a planar case it is not useful to consider right ascension of ascending node Ω and inclination i of the orbits, so they will be considered always null. In the results only the other four parameters will be shown.

- In this particular case the conditions of capture are particularly strict and only a representative orbit will be analyzed. Regardless how much the value of $C_{J,L1}$ is accurate, there are always infinite orbits all concentrated around a single point.

  The distinctive feature used to show the resulting characteristics is that everyone of the infinite orbits obtained has the same parameters of the one displayed in the following section, that is with an accuracy up to the seventh decimal point.

Table 7.4: Parameters used in the simulations for the Earth: mass of the Sun M_{Sun}, mass of Earth M_{Earth} and radius of its orbit around the Sun R_{ref}.

M_{Sun} [kg]	M_{Earth} [kg]	R_{ref} [km]
$1.988499251 \cdot 10^{30}$	$5.972430327 \cdot 10^{24}$	$149.6 \cdot 10^{6}$

7.3.2 Diagrams and duration of the internal generatrix orbit

In this section interesting figures and parameters for the internal generatrix orbit will be shown. The initial conditions for this orbit were presented in tables 7.2 and 7.3.

Keplerian energy relative to the second primary is negative for a time longer than 5000 years and this indicates a very important capture. That could be explained by considering the very small gap existing in the ZVC, which quite impede to enter or exit from the area in proximity of the planet.

In figures 7.3, 7.4, 7.5 and 7.6 is represented the trajectory of this peculiar orbit. First two figures (7.3 e 7.4) are taken in the synodic frame: the first is a complete view and a zoom around the planet; the second shows an additional zoom near the planet and a detail of the passage in the gap of L1. The last two figures (7.5 e 7.6) represent the orbit in the Cartesian inertial reference frame centered respectively in the first and the second primary.

Total duration of the simulation is 4 years, 2 in backward propagation (BW) and 2 in forward propagation (FW).

The transition to entry in the area near the planet lasts quite a year. This feature is particularly visible in figure 7.6, where the trajectory covers quite an entire circle near the Hill's sphere. Here relative velocities are very small and for this reason in the synodic frame the trajectory is almost still in proximity of the Lagrangian point L1.

In the inertial frame centered in the Sun (figure 7.5) this feature is visible between the square of the initial position and the moment when the trajectory begins to be diverted by the planet. In fact, between these two moments there is an entire circle in which the orbit slowly gets nearer to Earth's orbit.

Unfortunately, as in the case of Mars, these details are barely visible in the case of the Earth, because of the less importance in terms of mass of this second primary body. This feature takes to a packing of the characterising points near the planet and so they are not visible without any zoom in the diagrams.

7.3.3 Variation of orbital elements for internal generatrix

In figures 7.7, 7.8 and 7.9 the values of keplerian orbital elements a, e and ω are presented as a function of the distance of the body from the second primary. Besides, here semi-major axis a, eccentricity e and perigee argument ω are given for the internal generatrix orbit: $a = 0.9527$, $e = 0.0304$ and $\omega = -2.9056$. These values are taken in the figures mentioned above, where

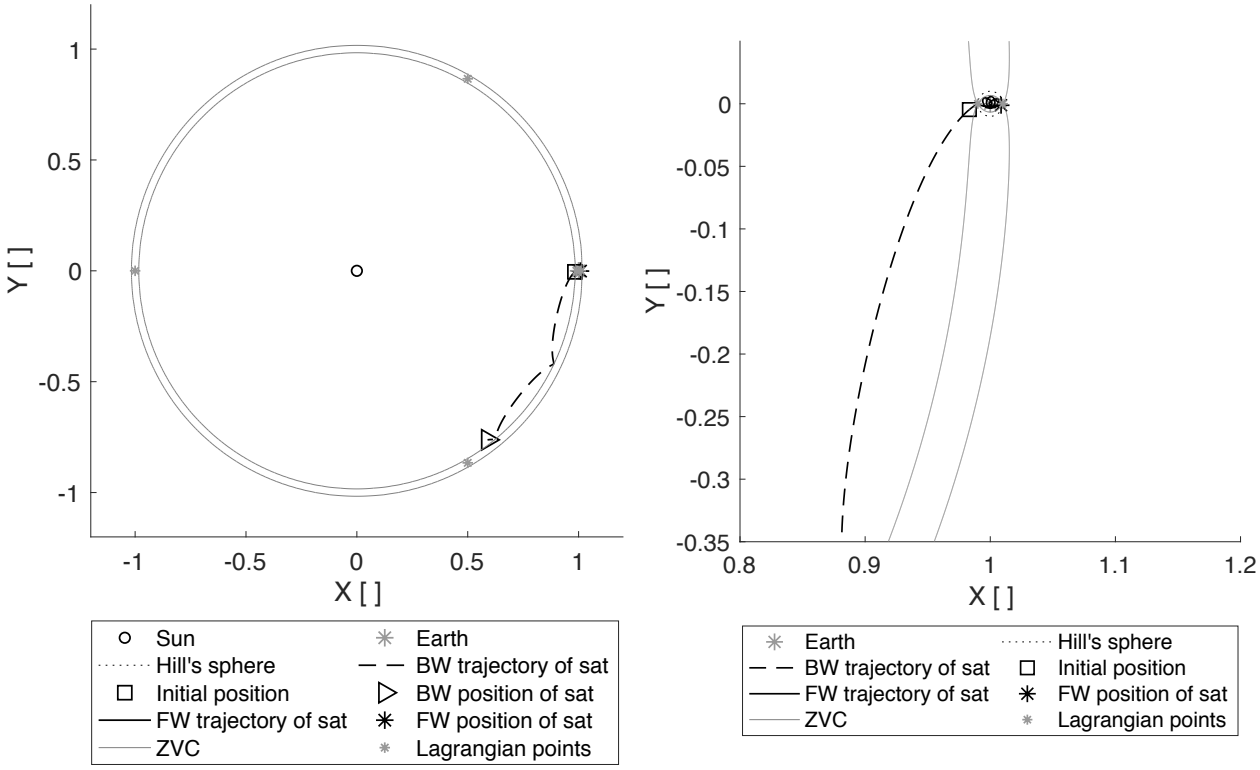

Figure 7.3: Internal generatrix trajectory of the satellite (sat) in the synodic frame centered in the Sun. On the left, the overall view; on the right, a zoom of the area containing the Earth. The trajectory propagated backward in time (BW) is dashed. Initial point of the propagation is represented by a square.

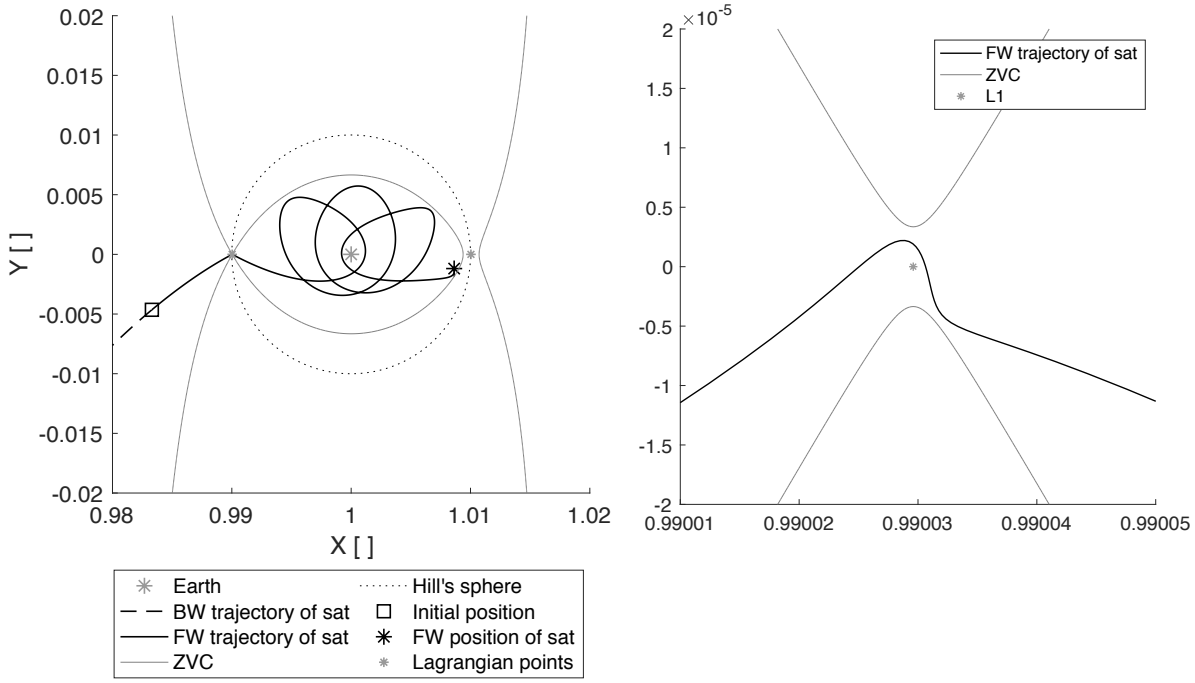

Figure 7.4: Internal generatrix trajectory in the synodic frame centered in the Sun. From left to right, additional zoom near planet and detail of the passage between the ZVC near L1.

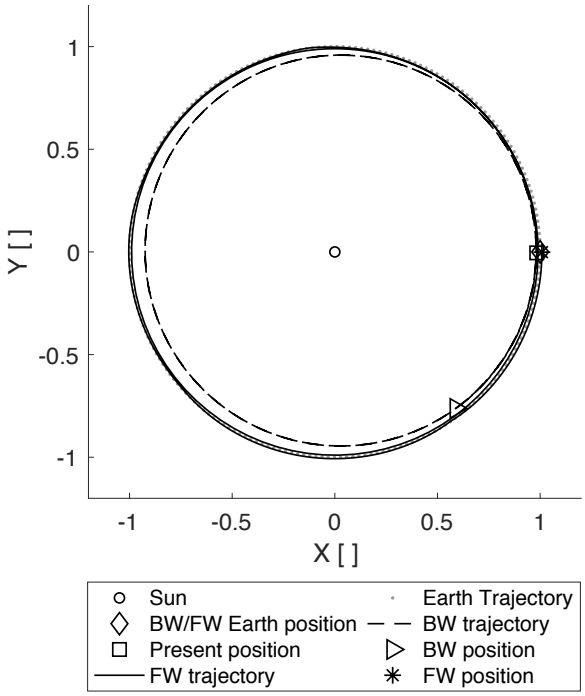

Figure 7.5: Internal generatrix trajectory in the inertial frame centered in the Sun.

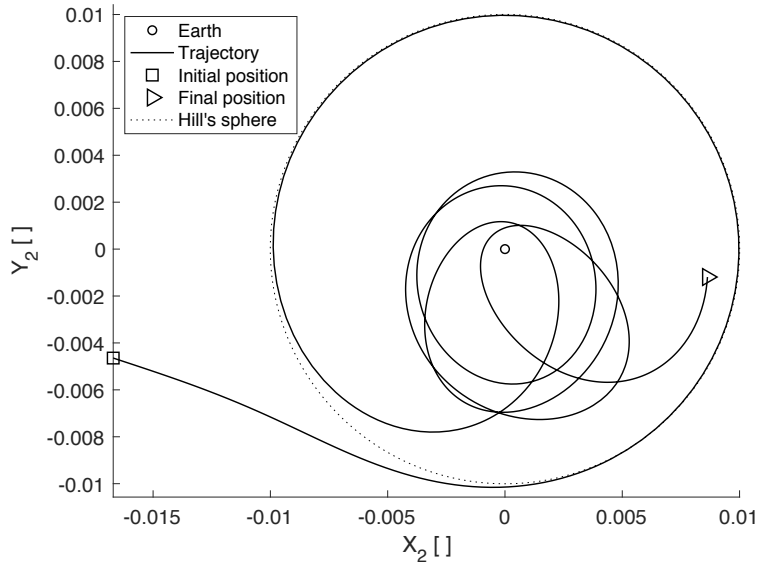

Figure 7.6: Internal generatrix trajectory in the inertial frame centered in the Earth.

the plotted parameters tend to be steady. On the contrary to Jupiter's case and analogously to Mars, they have a modest difference with the ones presented in table 7.2 obtained in the instant of beginning of the capture. It has to be highlighted that they continuously change and can not be considered reference parameters for the analysis, if not when some criteria are specified.

7.3.4 Diagrams and duration of the external generatrix orbit

In this section interesting figures and parameters for the external generatrix orbit will be shown. The initial conditions for this orbit were presented in tables 7.2 e 7.3.

In figure 7.10 is represented the keplerian energy relative to Earth for a time span of 5.4 years. All along this energy is negative and this indicates a very important capture, longer than 5 years. In figure is also shown the trajectory in the proximity of the planet with the detail of closed ZVC in L2 and slightly more open in L1.

Analogously to the case of Mars, the difference between the gap in L1 and the one in L2 depends on the mass ratio μ. In this case it is very small, hence this difference is very tiny. For this reason and thanks to the particular value of C_J studied, a trajectory entering by the gap of L2 stays longer in

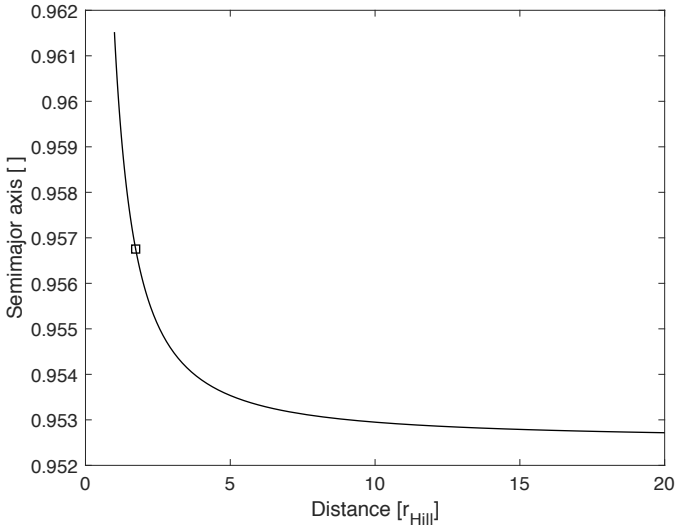

Figure 7.7: Semi-major axis of the internal generatrix computed in the inertial system of reference centered in the Sun. Its variation is shown as a function of the distance from the second primary in Hill's radii. The square indicates the moment when the capture begins. On its left there are the values for the FW propagation, nearer to the second primary; on the right there are the values for the BW propagation, where the body gets further from the planet.

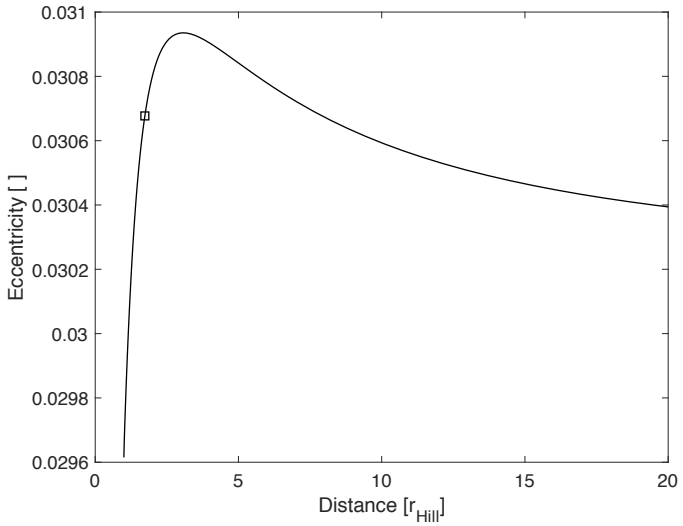

Figure 7.8: Eccentricity of the internal generatrix in the inertial system of reference centered in the Sun. Its variation is shown as a function of the distance from the second primary in Hill's radii. The square indicates the moment when the capture begins.

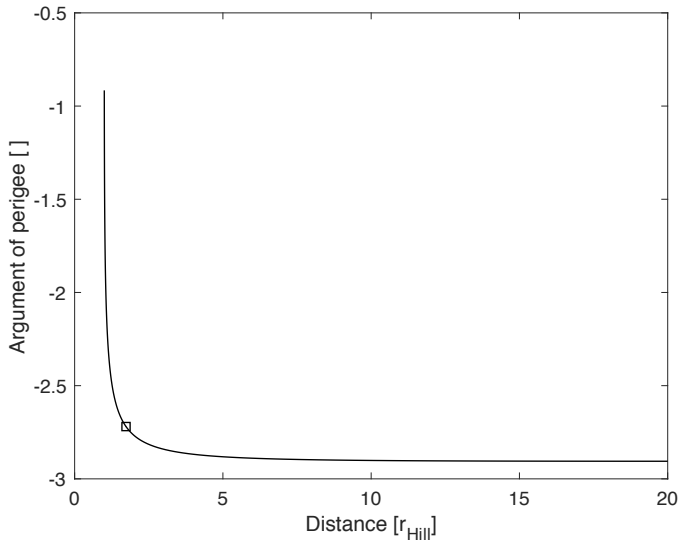

Figure 7.9: Perigee argument of the internal generatrix in the inertial reference centered in the Sun. Its variation is shown as a function of the distance from the second primary in Hill's radii. The square indicates the moment when the capture begins.

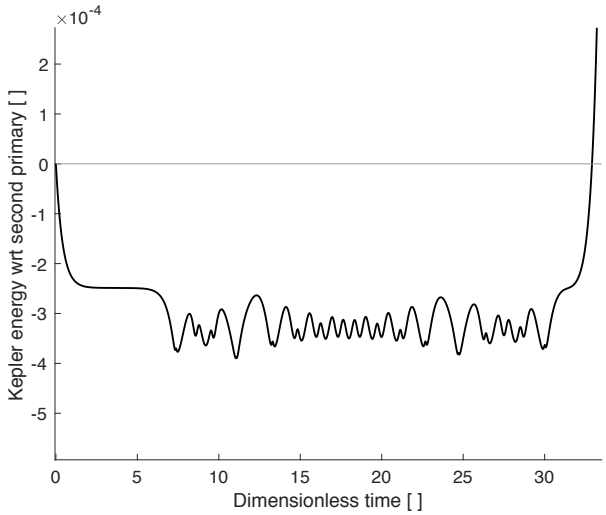

Figure 7.10: External generatrix Keplerian energy relative to the second primary for 5.4 years from the beginning of the capture.

orbit near the planet. It is more difficult for it to exit from the narrow gap in L1.

In figures 7.11, 7.12, 7.13 and 7.14 is represented the trajectory of this peculiar orbit. First two figures (7.11 and 7.12) are taken in the synodic frame: the first is a complete view and a zoom around the planet; the second shows an additional zoom near the planet and a detail of the passage in the gap of L2. The last two figures (7.13 and 7.14) represent the orbit in the Cartesian inertial reference frame centered respectively in the first and the second primary.

Total duration of the simulation is 4 years, 2 in backward propagation (BW) and 2 in forward propagation (FW).

The transition to entry in the area near the planet lasts quite a year. This feature is particularly visible in figure 7.14, where the trajectory covers quite an entire circle near the Hill's sphere. Here relative velocities are very small and for this reason in the synodic frame the trajectory is almost still in proximity of the Lagrangian point L2.

In the inertial frame centered in the Sun (7.13) this feature is visible between the square of the initial position and the moment when the trajectory begins to be diverted by the planet. In fact, between these two moments there is quite an entire circle in which the orbit slowly gets nearer to the Earth's orbit.

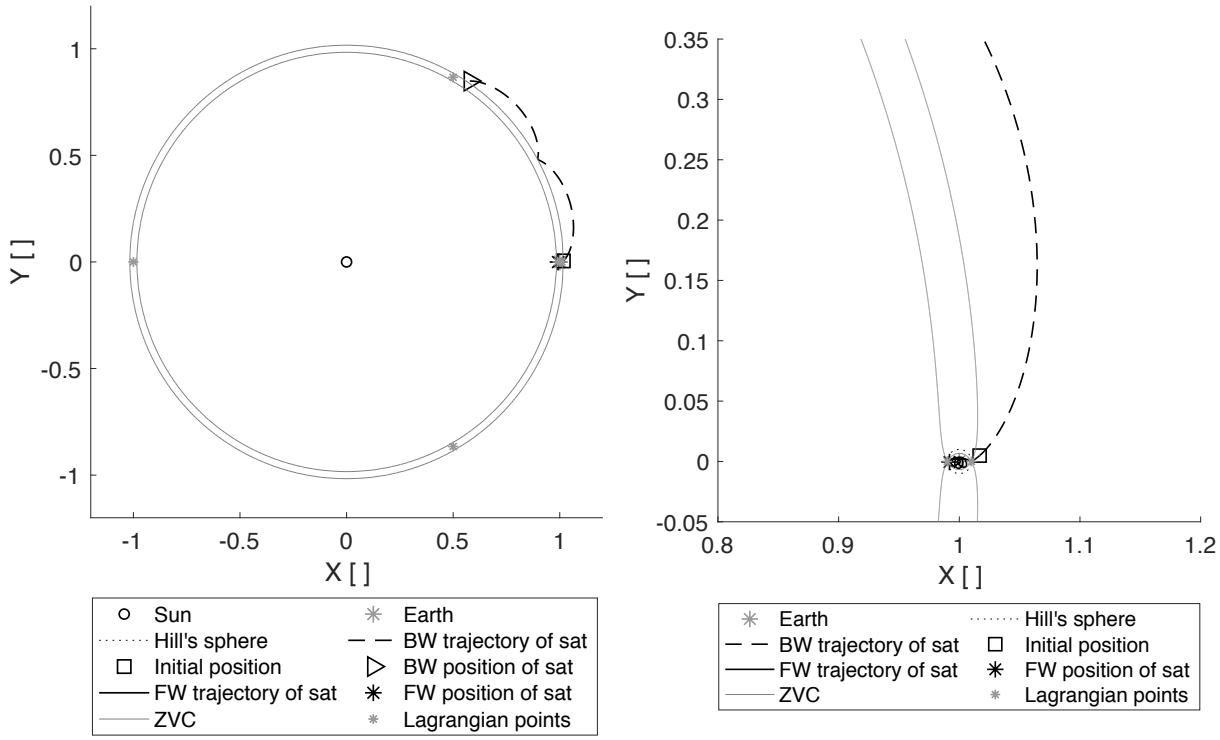

Figure 7.11: External generatrix trajectory of the satellite (sat) in the synodic frame centered in the Sun. On the left, the overall view; on the right, a zoom of the area containing the Earth. The trajectory propagated backward in time (BW) is dashed. Initial point of the propagation is represented by a square.

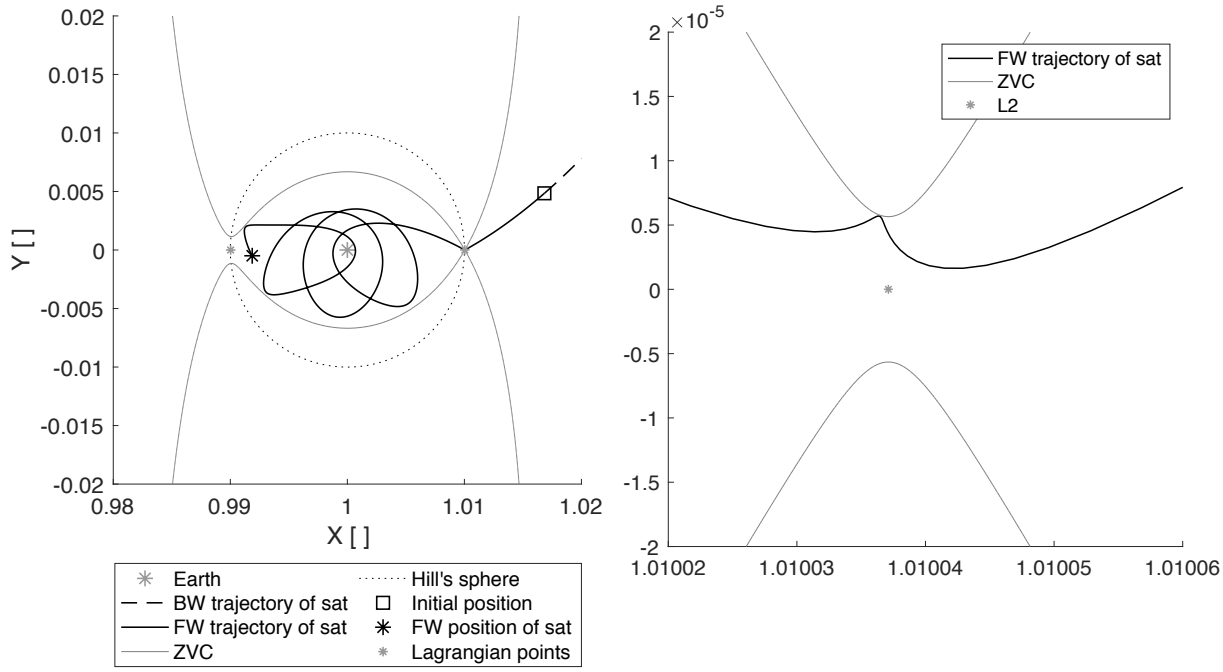

Figure 7.12: External generatrix trajectory in the synodic frame centered in the Sun. From left to right, additional zoom near the Earth and detail of the passage between the ZVC near L2.

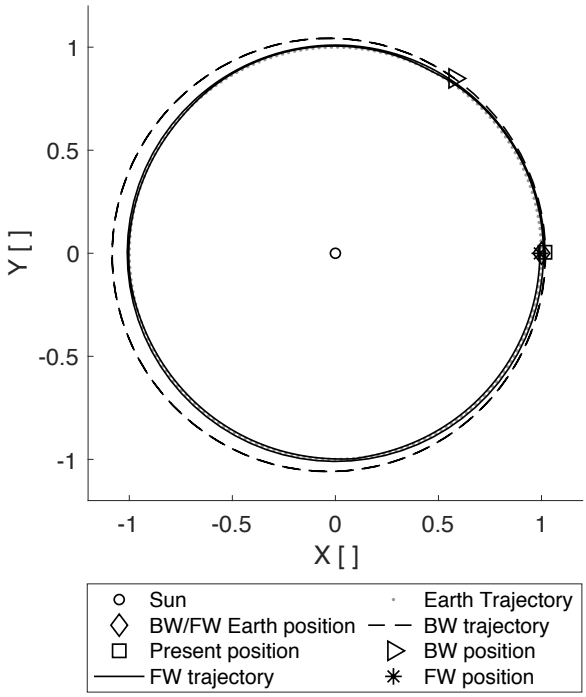

Figure 7.13: External generatrix trajectory in the inertial frame centered in the Sun.

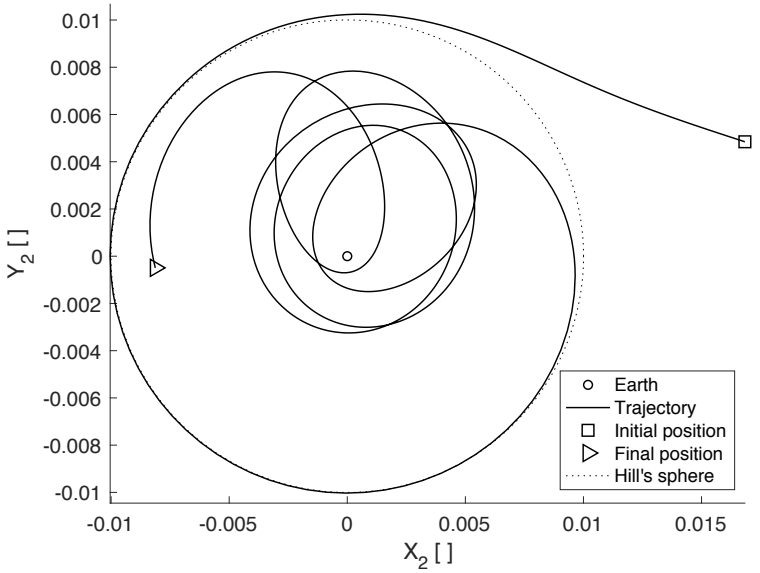

Figure 7.14: External generatrix trajectory in the inertial frame centered in the Earth.

Unfortunately, these details are barely visible in the case of the Earth, because of the less importance in terms of mass of this second primary body. This feature takes to a packing of the characterising points near the planet and so they are not visible without any zoom in the diagrams.

7.3.5 Variation of orbital elements for external generatrix

In figures 7.15, 7.16 and 7.17 the values of keplerian orbital elements a, e and ω are presented as a function of the distance of the body from the second primary. Besides, here semi-major axis a, eccentricity e and perigee argument ω are given for the external generatrix orbit: $a = 1.0515$, $e = 0.0313$ and $\omega = 0.2444$. These values are taken in the figures mentioned above, where the plotted parameters tend to be steady. On the contrary to Jupiter's case and analogously to Mars, they have a negligible difference with the ones presented in table 7.2 obtained in the instant of beginning of the capture.

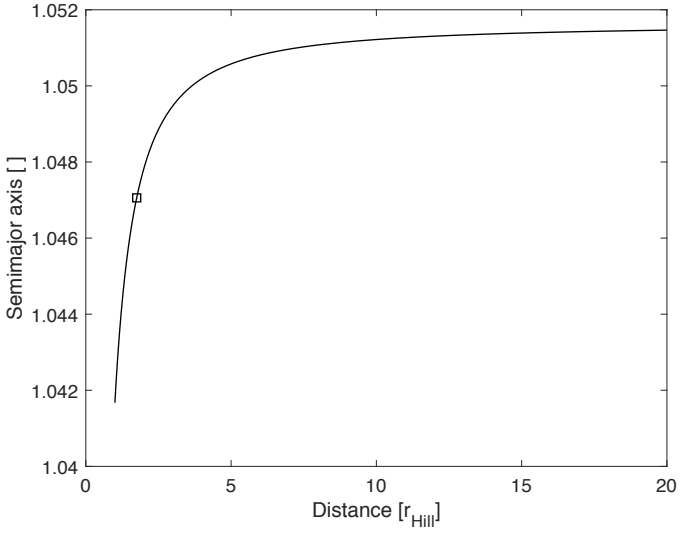

Figure 7.15: Semi-major axis of the external generatrix orbit computed in the inertial system of reference centered in the Sun. Its variation is shown as a function of the distance from the second primary in Hill's radii. The square indicates the moment when the capture begins. On its left there are the values for the FW propagation, nearer to the second primary; on the right there are the values for the BW propagation, where the body gets further from the planet.

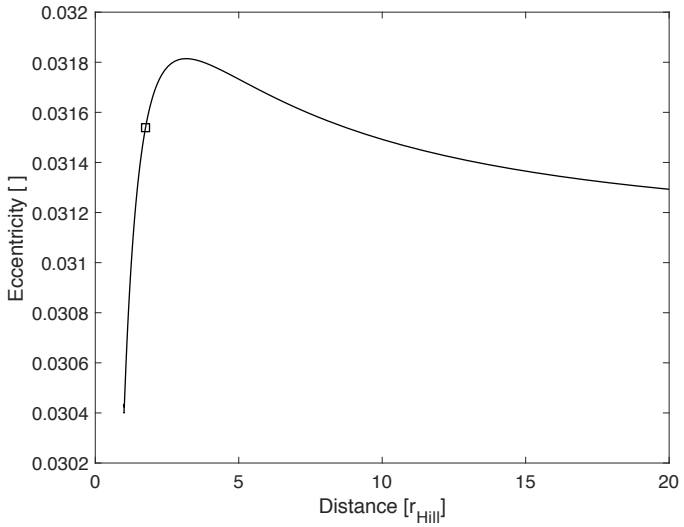

Figure 7.16: Eccentricity of the external generatrix orbit computed in the inertial system of reference centered in the Sun. Its variation is shown as a function of the distance from the second primary in Hill's radii. The square indicates the moment when the capture begins.

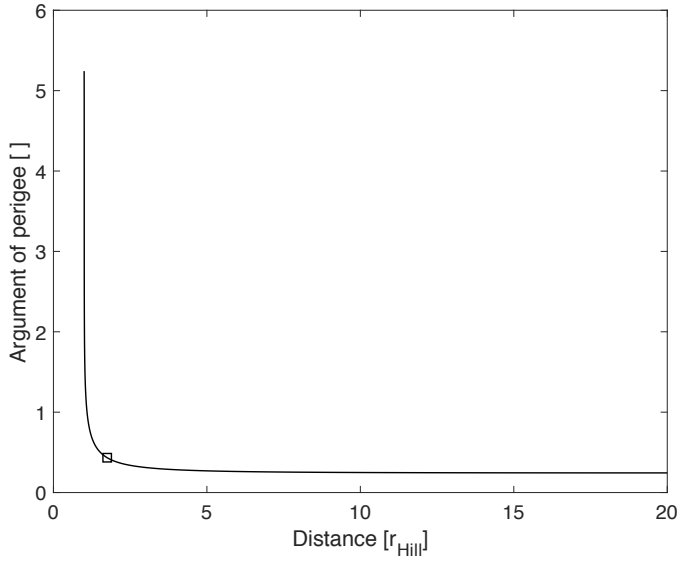

Figure 7.17: Perigee argument of the external generatrix orbit computed in the inertial system of reference centered in the Sun. Its variation is shown as a function of the distance from the second primary in Hill's radii. The square indicates the moment when the capture begins.

7.4 Keplerian orbital elements in the capture structure

In the same way for keplerian orbital parameters of the generatrix orbits, in this section keplerian orbital elements for orbits in section 7.1 will be studied. For everyone on the captures inside the structures of figure 7.1, semi-major axis a, eccentricity e, perigee argument ω and true anomaly ν were computed. These results are shown in figures 7.18 and 7.19. The first one is for initial position between the primaries and $C_J = 3.00088868 = \frac{C_{J,L1} + C_{J,L2}}{2}$, while the second is for external initial position and $C_J = 3.00088568 = C_{J,L2} - 10^{-6}$.

It has to be noted that these values are equally distributed around the values given in table 7.2.

Besides, the elements of perigee argument and true anomaly are strictly linked between them for all the orbits. In the internal case ω and ν are quite opposites: it is the situation sketched in figure 7.20, where ballistic capture occurs usually when the satellite reaches about 24.5° before the apoapsis. In the external case ω and ν are quite explementary (the sum is slightly more than 360°): it is the situation sketched in figure 7.21, where ballistic capture occurs usually when the satellite reaches about 24.5° before the periapsis. These results completely agree with the one found for Jupiter and Mars.

These results are also logical, but they highlight how the ballistic capture could take place only with these particular characteristics, which in all the cases analyzed diverge of only a few degrees from the configurations exposed here. In particular, a rotation of the red orbit in figure occurs, but the position of the beginning of the capture with respect to the apoapsis and periapsis remains substantially fixed.

Obviously, diminishing C_J and so enlarging ZVC and captures structures, the orbits get more variable but they remain meanly the ones analyzed previously. For example, it could be seen that in the internal case where there is a higher number of orbits propagated thanks to the higher dimensions of the gap in ZVC and therefore of the "bubble", also the orbital elements have a wider range of values.

Finally, it has to be underlined that as expected the initial position (where capture begins) for an internal orbit is delayed with respect to the planet. In fact, Earth is about 0.3° forward counterclockwise in the reference frame of the Sun. In addition, the velocity of the satellite is slightly lower than the one of the planet, but the minor length of the path will allow it to recover the lacking phase, entering in proximity of Earth. On the contrary,

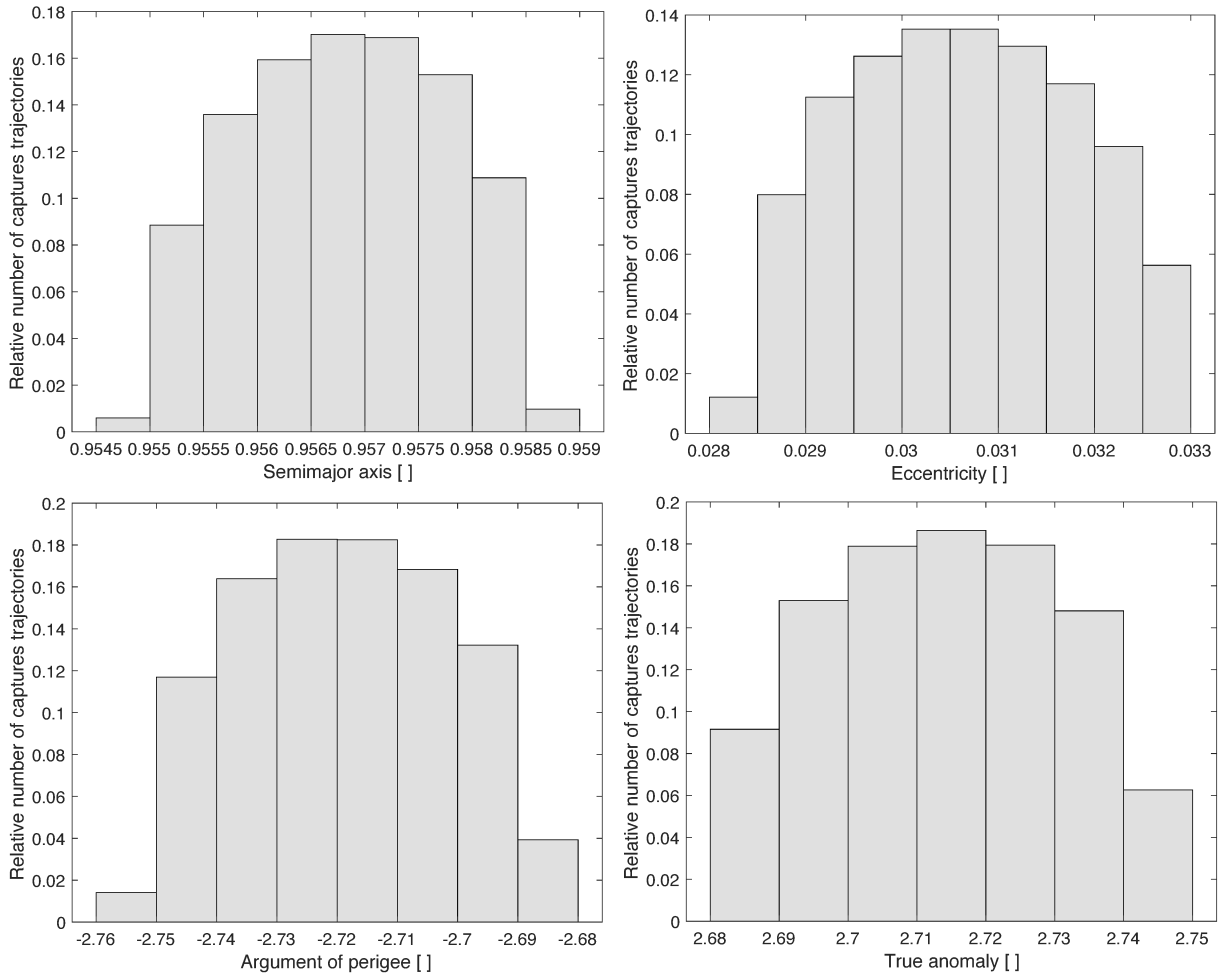

Figure 7.18: Keplerian orbital parameters for orbits inside the internal capture structure (or internal "bubble") for $C_J = C_{J,L1} + C_{J,L2}/2$. This values are distributed around the value of the internal generatrix orbits shown in table 7.2.

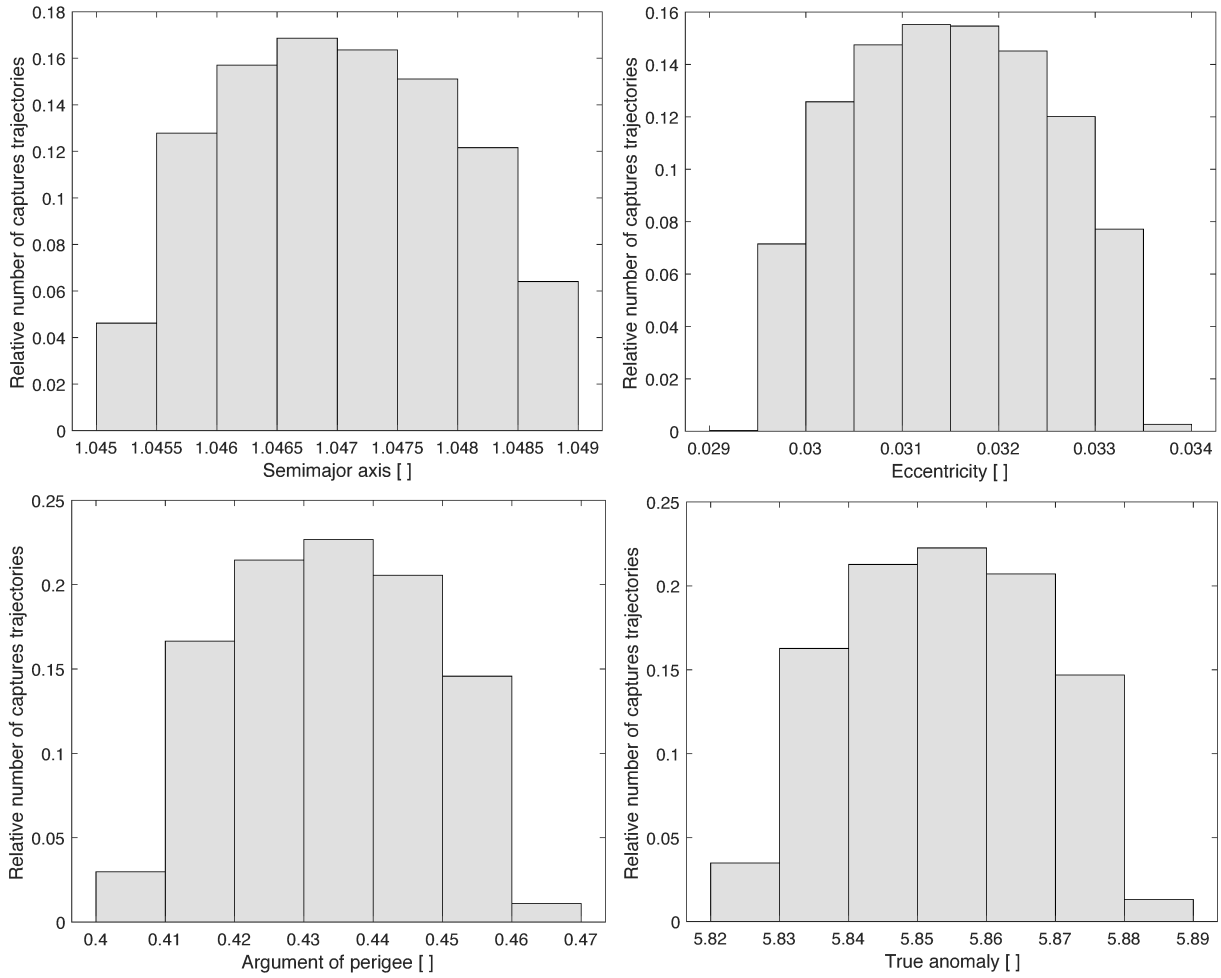

Figure 7.19: Keplerian orbital parameters for orbits inside the internal capture structure (or internal "bubble") for $C_J = C_{J,L2} - 10^{-6}$. This values are distributed around the value of the external generatrix orbits shown in table 7.2.

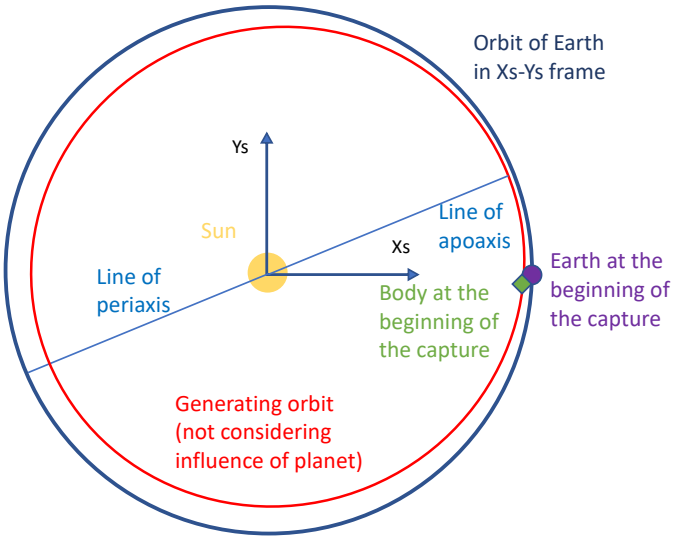

Figure 7.20: Schematic representation of the position of the body in its orbit around the Sun in the moment of the capture for the internal case. The red trajectory would be the one obtained not considering Earth attraction. Coloured signs are linked to the sketched elements in the same colour.

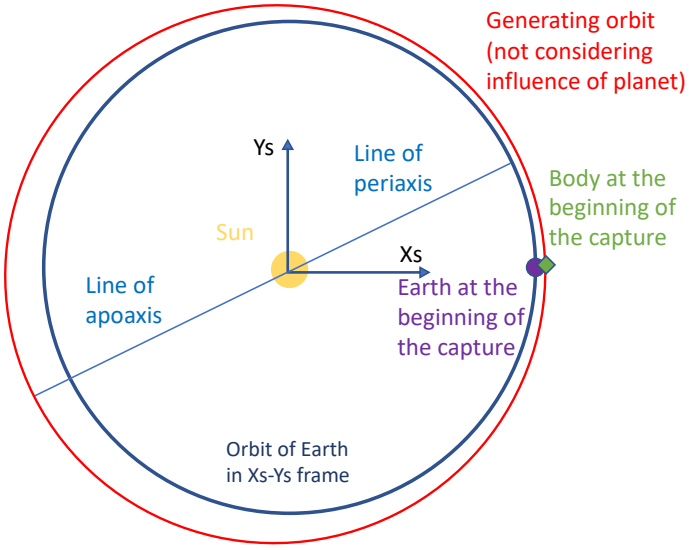

Figure 7.21: Schematic representation of the orbit around the Sun in the moment of the capture for the external case. The red trajectory would be the one obtained not considering Earth attraction. Coloured signs are linked to the sketched elements in the same colour.

for external orbits initial position is in advance of about 0.3° with respect to the planet and this difference will be recovered when the keplerian energy relative to the second primary is already negative. The velocity of the satellite is slightly higher than the one of the planet, but the advantage will be lost thanks to the longer path of the external orbit.

These characteristics are consistent with the ones observed in Jupiter case, but they present minor values for advance and delay (like the case with Mars). The reason is in the much lower mass ration, as indicated also previously.

7.5 Similarities and differences between Jupiter, Mars and Earth

The mass ratio μ for Mars and Earth is much lower than the one obtained considering Jupiter. This influences several aspects of the developed analysis.

- Jacobi constants of the Lagrangian points are more close to each other in Mars and Earth and also diagrams are more compact near Mars and Earth. Zooms will be needed to examine the behaviour for these cases.
- The previous point influences also capture structure. They are smaller, nearer to the planet and more influenced by a little change in the C_J.
- Also orbital keplerian elements are influenced. Semi-major axis and eccentricity are more modest (nearer respectively to 1 and 0), while angular parameters are less affected as they are similar to the ones obtained considering Jupiter. The only difference concerns the advance and the delay, which are considerably less important for Mars and Earth.
- The internal generatrix orbit for the Earth has a longer duration than the one for Mars, but the external one is shorter due to the fact that the gap in L1 in slightly more open for the Earth. This is the only behaviour where Earth and Jupiter are similar, with longer internal capture and shorter external ones. All the other characteristics are similar to the ones obtained for Mars.
- Other features are consistent with the cases of Jupiter and Mars.

Chapter 8

Advantages of the ballistic capture

In this chapter the orbits analyzed so far will be addressed, to find out when and how they could be exploited for interplanetary trajectories.

8.1 Orbital dynamics of interplanetary orbits

Interplanetary orbits are generally divided into three parts using the *patched conics method* [1]: hyperbolic orbit in the reference frame of the departure planet; elliptic orbit in the heliocentric reference frame linking the departure and the arrival planet; hyperbolic orbit in the reference frame of the arrival planet.

Ballistic capture could be exploited to avoid the impulsive maneuver mandatory in the case of a general interplanetary transfer. In fact, using patched conics method the "breaking" ΔV at the arrival planet must be considered and computed. This is to transform the hyperbolic orbit to an elliptic orbit in the frame of the arrival planet. Different considerations will be discussed in the following sections.

Therefore, the saving of a ballistic capture trajectory stays in the third part of the interplanetary trajectory. Equations and parameters for it will be detailed in the next section.

The characteristic of long duration of the ballistic capture will be considered equal to a permanent capture just like the one obtained with an impulsive burn. As it was shown in the previous chapters, also internal generatrix orbits give long time spent in capture sufficient for a mission involving a spacecraft.

In reality, a large number of long orbits with initial conditions inside the "bubbles" were propagated, giving similar results in terms of duration of the capture. So, the considerations discussed in this chapter are valid for a large number of orbits similar to each other.

An analogous discussion could be made for the time spent by the trajectory to reach the first close transit. As it was shown in the previous chapters, generatrix orbits spend a long time (from half to an entire planet year) to pass through the gap near the Lagrangian point. This could be a great disadvantage, but enlarging the "bubble" (therefore diminishing C_J) these periods drop to only a couple of planetary months or less. Hence, also from the point of view of the necessary time to reach the arrival planet the characteristics of ballistic capture and impulsive capture will be considered totally similar.

8.2 Considerations over orbital elements

It is important to begin this section underlining that keplerian elements of the generatrix orbit and similarly the ones for all the other orbits analyzed are normally much different from the ones of an interplanetary transfer departing from the Earth to Mars or Jupiter. On the contrary, keplerian elements computed in the previous chapters are always very similar to the ones of the planet such that when made dimensionless they are more or less near to $a = 1$ and $e = 0$.

This fact will take to three considerations:

- The orbit analyzed needs additional maneuvers to be able to link Earth to Jupiter or any other couple of planets. These additional maneuvers will not be accounted in this preliminary study.
- Indirect and less onerous interplanetary trajectories than the ones departing from Earth will be studied.
- Consequently hyperbolic excess velocities v_∞ at the arrival planet will be much lower than the ones usually obtained. For example, for an interplanetary orbit departing from the Earth $v_\infty = 5.64$ km/s against $v_\infty = 1.755$ km/s when the generatrix orbit is considered.

Classical equations of the orbital dynamics are often used to compute the necessary ΔV to slow down the satellite and permit the insertion in an elliptical orbit. They are resumed in the following one [1]

$$\Delta V = \sqrt{v_\infty^2 + \frac{2\mu}{r_0}} - \sqrt{\frac{\mu(1+e)}{r_0}} \tag{8.1}$$

where μ is the gravitational dimensional constant of the planet, e is the eccentricity needed after the maneuver and r_0 is the periapsis where the impulsive burn occurs.

To analyze it deeply, this equation it has to be studied as a function of the three variables v_∞, e and r_0. The last one is obviously the most important one, because the optimal distance for the breaking maneuver has to be found. But also the other two variables have an influence on the ΔV requested by this burn. In particular v_∞ is important: if the hyperbolic excess velocity is negligible with respect to the term μ/r_0 which represents the velocity given by the planet during the approach to the periapsis, then the trend of the burn is monotone decreasing as a function of the distance from the periapsis. At high distances the behaviour becomes asymptotic to a minimum ΔV and here is where the burn is more convenient. The opposite behaviour could be obtained for much larger v_∞ where the cost of the maneuver is monotonically increasing. Hence, burns more near to the planet will be more convenient. For an intermediate value of v_∞ also the eccentricity of the required orbit will acquire importance. This is the case that will happen in the case studied here. The trend is similar to the ones described above, but it will vary very rapidly even if v_∞ is fixed. In figures 8.1, 8.2 and 8.3 these trends are shown. Additional analysis of this topic will not be object of this study.

Obviously, the cost of the burn decreases when the eccentricity of the requested orbit around Jupiter increases.

Instead, an example with a much higher excess velocity $v_\infty = 5.64$ m/s is shown in figure 8.4. In this case the influence of the excess velocity is clear. A trend like this with lower v_∞ could be obtained only for quite parabolic orbits.

For every second primary considered (Jupiter, Mars and also Earth), conclusions are analogue to the ones presented here.

8.3 Saving in the ΔV

The saving that could be reached by avoiding the breaking ΔV thanks to a ballistic capture will be considered equal to the estimation of the cost of the impulsive maneuver at the arrival planet.

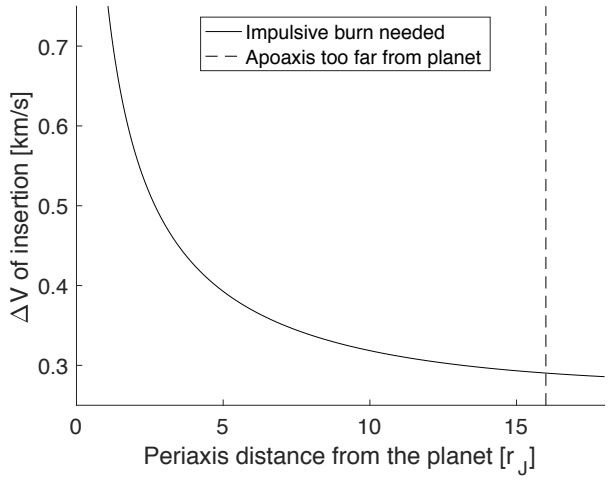

Figure 8.1: Insertion ΔV in an elliptic orbit with $e = 0.95$ and $v_\infty = 1.755$ km/s (coming from the generatrix orbit) as a function of the distance of the periapsis from the planet in Jupiter's radii. The trend is monotone decreasing. For the indicated distance from the periapsis the vertical black line says that the apoapsis is too far from the planet and near the Hill's sphere. So, orbits on its right will not be stable and must be discarded.

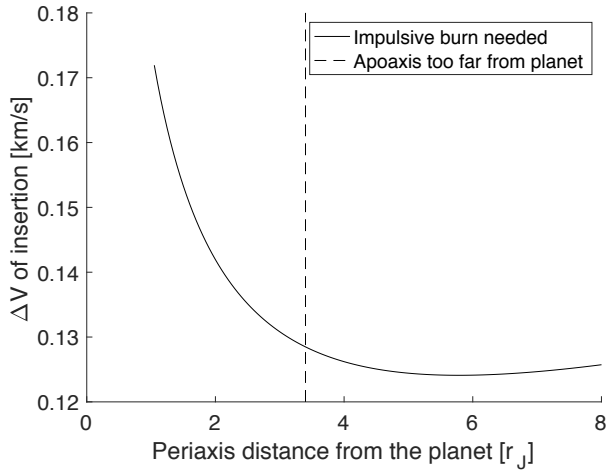

Figure 8.2: Insertion ΔV in an elliptic orbit with $e = 0.99$ and $v_\infty = 1.755$ km/s (coming from the generatrix orbit) as a function of the distance of the periapsis from the planet in Jupiter's radii. There is a minimum, so a optimal distance for the burn. As in the previous figure, orbits far on the right will must be discarded.

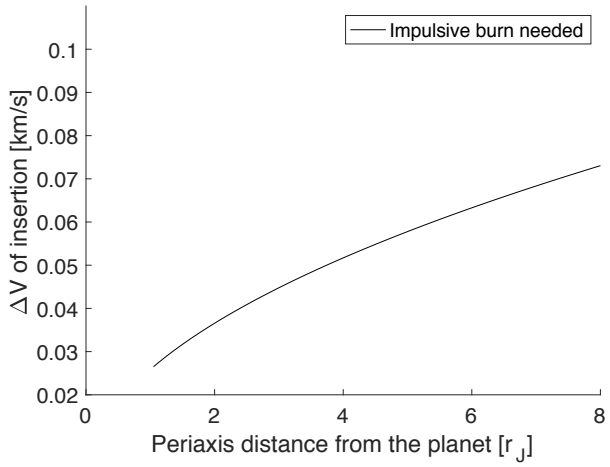

Figure 8.3: Insertion ΔV in an elliptic orbit with $e = 0.99$ and $v_\infty = 1.755$ km/s (coming from the generatrix orbit) as a function of the distance of the periapsis from the planet in Jupiter's radii.

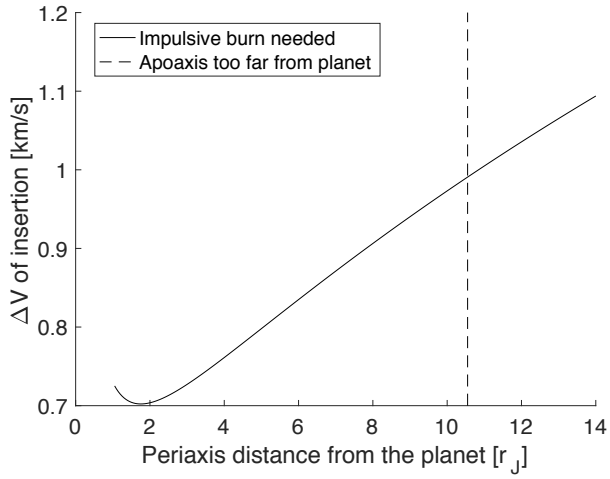

Figure 8.4: Insertion ΔV in an elliptic orbit with $e = 0.969$ and $v_\infty = 5.64$ km/s (coming from the orbit of the Galileo probe) as a function of the distance of the periapsis from the planet in Jupiter's radii. There is a minimum of the function.

To obtain an eccentricity of 0.95 the following ΔV has to be applied at the periapsis of the arrival hyperbolic orbit: for Jupiter it is of about 300 m/s; for Mars of about 36 m/s.

Considering a specific impulse $I_{sp} = 250$ s (typical value for hydrazine) respectively nearly the 13% and the 1.5% of the final mass of the satellite could be saved. For a net mass of the spacecraft of 1000 kg this is equal to a saving of nearly 130 additional kg for the insertion in Jupiter and nearly 15 kg in Mars.

It is worth to underline that in this case represented in figure 8.1 the trend is substantially decreasing (or asymptotic to a minimum value), so maneuvers have a minor cost if the burn is made when periapsis is distant from the planet. This distance can not get bigger than a certain value which will give an apoapsis too distant from the planet. This is due to the high eccentricity and could take the the satellite as far as the Hill's sphere taking to a significant perturbation of the Sun.

8.3.1 Considerations on orbits obtained

Results obtained from the present analysis show that ballistic captures for high values of the Jacobi constant keep always distant from the planet. Even the nearest point of the trajectories is quite far from the second primary, let alone the mean distance or the furthest points when the body is inside the capture phase. On the contrary, these last points are so distant that they are considerably deflected by the first primary as seen in the examples and genetrices examined.

This feature of the ballistic capture could be a severe drawback. In fact, for a mission that needs a passage near the planet, this trajectories could be not convenient at all.

Instead, this could be an advantage for orbits that need to stay for a period or for the entire mission at a great distance from the arrival planet. This is almost compulsorily the case of Jupiter, where the planet and the moon Io emit a huge quantity of radiations that could place at risk a probe. So, for this planet a ballistic capture could be interesting and cheaper than classic missions.

In particular, a ballistic capture as studied in this thesis hardly reaches a distance of less than 40 planet radius, that is to say about $3 \cdot 10^6$ km. This is equal to almost 5 times the semi-major axis of Europa and 2 times the one of Callisto. With these characteristics the trajectory stays always far from the zone near Jupiter and Io's orbit, where the important magnetic field of the planet ionizes particles coming from itself and the moon.

The conclusive deduction is that for ballistic captures radiations will be surely very low. Magnetic field will be weak, density of neutrals to be ionized will be low and the distance from sources of ionization is always considerable. Hence, calculus of the quantity of radiations typical for an orbit from a ballistic capture is far beyond the aim of this thesis. This aspect is let for a further improvement of the work.

Ballistic capture presents the classic feature of an orbit with the aim of be cheaper in terms of propellant needed than a normal interplanetary transfer. It is slower and therefore it will spend more time in the transfer orbit. In particular the time spent for classical missions to Jupiter is of nearly 5 years. Therefore a ballistic capture will be necessarily longer, but cannot take too long either.

When the internal generatrix orbit was taken into consideration, it was described the time spent from the point of beginning of the capture (which is relatively near to the planet) and the time when the trajectory went beyond the Lagrangian point L1. This was quantified in nearly 1 Jupiter's year, which means 12 years. A period like this is not suitable at all for a transfer, let alone for only a small portion. So it could be deduced that generatrices are not useful in practice, even if they are significant to understand the features in common to all the ballistic captures obtained for high Jacobi constant values.

Instead, for other cases obtained with lower Jacobi constant values the following periods were calculated:

- For $C_J = C_{J,L1}$ a trajectory takes nearly a Jupiter's year to reach a close encounter with the planet.
- For $C_J = (C_{J,L1} + C_{J,L1})/2$ this period decreases to nearly 6 Jupiter's months.
- For $C_J < C_{J,L2}$ this time falls neatly up to 2 Jupiter's months, which means up to 2 years.
- Inferior values of the Jacobi were not taken into consideration as they are out of the range studied here, but it is expected that they follow the trend and therefore the time span gets even lower.

As far as it could be seen, a period of 2 years spent from the beginning of the capture and the first close encounter could be considered satisfactory for a probe mission. This time is to be compared to the time spent by a classical orbit to reach the planet starting from a similar point and this

time span is nearly of 1 Jupiter's month (or nearly 1 year), so the difference is remarkable but not too great. In addition to both, more years had to be considered for the portion of the trajectory from the departure point or planet to the beginning of the capture.

It has to be underlined that the period of time necessary for the generatrix is useless because this orbit is obtained by taking the limit case. Just broadening a little the values of the Jacobi constant considered and therefore ZVC it is possible to reach suitable values for the period after the beginning of the ballistic capture.

The study stops here, as it wants only to give an idea of the time spans at stake and show that they could be suitable for a mission.

Conclusions and further improvements

The aim of this thesis was to implement a proper simulator for the circular restricted three body problem (CRTBP) capable of finding ballistic captures. These ones were defined and found by an algorithm developed to study trajectories coming from a point where keplerian energy relative to the planet is null. In fact, it is the planet itself the one which captures bodies freely orbiting around the Sun. In addition, a condition over the Jacobi constant was added for a more linear and simpler study of the problem. In particular, high values of the constant were considered, making the shape of ZVC only slightly open around the second primary and the Lagrangian points L1 and L2.

The analysis showed the following results:

- A locus of points leading to ballistic capture was discovered and studied as a function of the Jacobi constant.
- The time spent in capture by the planet in every trajectory considered was measured and orbits were catalogued by using this feature.
- Examples of different peculiar trajectories were studied for a better comprehension of the problem.
- Characteristics and orbital elements of these orbits were computed, showing that for high Jacobi there is always the same pattern for the orbit to be captured.
- A special orbit called "generatrix" was analyzed as it is the one that could resume common features of ballistic capture, and other special trajectories useful for the study were addressed.

- Jupiter, Mars and Earth were analyzed as second primaries. Similarities and differences were exposed, in particular regarding the orbital elements and the peculiarities of the pattern of capture in each case.
- An example of the application of this study was presented, showing how a ballistic capture could be used to save mass of propellant in an interplanetary trajectory. This is done by avoiding the maneuver of "breaking" at the arrival planet thanks to the exploitation of ballistic capture. A saving of ΔV of about 300 m/s and 36 m/s for respectively Jupiter and Mars was found for an orbit like the generatrix, which can not come directly from the Earth.
- The only drawback of a ballistic capture is an obvious increase of the transfer time. But it was shown that this time span could be reduced if an orbit with $C_J < C_{J,L2}$ was considered.
- All orbits obtained for high values of the Jacobi constant kept distant from the arrival planet. This feature could be an advantage if the target is an orbit with high semi-major axis like is usual in Jupiter, where radiations are important near to the planet.

Further improvements

Deepening the study from the perspective of the usefulness of ballistic captures for interplanetary orbit is surely important.

More interesting results could be obtained by extending this study for lower values of the Jacobi constant. In particular, a preliminary study was developed and the structure deflects from the shape of the "bubble" increasing a lot the computational cost of the analysis.

Another object of a further improvement could be to find analytical relations between the initial conditions and in particular initial direction of the velocity and whether the trajectory will be captured or not, as introduced in section 4.7.

It is well known that CRTBP is not enough accurate for the predictions of real systems [10]. A further improvement could be developed with the introduction of the elliptic problem (ERTBP) which is essential for better simulations of bodies in the Solar system. Even this could not be enough accurate, so eventually it could be considered the four body problem, other perturbations or the whole ephemeris model.

Another potential use of the results obtained here is the study of the ballistic capture of asteroids, finding out from where they are likely to be

captured and how the could be detected. Maybe also interesting results could be found in the field of planet and moon formation in the Solar system or deflection of asteroids and comets thanks to the interactions of Jupiter.

In addition, an analysis of the a well known example of ballistic capture could be conducted. The asteroid 2006 RH120 is emblematic and it could be interesting to verify if it belongs to a pattern found with this work. Preferably, for a wise study the analysis should be conducted after the extension of the values of C_J examined (it has a value of C_J much lower than the ones examined in this thesis) and the implementation of a more accurate model, as said before.

Bibliography

[1] Richard H Battin. *An introduction to the mathematics and methods of astrodynamics*. Aiaa, 1999.

[2] O.C Winter, E Vieira Neto, and A.F.B.A Prado. "Orbital maneuvers using gravitational capture times". In: *Advances in Space Research* 31.8 (2003). Integrated Space Geodetic Systems and Satellite Dynamics, pp. 2005–2010. ISSN: 0273-1177. DOI: https://doi.org/10.1016/S0273-1177(03)00176-5. URL: https://www.sciencedirect.com/science/article/pii/S0273117703001765.

[3] Sergey A. Astakhov and David Farrelly. "Capture and escape in the elliptic restricted three-body problem". In: *Monthly Notices of the Royal Astronomical Society* 354.4 (Nov. 2004), pp. 971–979. ISSN: 0035-8711. DOI: 10.1111/j.1365-2966.2004.08280.x. eprint: https://academic.oup.com/mnras/article-pdf/354/4/971/3608355/354-4-971.pdf. URL: https://doi.org/10.1111/j.1365-2966.2004.08280.x.

[4] Francesco Topputo, Massimiliano Vasile, and Franco Bernelli-Zazzera. "Low energy interplanetary transfers exploiting invariant manifolds of the restricted three-body problem". In: *The Journal of the Astronautical Sciences* 53.4 (2005), pp. 353–372.

[5] Francesco Topputo and Edward Belbruno. "Computation of weak stability boundaries: Sun–Jupiter system". In: *Celestial Mechanics and Dynamical Astronomy* 105.1 (2009), p. 3. DOI: 10.1007/s10569-009-9222-5. URL: https://doi.org/10.1007/s10569-009-9222-5.

[6] Victory Szebehely. *Theory of orbit: The restricted problem of three Bodies*. Elsevier, 2012.

[7] E. Belbruno, M. Gidea, and F. Topputo. "Geometry of Weak Stability Boundaries". In: *Qualitative Theory of Dynamical Systems* 12.1 (2013),

pp. 53–66. DOI: 10.1007/s12346-012-0069-x. URL: https://doi.org/10.1007/s12346-012-0069-x.

[8] Z.-F. Luo and F. Topputo. "Analysis of ballistic capture in Sun–planet models". In: *Advances in Space Research* 56.6 (2015), pp. 1030–1041. ISSN: 0273-1177. DOI: https://doi.org/10.1016/j.asr.2015.05.042. URL: https://www.sciencedirect.com/science/article/pii/S0273117715003993.

[9] F. Topputo and E. Belbruno. "Earth–Mars transfers with ballistic capture". In: *Celestial Mechanics and Dynamical Astronomy* 121.4 (2015), pp. 329–346. DOI: 10.1007/s10569-015-9605-8. URL: https://doi.org/10.1007/s10569-015-9605-8.

[10] Hodei Urrutxua et al. "Temporarily Captured Asteroids as a Pathway to Affordable Asteroid Retrieval Missions". In: *Journal of Guidance, Control, and Dynamics* 38.11 (2015), pp. 2132–2145. DOI: 10.2514/1.G000885. URL: https://doi.org/10.2514/1.G000885.

[11] Hodei Urrutxua and Claudio Bombardelli. "A look at the capture mechanisms of the "temporarily captured asteroids" of the earth". In: *26th International Symposium on Space Flight Dynamics, ISSFD-2017*. Vol. 74. 2017, pp. 1–7.

[12] Claudio Bombardelli and Pablo Bernal Mencia. "The circular restricted three-body problem in curvilinear coordinates". In: *Celestial Mechanics and Dynamical Astronomy* 130.11 (2018), pp. 1–16.

[13] Diogene A Dei Tos, Ryan P Russell, and Francesco Topputo. "Survey of Mars ballistic capture trajectories using periodic orbits as generating mechanisms". In: *Journal of Guidance, Control, and Dynamics* 41.6 (2018), pp. 1227–1242.

Ringraziamenti

Al professor Bombardelli, che mi ha guidato dentro e fuori da questa tesi, e al professor Lorenzini.
Ai compagni di questa avventura universitaria e in particolare ai "Bulli", il migliore gruppo di compagni di studio e di progetti, di gioie e dispiaceri.
Al "Comitato", alle mie "A-Misce", a Pietro e Davi, a Irene e a quanti mi hanno accompagnato in questi anni universitari, per essermi stati sempre vicini e aver condiviso delle amicizie fantastiche.
Alla mia famiglia, per avermi spronato e supportato in qualsiasi percorso volessi intraprendere.
A chi è arrivato fin qui sfogliando queste pagine.

Grazie.